Experimental Innovation and Performance Assessment of a Solar HDD System

Maher Ghazal

Submitted to the
Institute of Graduation Studies and Research
in Partial Fulfillment of the Requirements for the Degree of

Doctor of Philosophy
in
Mechanical Engineering

Eastern Mediterranean University
February 2015
Gazimagusa, North Cyprus

Approval of the Institute of Graduate Studies and Research

Prof. Dr. Serhan Ciftcioglu
Acting Director

I certify that this thesis satisfies the requirements as a thesis for the degree of Doctor of Philosophy in Mechanical Engineering.

Prof. Dr. Ugur Atikol
Chair, Department of Mechanical Engineering

We certify that we have read this thesis and that in our opinion it is fully adequate in scope and quality as a thesis for the degree of Doctor of Philosophy in Mechanical Engineering.

Prof. Dr. Fuat Egelioglu
Co-Supervisor

Prof. Dr. Ugur Atikol
Supervisor

Examining Committee

1. Prof. Dr. Ugur Atikol
2. Prof. Dr. Fuat Egelioglu
3. Prof. Dr. Arif Hepbasli
4. Prof. Dr. Adnan Midilli
5. Prof. Dr. Ibrahim Sezai

ABSTRACT

The solar humidification dehumidification desalination (HDD) systems described in the literature have four main components, namely, the air heater, the water heater, the humidifier, and the dehumidifier. The heating of air and water are carried out in thermal solar collectors. These components physically occupy a considerable amount of space and the performances of the HDD systems still possess room for improvement.

In the present work a novel humidification mechanism is developed, in which the processes of water and air heating and humidifying are contained in the same unit, giving opportunity to designing smaller sized HDD systems. The unit is essentially a solar collector filled with water. Air is driven in the form of bubbles while some water vapor mixes with it. By the time bubbles reach the outlet of the unit at the top, it is possible to have almost 100% relative humidity.

The solar unit was designed and constructed using the experience gained from a preliminary experiment conducted in the laboratory. In this experiment air was charged through a sparger that was immersed in water and located at the bottom of the humidifier. The experiment was performed under different configurations. Water temperature, air mass flow rate, water level, and the pitch distance between the holes in the spargers are the variables under which the humidification unit was tested. Higher water temperature, higher air mass flow rate, and higher water level resulted in the highest performance when the pitch distance was 10 mm. In an attempt to

increase the performance of the unit, intermediate bubble regeneration stages were added. As a result, significant increase in the humidification effectiveness of the unit was observed. The number of bubble regeneration stages for obtaining the maximum humidification effectiveness at any temperature and air flow rate was found to be eight. The effectiveness of the humidification process at a water level of 40cm with 8 bubble-regeneration stages was 100%.

Experiments of the solar unit were conducted under the weather conditions of North Cyprus. Outlet air approaches saturation and its temperature is found to reach the hot water temperature in the collector (thus increasing the vapor carrying capacity). Moreover, the effectiveness of the humidification process is found to be maximized. The system is capable of producing 15kg/m^2 of fresh water per day. The normalized production of the system is compared with different pilot and commercial scale solar systems. It is found that the present design has a superior performance.

Keywords: Solar Desalination, HDD, Bubble regeneration, Heat and Mass Transfer, GOR

ÖZ

Literatürde anlatılan güneş enerjili nemlendirme-nemalma damıtma sistemlerinin dört ana elemanı vardır, bunlar, hava ısıtıcısı, su ısıtıcısı, nemlendirici, ve nem alıcıdır. Hava ve su ısıtması güneş termal kolektörleri ile yapılmaktadır. Bu elemanlar fiziksel olarak önemli yer kaplamaktadırlar ve nemlendirme-nemalma damıtma sistemlerinin performansları geliştirilmeye uygundur.

Bu çalışmada yeni bir nemlendirme mekanizması geliştirilmiştir, burada su ve hava ısıtması ile nemlendirme işlemleri aynı ünite içerisinde yapıldığından küçük boyutlu nemlendirme-nemalma damıtma sistemlerinin tasarımına fırsatı verildi. Ünite esas olarak su ile doldurulmuş bir güneş kolektörüdür. Hava kabarcıklar halinde sürülürken içerisine bir miktar su buharı karışır. Kabarcıklar üst kısımdaki ünitenin çıkışına ulaştığında, bağıl nemin hemen hemen %100 olması mümkündür. Güneş ünitesi laboratuvarda yapılan ön deneylerden elde edilen deneyimlerden tasarlanıp inşa edilmiştir. Bu deneyde hava su içerisine daldırılan nemlendiricinin alt kısmındaki süzgeçten geçirilerek tahrik edildi. Deney farklı konfigürasyonlarda yapıldı. Nemlendirme ünitesi, su sıcaklığı, hava kütle akış hızı, su seviyesi, ve süzgeçlerdeki delikler arasındaki perde mesafesi değişkenlerine göre test edildi. Süzgeç delikleri arasındaki mesafe 10 mm iken yüksek su sıcaklığı, yüksek hava kütlesi debisi ve yüksek su seviyesi en yüksek performans verdi. Ünitenin performansını artırmak için bir ara kabarcık yenileme aşaması ilave edildi. Bunun sonucu olarak, cihazın nemlendirme etkinliğinde önemli bir artış gözlenmiştir. Herhangi bir sıcaklık ve hava akış hızında en yüksek nemlendirme etkinliğini elde

etmek için kabarcık rejenerasyon aşamalarının sayısı sekiz olarak bulunmuştur. Sekiz kabarcık-rejenerasyon aşaması ile 40cm'lik su seviyesinde nemlendirme sürecinin etkinliği% 100 idi.

Güneş ünitesinin deneyleri Kuzey Kıbrıs hava koşullarında yürütülmüştür. Çıkış havası doymuş ve sıcaklığı kollektördeki suyun sıcaklığına ulaştığı bulunmuştur. Ayrıca, nemlendirme işleminin verimliliğinin maksimize olduğu bulundu. Sistem günde 15 kg/m2 taze su üretme yeteneğine sahiptir. Sistemin normalize üretimi farklı pilot ve ticari ölçekli güneş enerjisi sistemleri ile karşılaştırıldı. Mevcut tasarımın üstün performansa sahip olduğu bulunmuştur.

Anahtar kelimeler: Güneş su damıtma, Nemlendirme-nemalma arıtma, kabarcık rejerasyonu, ısı ve kütle transferi, kazanç-verim oranı

This thesis work is dedicated to my deceased father, Tawfeeq, whom I miss very much. I am highly indebted to him, for his guidance, blessings, constant backing, and for providing the necessary support in completing this work.

I also dedicate this work to my caring mother, Wafa, and would like to express my gratitude towards her for her kind encouragement and continuous support. God bless you.

Finally, I dedicate this work to my steadfast loving wife, Mai, for her patience and motivation which helped me during the challenges of my Ph.D. study. I am truly thankful for having you in my life.

ACKNOWLEDGMENT

I have taken great efforts in this work. However, it would not have been possible without the kind support and help of many individuals. I would like to extend my sincere thanks to all of them.

I would like to express my special gratitude and thanks to my supervisor Prof. Dr. Ugur Atikol and my Co-supervisor Prof. Dr. Fuat Egelioglu for giving me such attention and time. This thesis would not have been complete without their expert advice and unfailing patience.

My thanks and appreciations also go to all people who have willingly helped me out with their abilities and knowledge.

TABLE OF CONTENTS

ABSTRACT iii

ÖZ v

DEDICATION vii

ACKNOWLEDGMENT viii

LIST OF TABLES xiii

LIST OF FIGURES xiv

LIST OF ABBREVIATIONS xviii

LIST OF SYMBOLS xix

LIST OF SUBSCRIPTS xxi

1 INTRODUCTION 1

1.1 Background 1

1.2 Humidification-Dehumidification Desalination (HDD) 2

1.3 Scope and Objective of the Study 2

1.4 Organization of the Thesis 3

2 LITERATURE REVIEW 5

2.1 Humidification Dehumidification Desalination 5

2.1.1 Closed-Air, Open-Water, Water & Air-Heated (CA-OW-WAH) System .. 7

2.1.2 Closed-Air, Open-Water, Water-Heated (CA-OW-WH) System 8

2.1.3 Closed-Air, Open-Water, Air-Heated (CA-OW-AH) System..... 12

2.1.4 Closed-Water, Open-Air, Water & Air-Heated (CW-OA-WAH) System 16

2.1.5 Closed-Water, Open-Air, Water-Heated (CW-OA-WH) System 19

2.1.6 Batch -Water, Open-Air, Water-Heated (BW-OA-WH) System 20
2.2 Bubble Columns 24
2.2.1 Column Hydrodynamics and Flow Regimes 25
2.2.2 Dynamics of Gas Bubbles 33
2.2.3 Final remarks 41
3 METHODOLOGY 43
3.1 Experimental method 43
3.2 Performance Measures and Evaluations 44
3.2.1 Efficiency and Effectiveness 45
3.2.2 Gas Holdup 47
3.2.3 Gained Output Ratio 48
3.2.4 Normalized Production (NP) 49
3.2.4 Normalized Gain (NG) 49
3.3 Uncertainty Estimation 50
3.4 Optimization Method 50
4 UTILIZING THE BUBBLING TECHNIQUE FOR HUMIDIFICATION: AN EXPERIMENTAL ASSESSMENT 52
4.1 Design and experimental setup of the bubble column 52
4.1.1 Experimental setup 52
4.1.2 The humidification unit 53
4.1.3 Data acquisition 59
4.2 Experimental procedure 62
4.3 Flow rate measurement and superficial gas velocity 62
4.4 Results and discussion 64

4.4.1 The flow regime 64
4.4.2 Air temperature and humidity 65
4.4.3 Efficiency and effectiveness 70
4.5 The modified bubble column 75
4.5.1 Apparatus setup and procedure 78
4.5.2 Results and discussion 78
5 SOLAR HUMIDIFICATION UNIT 86
5.1 Solar Heating and Humidification 86
5.2 Test apparatus 88
5.2.1 The humidifier bed 89
5.2.2 Compressor and controllers 90
5.2.3 Data acquisition and measuring devices 90
5.3 Experimental procedure and data processing 91
5.3.1 Setup 1: The basic design 91
5.3.2 Setup 2 93
5.3.3 Setup 3 95
5.3.4 Data processing 95
5.4 Results and discussion 97
5.5 Final remarks 103
6 SOLAR HDD SYSTEM – THE COMPLETE SYSTEM 105
6.1 The humidifier design 105
6.2 Experimental setup 108
6.3 Experimental procedure 111
6.4 Results and discussion 111

6.4.1 Temperature and humidity changes 111
6.4.2 Productivity and performance measure 114
6.5 Final remarks 121
7 INNOVATION IMPLICATIONS IN THE DESIGN OF SOLAR HDD SYSTEMS 123
8 CONCLUSION 130
REFERENCES 132

LIST OF TABLES

Table 2.1. Comparison of available HDD systems in literature ……..……..…23

Table 4.1. Characteristics of bubble under different temperatures……..57

Table 4.2. The parameters under which the humidifier was tested……62

Table 4.3. Characteristics of the air flow……64

LIST OF FIGURES

Figure 2.1. Rain cycle 6

Figure 2.2. Typical CA-OW-WAH HDD cycle 8

Figure 2.3. Closed-Water, Open-Air, Water & Air-Heated (CW-OA-WAH) scheme 17

Figure 2.4. Modofoed Closed-Water, Open-Air, Water & Air-Heated cycle..... 18

Figure 2.5. Schematic diagram of typical bubble column 24

Figure 2.6. Flow regime map for air-water system at atmospheric pressure (Deckwer et al., 1980; Shah et al., 1982). (D_c is column diameter) 26

Figure 2.7. Experimental data on gas holdup in a 0.1 m diameter bubble column operating with the air-water system (Krishna and van Baten, 2003)..... 30

Figure 2.8. Various types of gas spargers used in bubble columns 33

Figure 2.9. Air bubble formation regime at the orifice (Heijnen and Van't Riet, 1984) 35

Figure 2.10. Shape regime map (Clift, 1978) 37

Figure 2.11. Numerical results and experimental observations of side by side coalescence between two identical bubbles (Krishna and van Baten, 2003)..... 40

Figure 2.12. Numerical results and experimental observations of in-line coalescence between two identical bubbles (Krishna and van Baten, 2003)..... 41

Figure 3.1. humidification by bubbling 44

Figure 4.1. Experimental setup 53

Figure 4.2. The humidification unit 54

Figure 4.3. Moisture content of fully saturated air at different pressures and temperatures (produced using EES program) 56
Figure 4.4. The sparger device 58
Figure 4.5. Configurations of the sparger's lid 59
Figure 4.6. Air compressor and controlling unit 61
Figure 4.7. Outlet air temperatures with respect to water temperature for different flow rates 66
Figure 4.8. Outlet air relative humidity with respect to water temperatures for different flow rates 68
Figure 4.9 Absolute humidity changes with respect to water temperatures 69
Figure 4.10. Humidifier efficiency vs. water temperature 72
Figure 4.11. Humidification effectiveness vs. water temperature 73
Figure 4.12 performance of the humidification unit, in terms of absolute humidity difference under different parameters 74
Figure 4.13. a) the perforated sieve, b) the modified humidifier with 8 sieves configuration. 76
Figure 4.14. The modified humidifier testing unit 77
Figure 4.15. Temperature variation of the outlet air with bubbles regeneration 79
Figure 4.16. Thermal efficiency of the humidification unit with bubbles regeneration 81
Figure 4.17. Effectiveness of the humidification unit with bubbles regeneration 82
Figure 4.18. Absolute humidity differences between the outlet and the inlet points of the humidifying unit 84

Figure 4.19. Comparison of the absolute humidity difference, between the inlet and outlet of the humidifier, of the best performed configuration of the basic bubble column and the modified column 85
Figure 5.1. The proposed humidifier schematic diagram 88
Figure 5.2. Schematic diagram of the experimental setup 89
Figure 5.3. The cross-sectional view of Setup 1 showing the process 92
Figure 5.4. A stack of Inverted sieves (heat absorber and bubble regenerator) 93
Figure 5.5. The cross-sectional view of Setup 2, where sieves are used to regenerate bubbles 94
Figure 5.6. The inlet and outlet relative humidity of air for different setups at a flow rate of 8.2 kg/h. a) setup 1, b) setup 2, c) setup 3 98
Figure 5.7. The effect of the improved design on the outlet temperature of air for air flow rate of 8.2 kg/h. a) setup 1, b) setup 2, c) setup 3 99
Figure 5.8. The efficiency and effectiveness of the humidification process. a) Setup 1, b) Setup 2, c) Setup 3 101
Figure 5.9. The effect of the improved design on the productivity of the system ... 102
Figure. 5.10. Effectiveness of the three setups plotted as a function of the normalized gain 103
Figure 6.1. A view of the humidification unit a) from inside showing the tray and the cover, and b) showing the bubble regeneration sieves 107
Figure 6.2. Comparison of a) the original design and b) the improved design 108
Figure 6.3. Schematic diagram of the experimental setup 109
Figure 6.4. Photo showing the humidifier and the experimental setup 110

Figure 6.5. Hourly change in temperature due to the change in solar radiation and heat extraction 113
Figure 6.6. Hourly changes in humidity due to humidification process 113
Figure 6.7. Hourly freshwater production for different flow rates 115
Figure 6.8. Cumulative freshwater production for different flow rates 116
Figure 6.9. Total freshwater production for different flow rates 117
Figure 6.10. Comparison of gas holdup with different suggested formulas 118
Figure 6.11. Comparison of gas holdup with different experimental results 119
Figure 6.12. GOR for different flow rates 120
Figure 7.1. Proposed flow chart of a HDD controller subroutine that insures maximum productivity 129

LIST OF ABBREVIATIONS

AH	Air heated
Bo	Bond number
CA	Closed air
CW	Closed water
GOR	Gain-output ratio
HDD	Humidification-dehumidification desalination
MED	Multiple-effect distillation
Mo	Morton number
MSF	Multi-stage flash
MSHH	Multi-stages heating and humidifying
NG	Normalized Gain
NP	Normalized Production
OA	Open air
OW	Open water
WAH	Water and air heated
WH	Water heated

LIST OF SYMBOLS

A	Area, m^2
d	Diameter, mm
I	Solar intensity, W/m^2
K	Mass transfer coefficient
ṁ	Mass flow rate (air or water), kg/h
NG	Normalized gain, $k.m^2/W$
P	Atmospheric pressure, kPa
PR	Productivity/moisture increment, kg_w/h
Pg	Saturated vapor pressure, kPa
T	Temperature, C°
U	Uncertainty
V	Volume, m^3
$\dot{V}$	Volume flow rate of air, m^3/h
α	Constant
Δ	Difference
η	Efficiency of the humidification process, %
σ	Surface tension, N/m
ϵ	Effectiveness of the humidification process, %
ε	Holdup ratio of a fluid in a mixture, %
ρ	Density, kg/m^3
μ	Dynamic viscosity, $N.s/m^2$

ω	Absolute humidity, kg water vapor/kg dry air
$\emptyset$	Relative humidity, %

LIST OF SUBSCRIPTS

a	Air
av	Average
b	Bubble
cr	Cross-section
G	Gas
h	Enthalpy
H	Humidifier
in	Inlet
J	Defined by Jaber and Webb
L	Liquid
o	Orifice
out	Outlet
PR	Product
sat	Saturated, saturation
T	Thermal
t	Terminal
Tot	Total
v	Vapor
w	Water

Chapter 1

1 INTRODUCTION

1.1 Background

The two main issues challenging the world today and in the future are the shortage of both energy and fresh water. Water scarcity threatens about one fourth of humankind. According to the UNESCO freshwater availability will be increasingly strained over a relatively short time period, and more than 40% of the global population is projected to be living in areas of severe water stress through 2050 (UNESCO, 2014).

Numerous desalination methods have been suggested during the last three decades, due to growing demand for fresh water by the rising human population. With the exponential growth in industry, techniques used in desalination have advanced too. Most of these systems, especially the high productive ones, rely highly on high quality energy (i.e. electricity or fossil fuels) for powering the desalination process. Unfortunately high quality energy is not available everywhere or to everybody on our plant.

At present Reverse Osmosis and Multi Stage Flash systems are the dominant large scale desalination systems. Reverse osmosis and Multi Stage Flash are high energy demanding desalination plants. On the other hand, medium and small scale

desalination techniques are competing for the lead in terms of independency, reliability, and desalination cost. Though less efficient than large scale plants, the importance of the small scale plants manifests itself in the rural areas, countryside and remote places, where energy availability is seldom. In such places solar stills can be utilized to provide freshwater. Solar stills were the first devices to incorporate renewable energy to produce freshwater. However, under the most favorable conditions of high solar radiation and low water depth, the solar still efficiency does not exceed the 50% (Cooper, 1973) with a freshwater production of about 4 L/m^2 day for a standalone unit. This is due to the high loss of the latent heat upon condensation from the glass cover.

1.2 Humidification-Dehumidification Desalination (HDD)

HDD techniques were recently introduced as economically attractive techniques for small scale desalination systems. HDD systems like solar stills mimic the nature in producing freshwater. The evaporation of water is enhanced in different ways to humidify dry air, then the vapor is extracted from the carrier air in a dehumidification process that takes place in a condenser. Coupling a HDD system with solar energy should lead to increase in the overall efficiency of the process. Many promising techniques of humidification and dehumidification of air were introduced in the last two decades. HDD systems are witnessing continuous improvement and modifications that not only increase their productivity, but also decrease their energy consumption.

1.3 Scope and Objective of the Study

In previous studies researchers have been trying to increase the performance of solar HDD systems by suggesting alternative cycles. The cycles varied between open to

close, water heated and/or air heated. However, the increasing foot print of such systems overweighs the slight gain in the accomplished performance. This study aims at improving the HDD cycle performance while minimizing the space needed for the system.

The main objective of this work is to investigate experimentally the possibility of employing a humidification technique, namely humidification by bubbling, in a solar HDD process. Moreover, it is aimed to examine the possibility of integrating some of the processes of the HDD cycle in one process in an attempt to decrease the foot print of such systems. The optimum working conditions are to be identified by conducting a thorough and comprehensive thermodynamic analysis and efficiency assessment of the humidification unit. Performance and productivity of the proposed compact humidification unit are the main key points to be studied in this research.

1.4 Organization of the Thesis

The upcoming chapters in this thesis are as follows:

Chapter 2: The first part presents a comprehensive literature review of HDD systems. The second part investigates the bubbling technique and its use in industry.

Chapter 3: The methodology, mainly the performance measures, is presented in this chapter.

Chapter 4: The laboratory based humidifier unit is presented in this chapter. The unit is tested under different configurations, working conditions and the results were presented.

Chapter 5: The solar energy based humidification unit and its performance were presented.

Chapter 6: Experimental investigation of the completed pilot HDD system was presented.

Chapter 7: This chapter discusses innovation implications for solar HDD system design.

Chapter 8: This chapter sums up the whole study by presenting some concluding remarks.

Chapter 2

2 LITERATURE REVIEW

2.1 Humidification Dehumidification Desalination

One of the most attractive small scale desalination techniques is the HDD system. This process resembles the rain cycle in the nature (Fig. 2.1). In this cycle, solar energy heats the oceans, stimulating surface water to evaporate. Evaporated water then mixes with the air mass above the surface in a similar manner to the humidification process. The humidified air then rises and forms the clouds. Eventually the clouds are dehumidified as condensation takes place when they come into contact with a cooler area in the atmosphere. The condensed water falls as rain to complete the cycle. The rain water is pure water by nature. This cycle has inspired us to create a man-made version and deploy it to desalinate water in a system called humidification-dehumidification desalination (HDD) system.

Several works have been conducted on this kind of desalination method using different setups and systems. The functioning principle of the HDD systems were reviewed by several researchers (Bourouni et al., 2001; Narayan et al., 2010; Parekh et al., 2004). They provided comprehensive overviews of solar-driven HDD with their various classifications.

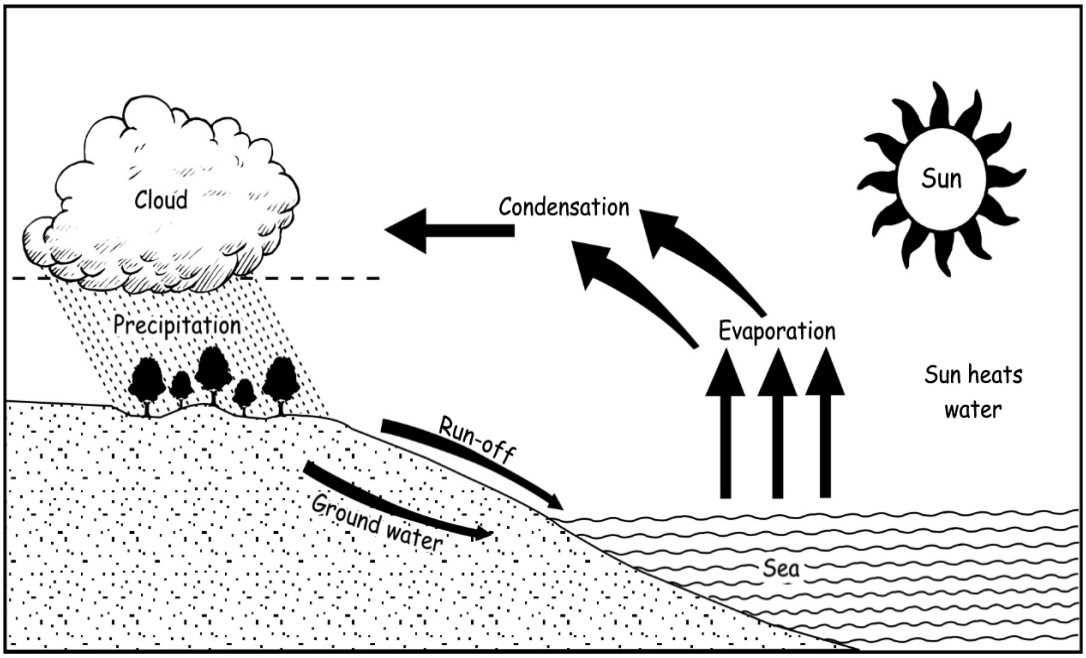

Figure 2.1. Rain cycle

These systems can be set up as open or closed cycle systems with heated air or/and heated water options:

- Closed-air, open-water, water & air-heated (CA-OW-WAH) system
- Closed-air, open-water, water-heated (CA-OW-WH) system
- Closed-air, open-water, air-heated (CA-OW-AH) system
- Closed-water, open-air, water & air-heated (CW-OA-WAH) system
- Closed-water, open-air, water-heated (CW-OA-WH) system
- Still-water, open-air, water-heated (SW-OA-WH) system

The technique is versatile but the main idea is to bring the dry air into contact with water in an evaporator to facilitate its humidification before passing it through a condenser in which air is dehumidified to give fresh water. Following are the details of the various techniques found in literature.

2.1.1 Closed-Air, Open-Water, Water & Air-Heated (CA-OW-WAH) System

Figure 2.2 is a schematic view of a general CA-OW-WAH HDD system, showing diagrammatically the water and air streams and the processes of heating, evaporation, and condensation. Generally air is humidified in the evaporator before fresh water extracted in the condenser. In this arrangement water is heated in solar water collector (or any other source of heat) before entering to the humidifier. A counter air flow is preheated in a solar air collector before it comes into direct contact with water in the evaporator. Heat and mass transfer take place during this direct contact which ideally results in hot saturated air at the humidifier exist. The temperature of air stream exiting the humidifier could be as high as the highest temperatures of the two steams. The hot humid air then is fed to heat exchanger to be cooled, and thus dehumidified, by the seawater stream. This indirect contact process between seawater and the humid air results in cooling and dehumidifying the humid air. The latent heat resulted from condensation of vapor on the heat exchanger's walls is transferred to the cooling seawater resulting in preheating the water stream before it is fed to the solar heater. Fresh water is collected from the dehumidifier upon the condensation process. The air circulation is cyclic within system. Unlike air, water is not circulated in the system and exits the humidifier as brine with higher salt concentration as a result of vapor extraction in the humidifier.

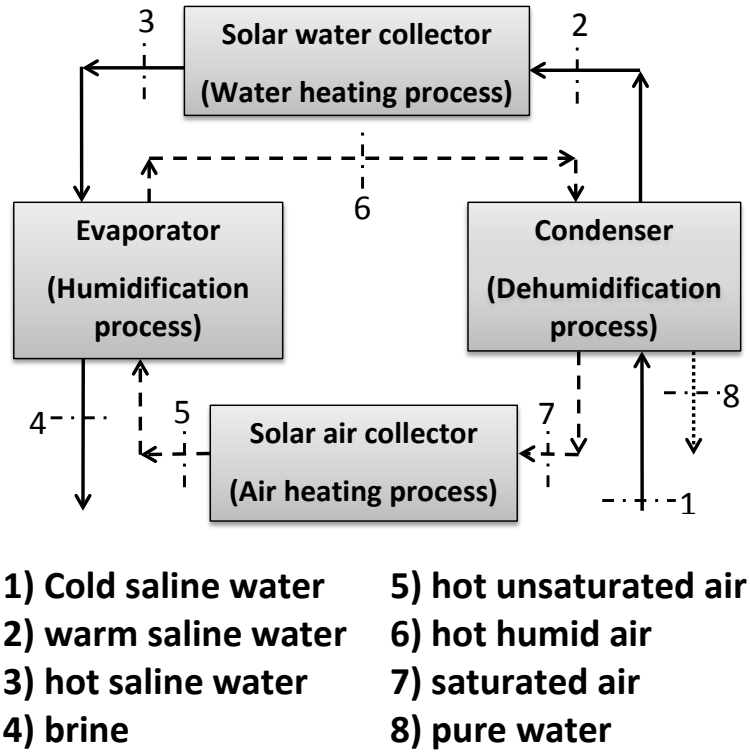

Figure 2.2. Typical CA-OW-WAH HDD cycle

This unique setup in which heating was applied to both of the streams was tackled by Nafey et al. (2004). They have presented an experimental investigation of HDD process using solar energy to heat both air and water streams. Water was heated using a 1 m wide and 2 m long solar concentrating collector. Circulating air was heated using a 0.5 m^2 flat air solar heater. They used canvas as packing material in the evaporator. The authors reported maximum fresh water production of 1.3 L/h, they reached a total of 8 L/day and indicated that at high air flow rate fresh water yield decreases.

2.1.2 Closed-Air, Open-Water, Water-Heated (CA-OW-WH) System

This cycle is similar to the CA-OW-WAH cycle except, the heating is applied to the water stream alone. Air stream heating process (i.e., process between 5 and 7) does not exist in this cycle. Instead air stream is fed directly after being cooled and

dehumidified in the condenser to the evaporator. Sensible and latent heat are transferred from the hot seawater stream to the air stream during the humidification process. As a result, air stream temperature depends extremely on its residence time in the humidifier. This cycle demands a sophisticated evaporator in order to enhance the heat and mass transfer for a better cycle efficiency.

Several studies have been done on this type of systems. These systems could be further classified in terms of the way air is circulated. Some of the researchers favored natural convection to drive the circulation of air in order to decrease the energy needed per unit of fresh water yield (Bacha et al., 2003; Garg et al., 2003; Müller-Holst, 2007). Usually these types of setups facilitate water storages to elongate operation hours, and thus increase the freshwater yield. Some other researchers preferred controlling the air flow rate by forcing the air stream to circulate mechanically for higher yield (Farid and Al-Hajaj, 1996; Younis et al., 1993). In order to compare the performances of both natural and forced convections systems Al-Hallaj et al. (1998) and Nawayseh et al. (1999) examined the two systems.

2.1.2.1 CA-OW-WH with natural convection

Bacha et al. (2003) utilized 6 m^2 of solar water heater with a water storage that runs at minimum temperature constraint. Hot water then fed to a humidifier bed which is packed with thorn trees. The cooling water for the humidifier (made up of polypropylene plates), was provided by brackish water from a local well. The system produced 19L/day with the thermal storage that elongated production period. They claimed the possibility to get the same amount of product without storage provided

the solar collector area was $7m^2$ instead of $6m^2$. They stated that the system performance is largely affected by the temperatures of water and air besides to the packing material which directly affect the mass transfer to the air stream. In addition, water and air flow rates played an important role in the system productivity.

Another pilot system that used natural convection for air circulation is found in (Garg et al., 2003). Water was heated in a $2m^2$ solar water collector in a system that has a thermal storage of 5 liters. A separate water stream that runs in the humidifier and the dehumidifier was preheated in the dehumidifier before it was fed to the thermal storage which allowed for partial latent heat recovery. The daily product was not available in the study. Instead condensate water was plotted with respect to the water temperature at the humidifier inlet. They reported a product of 1gr/s at water temperature of 45 °C increasing linearly to 2.2gr/s at 70 °C. Accordingly they concluded that the inlet water temperature has the highest effect on the fresh water product, and thus on the efficiency, of the system.

In an attempt to enhance the heat recovery of the system, Müller-Holst (2007) proposed the employment of the multi-effect concept in the HDD systems. In the system heat recovery was possible by extracting air from the humidifier at different stages and supplying the extracted air to the dehumidifier at corresponding points. The author claims that the temperature of the water at the dehumidifier outlet has reached to 75 °C as a result of the latent heat recovery alone. Additional heat was supplied to the water by employing a total of 38 m^2 solar water collectors before it was fed to the humidifier. Solar collectors have increased the water temperature to 80-90 °C. The system has a $2m^3$ of thermal storage tank thus, the process could run

24 hours (i.e., continuously). Hence, the fresh water yield of the system was reported to be 500L/day. Müller-Holst also emphasized the importance of the water inlet temperature to the humidifier.

2.1.2.2 CA-OW-WH with forced convection

Farid and Al-Hajaj (1996) presented a system in which air was forced to circulate through a humidifier that was packed by wooden shavings. Water was heated in a solar water collector with an aperture area of 1.9m^2. Dehumidification process was achieved by passing the saturated air in a multi-pass shell and tube heat exchanger. They claimed a 12L/m^2 freshwater yield from the system. Younis et al. (1993) used a solar pond to provide vapor to the air stream in a HDD system. The 1700m^2 solar pond acted as a solar heater as well as a thermal storage in the system. Air was forced to flow on the surface of the water of the pond to carry vapor to the condenser. Upon condensation, latent heat is recovered by the water stream in the condenser before it is fed to the solar pond. The authors indicated that the air flow rate has the major impact on system's productivity.

2.1.2.3 CA-OW-WH with natural and forced convection

Some researchers have tested the performance of HDD systems under both natural and forced air circulation. Al-Hallaj et al. (1998) compared the effect of air circulation mode in a system that utilizes a 2m^2 tubeless flat-plate type solar collector which heated water to 50-70 °C. The highest reported daily fresh water yield of the unit was 3.55L/m^2 during October 5th with expectation of being 8L/m^2 in summer time. They claimed that the production of the plants achieved maximum yield at an optimum value of water flow rate. Regarding to the air circulating mode, they found that at higher top temperature (i.e., at the humidifier exit) natural circulation was

advantageous. But at lower top temperature forced circulation gives better performance.

Nawayseh et al. (1999)worked on configurations and design aspects of the humidifier and the dehumidifier and compared their system with Al-Hallaj et al., system. The design changes they promote resulted in an increase in the production. The daily specific yield of fresh water was 6.2L/m^2. They observed that the effect of air flow rate on the production of freshwater was low and thus, they favored the natural circulation to the forced air circulation.

2.1.3 Closed-Air, Open-Water, Air-Heated (CA-OW-AH) System

Heating in this cycle is applied to the air stream alone. The top temperature in this system belongs to air stream at the humidifier inlet. Generally, air stream is heated in solar air collectors to a temperature as high as 90 °C. Water in this system could be preheated in the condenser before it is fed to the humidifier, though water temperature would be very low comparing to the air temperature at the humidifier's inlet. Upon direct contact of both streams air is cooled and humidified, ideally saturated. The major disadvantage of these systems is the big difference in temperatures between the two streams. Ideally, adiabatic saturation occurs at the outlet of the humidifier. But if the full saturation state of the air stream is reached at any point in the middle of the humidifier, with the continuous contact between the colder water stream and the air stream, condensation would take place starting from that point. Condensation of vapor in the humidifier hinders fresh water productivity and decreases the cycle efficiency.

Generally, air in air-heated systems circulates mechanically by means of blowers, air pumps, or compressors. Natural convection in these systems is reported to give poor results and thus none of the available studies favored it.

Single humidification chambers were used as well but the fresh water yield was low and didn't exceed, at their best, the production of solar stills (Orfi et al., 2004; Yamali and Solmus, 2008). Both of the researchers suggested water heating along with solar air heating in order to enhance the evaporation process to increase productivity.

The first breakthrough came from Chafik (2003a, b, 2004) who introduced the concept of Multi-effect-heating-humidification process to these kind of air heated HDD systems. Based on this concept, other researchers (Ben Amara et al., 2004; Houcine et al., 2006) have built their own systems. In literature this concept is sometimes referred to as multiple effect heating and humidification or multi stage heating and humidifying systems. In order to differentiate between the well-known Multiple-effect distillation (MED) and Multi-stage flash distillation (MSF) systems it is convenient to state out the difference among them at this stage.

As an evolution of the simple distillation process, MED is one of the first developed thermal processes that have been used for freshwater produce. It encompasses successive chambers in which seawater is being heated and allowed to evaporate. Energy is given from an outer source to heat water at the first chamber. Boiling water at this chamber releases vapor that is fed to the next chamber for condensation by means of indirect contact with the water in that chamber. Water in the next chamber

is heated by the effect of the latent heat of condensation that is transferred to it at that stage. By this effect, water temperature increases and releases vapor (or steam) to the next chamber and this process continues as many as the chambers in the system.

MSF distillation is known for its simplicity and high productivity, the reason why it dominates almost 85% of the commercially available distillation systems. Similar to MED, MSF consists of many successive chambers or stages in its case. MED uses the heat directly for water evaporation. On the other hand, MSF uses the heat at each stage to preheat the water by the latent heat of condensation before it is fed to the boiler for further heating. The boiling water is then fed backwardly to the stages at decreasing pressures and so water partially flashes.

In the case of multiple stages heating and humidifying system heat is added to air stream before it is fed to the next chamber. At each air heater temperature is increased and thus the vapor carrying capacity of air increases. Consequently, at each humidifying chamber the absolute humidity is increased. Since there is no heat addition in the humidifier, the temperature of air at the humidifier decreases which makes it important to be reheated before fed to the next chamber.

For that, it is more convenient to present the concept suggested by Chafik (2004) as a Multi-stages heating and humidifying (MSHH) process for HDD systems. It is important to note that in the MSHH case, air is a non-condensable fluid that acts as energy carrier in the system. However in both systems the presence of non-condensable gas is undesirable as it affects the controlled pressure and the heat transfer coefficient.

2.1.3.1 Single-stage CA-OW-AH with forced convection

An experimental and theoretical study of a single-stage CA-OW-AH with forced convection was presented by Orfi et al.(2004). In this study, the authors utilized a $2m^2$ of solar heater for air heating but simulated water heating by applying water heater. Heat recovery was present in the system and they suggested pre-heating of the water before it was fed to the humidifier. The humidifier was equipped with spongy material besides to wetting many vertical plates, through which air stream passes, by capillary effect. Productivity of the system is reported to be maximized under some optimum water and air mass flow rates.

2.1.3.2 Multi-stages heating and humidifying (MSHH) CA-OW-AH with forced convection

This system was first introduced by Chafik (2003a) followed by application for the process in two more publications (Chafik, 2003b, 2004) in which he used solar collectors to heat air stream. The collectors were 15 parallel, four-fold-web-plate type 2.94 m^2 each. The heating and humidification processes were broken to four stages. Two types of humidifiers were tested; a) pad humidifier that contains cassette made of corrugated cellulosic material, and b) a 4m long U-tube spray chamber humidifier. The author expected 400L/day of freshwater yield from the system. He simulated a system that is able to feed a small community with 10m3/day of freshwater. Although the idea is promising, it was reported that the initial investment of the system was too high and that the air heaters made up 40% of the total cost.

Following Chafik's idea of MSHH, Ben-Amara et al. (2004) and Houcine et al. (2006) have used the same equipment but with different solar heaters and heating

configurations. Ben-Amara et al., (2004) constructed a one stage heating and humidifying system. The results from this system were used to simulate eight heating and humidifying stages. The results show occurrence of adiabatic humidification after the fifth stage. They reported a huge effect of wind velocity on the whole process. Based on these results, Houcine et al.(2006) used 5 heating and humidifying stages in their configuration. The collection areas of the first and second stages are 44.1m^2 each. The third and fourth stages were 45m^2 of area each. The fifth stage was 27m^2 of solar collection area. They reported that the freshwater production strongly depends on the climatic conditions and especially on the solar insolation. For six months of testing period, from March to August, the highest monthly average freshwater production was 316 L/day in August.

2.1.4 Closed-Water, Open-Air, Water & Air-Heated (CW-OA-WAH) System

Similar to any HDD system, air in CWOAWAH systems is humidified in a humidifier upon the direct contact with water. Then it is dehumidified in a condenser to produce freshwater. In CWOAWAH systems however, air does not circulate in the system. Instead water is the circulating fluid (Fig. 2.3). Air heating take place before it is fed to the humidifier. Air and water streams come in to an indirect contact in the dehumidifier were freshwater was extracted from the air stream. Condensation takes place in the dehumidifier provided that the temperature of the water stream is lower than the temperature of the air stream. If the cooling effect of the humidification process does not decrease the temperature of the water stream sufficiently, the dehumidifier's inlet water temperature would be high and condensation would be limited. Theoretically, in order to overcome this problem, the enthalpy flow rate of the cycle should be carefully controlled and, more importantly, the humidifier should

be highly efficient to result in better water cooling. Though, there is no success story for this cycle in its present scheme. The cycle was modified to allow the separation of the closed hot water cycle and the cooling cycle (see Fig. 2.4) when some of the researchers succeeded in fresh water production.

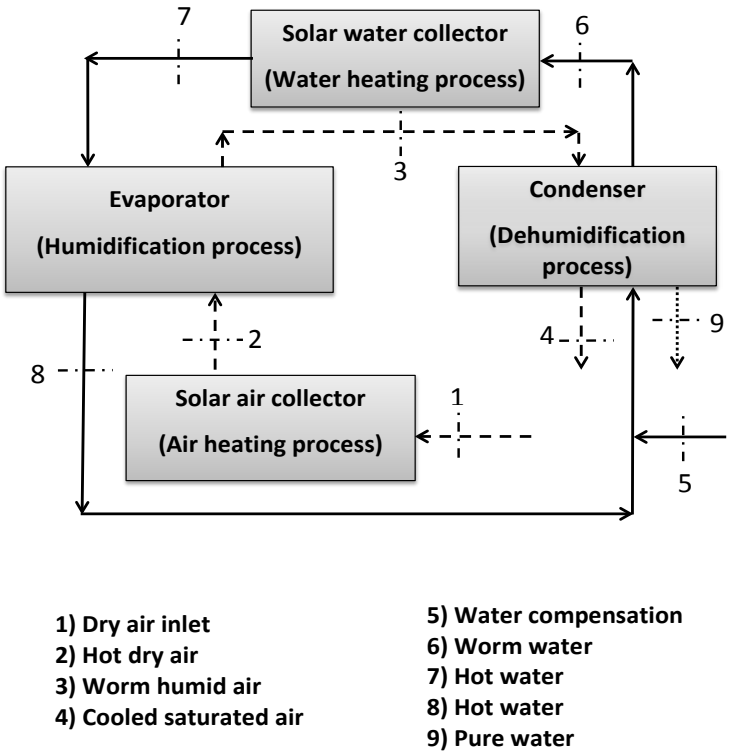

Figure 2.3. Closed-Water, Open-Air, Water & Air-Heated (CW-OA-WAH) scheme

Yamali and Solmus (2008) have built a single stage heating and humidifying system utilizing solar energy to heat air in a 50cmx100cm double-pass flat-plate solar air collector. The preheated air is then passed to a pad humidifier which consisted of four pads in series. The pads that form the wetted surface are made of plastic material. The water cooling system circulating in the humidifier was separate. The plant produced maximum of 4 L/day with air heating alone. When extra energy was

provided to circulating water from outer supply (evacuated tubular solar collector), the freshwater production has increased to 10 kg/day.

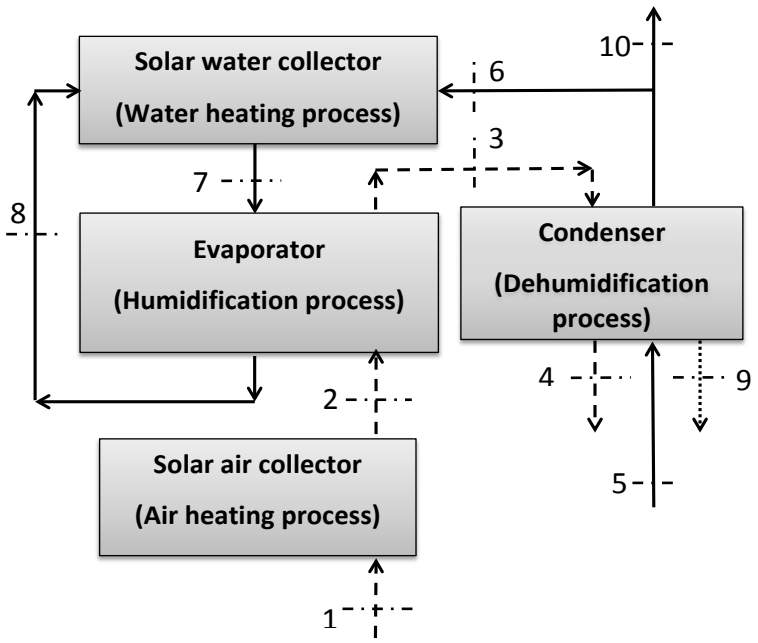

Figure 2.4. Modofoed Closed-Water, Open-Air, Water & Air-Heated cycle

Water heated systems suffer another problem regarding to the effect of water temperature on the system's parts and equipment. Working at high temperatures can cause fouling and corrosion of tubes especially if the fluid is seawater (Yuan et al., 2011). Yuan et al. (2011) performed an experimental study on a 1000 L/day solar HDD system aiming to keep the water temperature below 50°C. They arrayed 72 solar air heaters with total collection area of 100 m^2 and a total of 14 m^2 of solar water heating arrangement for water heating were used. On a daily basis the

production of the system was 8.8 L/m^2. The cooling water was provided from a water pond.

2.1.5 Closed-Water, Open-Air, Water-Heated (CW-OA-WH) System

In this system, air heating represented by process 1-2 from the schemes in Fig. 2.3 and Fig. 2.4 were eliminated. Heat is applied only to water. If air heaters were not used in the closed-water cycles, the scheme in Fig. 2.3 would have been thermodynamically more logical and demands less control. Water coming out from the humidifier could be potentially cooled by the air stream which enters the humidifier at the ambient temperature. The water could then circulate in the dehumidifier and would have the ability to cool the air stream. Though, in most of the researches, the scheme of Fig. 2.4 was favored.

Al-Enzi et al. (2006) tested a system that heats the water to top temperatures of 35-45 °C. A separate cooling cycle for the condenser was considered. Ambient air was forced in a humidifier which was packed with cylindrical-shaped plastic pieces. The humid air was fed to the condenser for water extraction. As being open-air cycle, air was dumped to the ambient after the condensation process. The cooled water at the humidifier water outlet is then fed to a heater (solar or other type) to gain energy before it circulates back in to the humidifier. The variation of production under different air and water flow rates, cooling water and hot water temperatures were studied. Heat and mass flow coefficients have been developed under different parameters. Their conclusion was that the higher the hot water temperature is, the higher the fresh water production. They reported that the high air flow rate, the low

hot water flow rate, and the low cooling water temperature enhance the freshwater production as well.

Likewise, Dai and Zhang (2000) and Dai et al. (2002) implemented the scheme in Fig 2.4 without the air heating process. Water vapor with a high temperature and pressure from a boiler was used as the heat resource instead of solar energy in order to acquire the test results more rapidly. The humidifier was packed with honeycomb paper. The air was forced to circulate in the humidifier then the dehumidifier before being damped to the ambient. Some of the water from the condenser outlet was fed to the hot water storage tank to compensate for the water loss upon evaporation and provide heat recovery. Different parameters like the hot water and air flow rates, hot water and air temperatures, and cooling water temperature and flow rate were studied. As in the previous study, the freshwater product was found to be strongly dependent on the humidifier inlet temperature. They have reported that there is an optimal air velocity at which the fresh water production was peaked.

2.1.6 Batch -Water, Open-Air, Water-Heated (BW-OA-WH) System

In BW-OA-WH systems water is dispersed in the bottom of a container that is filled with water. Humidification process takes place in the container by direct contact between air stream and the still water. This technique is widely used by chemists to diffuse gasses into liquid by dispersion of the gas in a container (usually referred to as column reactor) filled with liquid. The dispersion process is aided with a sparger that contains many holes and breaks the air stream into bubbles in order to increase the gas-liquid contact area. The spargers used in such systems could be perforated plates or manufactured by using porous material. The first attempt to use this

technique in HDD systems was made by El-Agouz and Abugderah (2008) and El-Agouz (2010). Experimental investigations have been conducted to test the influence of some operating conditions on the humidification process (El-Agouz and Abugderah, 2008). The evaporator chamber was made of steel with 50cm x 25cmm square cross section and 70cm height and was filled with water at different heights. Water was heated by an electrical heating element, Air dispersion was made by the aid of pipe with 32 drilled holes. Operating conditions such as water temperature in the humidifier, water height, air velocity and the inlet air temperature to evaporator chamber that could affect the humidification efficiency were studied. It was reported that, the vapor content difference and the humidification efficiency of the system was strongly affected by the saline water temperature in the evaporator chamber. Increasing water height in the humidifier and air mass flow rate resulted in an increased productivity as well. The humidifier inlet air temperature however, was found to have a negligible effect on the vapor content and thus on productivity.

After coupling such evaporator with a condenser to form a HDD system, El-Agouz (2010) reported fresh water production of 8.22 kg/h at water temperature of 75 °C.

In this section, different types of HDD systems available in literature were reviewed. A related comparison can be found in Table 2.1. The last type, which is the bubbling technique (BW-OA-WH), is the least studied one. The technique is the latest to be proposed for use in the HDD systems. In this study bubbling technique was analyzed and examined for its viability to replace some less efficient techniques used in HDD systems. The next section is devoted to give a better understanding of the bubbling

technique that is already in use for chemical diffusion of gas into liquid in a device called a bubble column or a column reactor.

Table 2.1. Comparison between available HDD systems in literature

Author	Closed Water	Closed Air	Water Heater	Air Heater	Evaporator	Production
Nafey et al. (2004)	✓	✓	2 m^2 concentrating collector	0.5 m^2 flat air solar heater	canvas as packing material	8 L/day
Bacha et al. (2003)	-	✓	6 m^2	-	packed polypropylene plates	19 L/day
Grang et al. (2003)	-	✓	2m^2	-	Multi stage extraction	2.2gr/s at water temperature of 70 °C
Müller-Holst (2007)	-	✓	38 m^2	-		500L/day (running 24)
Farid and Al-Hajaj (1996)	-	✓	1.9m^2	-	packed by wooden shavings	12L/day.m^2
Younis et al. (1993)		✓			1700m^2 solar pond	
Al-Hallaj et al. (1998)	-	✓	Tubeless flat plate 2m^2	-		3.55 L/day.m^2
Nawayseh et al. (1999)	-	✓				6.2 L/day.m^2
Orfi et al. (2004)		✓	Electrical water heater	2m^2		
Chafik (2004)	-	✓	-	15 collectors 2.94 m^2 each	Multistage humidifier	400 L/day Expected
Houcine et al. (2006)	-	✓	-	205.2 m^2 total of five stages	Multistage pad humidifier	316 L/day
Yamali and Solmus (2008)	✓	-	Evacuated tube collector	0.5 m^2 double pass flat plate	Made of four plastic pads in series	a)Air heated: 4 L/day b)Both air and water heated : 10 L/day
Yuan et al. (2011)	✓	-	14 m^2	100 m^2 evacuated tubes		8.8 L/day.m^2

2.2 Bubble Columns

Bubble columns are two-phase gas-liquid systems in which gas is dispersed into a liquid in a vertical column. The gas which is broken into bubbles travels upward by the buoyant force. Generally, the liquid flow can be co-current, counter current, or in batch mode with respect to the gas flow. Bubble columns offer numerous advantages when used as air humidifiers (Fig. 2.5). Advanced heat and mass transfer characteristics perhaps the best advantage of these columns besides their being easy to operate with no moving parts. This means that they are effective, cheap to operate, and offer low operating and maintenance coast.

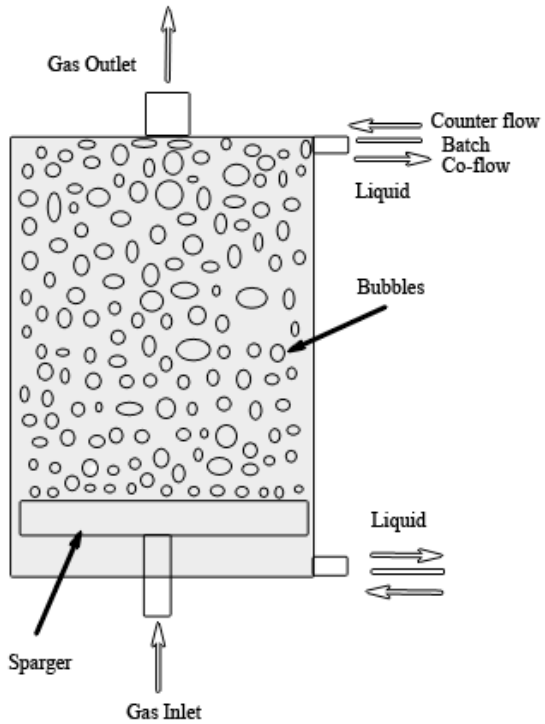

Figure 2.5. Schematic diagram of typical bubble column

Geometry of the column, operating conditions and design, are among the various factors that influences the hydrodynamics of the bubble columns and thus the mass

and heat transfer characteristics. To comprehend the hydrodynamics of the bubble columns we need to understand the flow regimes under which air bubbles are travelling. And thus, we would appreciate the influence of different regimes on heat and mass transfer to the bubbles.

2.2.1 Column Hydrodynamics and Flow Regimes

The hydrodynamics of two-phase bubble columns depend strongly on the flow regime. Despite the ubiquity of the topic in literature, no flow regime map is available that covers a wide range of industrial conditions (Urseanu, 2000). Nevertheless, there are three flow patterns that prevail in these bubble columns in literature (Deckwer et al., 1980; Shah et al., 1982; Wallis, 1969): 1) homogeneous flow; 2) heterogeneous flow; and 3) slug flow regimes (Fig 2.6). Since formation of these regimes depends on many parameters, the boundaries between them are not exact. Between each of these regimes there is a transition region. In these regions the experimental setup and operating parameters decide which of the regimes prevail. In the homogeneous regime, which is known as bubbly flow as well, there is a homogeneous distribution of small gas bubbles. Bubble rising velocity is usually low with limited interaction among the bubbles. As the gas flow rate is increased, the bubbles presence density increases in the liquid. And thus there is more interaction among bubbles. At this stage bubbles coalescence and break up is observed and the regime transition region is started. Upon increasing coalescence more of the larger bubbles are created. The larger gas bubbles move in a plug flow, creating large eddies, swirls, and result in back mixing and circulation as well. This is the heterogeneous flow, or churn-turbulent flow, regime which is observed in large diameter columns. However, in small diameter columns, as the gas flow rate

increase, bubbles coalescence result in bubbles with diameters near to that of the column itself. These bubbles are called slugs and they are the indicator of regime transition to the slug flow regime. As seen in Fig. 2.6, gas velocity plays a key role in defining the type of flow regime.

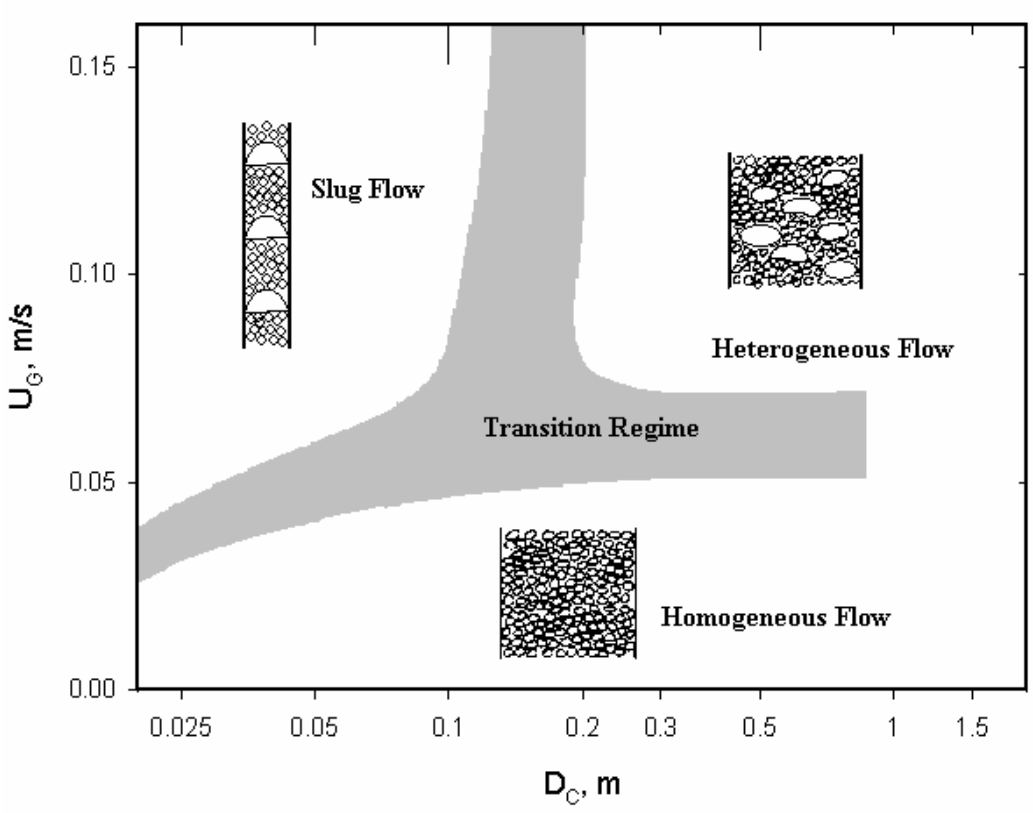

Figure 2.6. Flow regime map for air-water system at atmospheric pressure (Deckwer et al., 1980; Shah et al., 1982). (D_c is column diameter)

2.2.1.1 Gas Velocity

Gas velocity is directly connected to the gas mass flow rate in these systems. However, different studies are available in literature which deal with two-phase flow, test columns with different diameters. If the physical properties of those columns were not taken into account, comparison of results would be futile. If gases with

same flow rates were passed in two different columns with different diameters the flow regimes would vary for each of them. Therefore, normalization of the flow rate is crucial in flow regime comparisons. The normalized flow of gas is called the superficial gas velocity. The superficial gas velocity, in engineering and chemistry of multiphase flows, is a hypothetical fluid velocity calculated as if the given phase or fluid were the only one flowing or present in a column with a given cross sectional area. Other phases or particles present in the column are disregarded. It is a normalized velocity which gives idea of the volume flow rate of one phase through a given cross section area in terms of velocity. Superficial gas velocity is expressed as:

$$U_G = \frac{\dot{V}}{A_{cr}} \tag{2.1}$$

Where, $\dot{V}$ is the volume flow rate of air and A_{cr} is the horizontal cross sectional area of the humidifier. As expected for the same volume flow rate the superficial velocity increases with decreasing cross sectional area. Superficial gas velocity has a unit of (m/s).

As the gas flow rate increase, and thus the superficial gas velocity, the size of bubbles starts to increase decreasing the distance between the adjacent bubbles. This increases the possibility of coalescence and thus changes the flow regime to heterogeneous. In this regime ascending bubbles become irregular and the flow becomes rather turbulent. As the flow rate of the dispersed gas increases, the volume fraction of the gas, known as the gas holdup, in the liquid increases. This is indication of better heat and mass transfer to the gas stream.

2.2.1.2 Gas Holdup

Gas holdup ε_G has collected a high interest in literature by chemists as it serves a measure of mass transfer efficiency in bubble columns. In bubble columns of two-phase systems, the total volume, V_{Tot}, is given as:

$$V_{Tot} = V_G + V_L \tag{2.2}$$

Where V_G is the gas volume and V_L is the liquid volume in the bubble column. The gas holdup is defined as the volume fraction occupied by gas in the bubble column:

$$\varepsilon_G = \frac{V_G}{V_{Tot}} \tag{2.3}$$

Both analytical and experimental investigations suggested numerous relationships between mass transfer coefficients, at both the liquid side K_L and the gas side K_G, and ε_G. K_G is a useful parameter for system mass transfer characterization and predictive modelling. K_G relations, which are the main interest, are rather simplified than K_L relations. K_G relations are usually linear with a proportional factor α:

$$K_G = \alpha\varepsilon_G \tag{2.4}$$

Where α depends on column design and liquid medium. From the relation it is recognized that the higher the gas holdup ability of a system is, the higher the mass transfer coefficient and thus the higher the mass transfer efficiency would be. Chaumat et al.(2005), Krishna and Ellenberger (1996) , and Vandu and Krishna (2004) used α between 0.1 and 0.5 s^{-1}. Some other studies claimed no dependency of the superficial gas velocity and that K_G has a power relation with ε_G (Elgozali et al., 2002). It is important to mention that the effect of temperature of gas and liquid in such devices on the relations above was not studied.

2.2.1.2.1 Effect of the superficial gas velocity on the gas holdup

Gas holdup ability of bubble columns was studied both analytically and experimentally by many researchers. The majority of the studies concentrated on the relationship between gas holdup ability and the superficial gas velocity of the gas in the system. Most of these studies have shown positive effect of the superficial gas velocity on the gas holdup. Some researchers (Hikita et al., 1980; Kumar et al., 1976; Reilly et al., 1986) have suggested relatively complex relation to calculate ε_G analytically. On the other hand some other researchers (Camarasa et al., 1999a; Chaumat et al., 2005; Moshtari, 1999) have studied the gas holdup experimentally. These researchers have used the pressure difference method (but using different techniques) to measure the average gas holdup value. There are more advanced techniques to measure gas holdup including particle image velocimetry, and gamma-ray densitometry, and gamma-ray and X-ray attenuation together with computer tomography are some of them (Wu et al., 2001).

The simplest form of the relation between gas holdup and superficial gas velocity is best defined by a power-law expression as follows (Winterbottom, 1993):

$$\varepsilon_G \propto U_G^n \tag{2.5}$$

Where *n* is an exponent that depends on the flow regime. In the homogeneous flow regime, where there are low superficial gas velocities, the exponent *n* is reported to be in the range of 0.7-1.2 (Deckwer et al., 1980; Shah et al., 1982). Thus the holdup increases sharply with the increase in superficial velocity. When the transition to heterogeneous flow occurs, the more none linear, but gentler, increase of gas holdup is observed as the superficial velocity was increased. The exponent *n* in this region

was reported to be in the range of 0.4-0.7(Deckwer et al., 1980; Shah et al., 1982). The range of the exponent n is largely affected by the operating variables, the design and size of bubble column. Krishna et al. (Krishna and van Baten, 2003)presented a map of the gas holdup with respect to superficial gas velocity for a bubble column with 0.1 m diameter (Fig. 2.7).

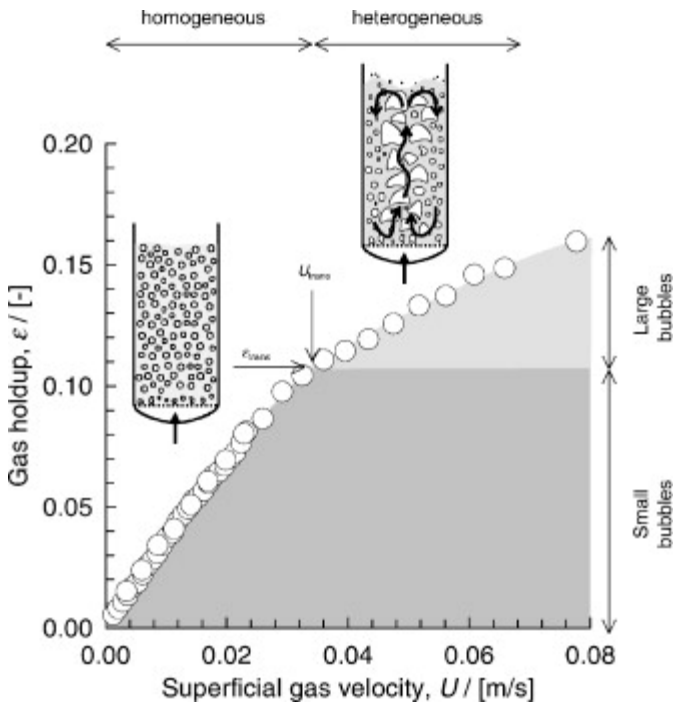

Figure 2.7. Experimental data on gas holdup in a 0.1 m diameter bubble column operating with the air-water system (Krishna and van Baten, 2003)

2.2.1.1.2 Effect of Column Size on ε_G

It has been reported that the geometry of the bubble columns affect the hydrodynamics of the system (Winterbottom, 1993). Based on the column geometry, three different regions were reported in terms of gas holdup (Thorat et al., 2001; Yamashita, 1998): (1) sparger region; (2) bulk region; and (3) top region. Gas holdup in the sparger region depends on the sparger design. However, in the bulk region, gas

holdup is ruled by liquid circulation. In the top region, formation of froth above the surface enhances gas holdup. In bubble columns, considering these regions, the sum of holdups would give the average holdup of the system. However, the column could be tall enough to be ruled by the second region alone where the influence of the other regions is insignificant(Wilkinson et al., 1992). The ratio of height of the column to its diameter is reported to decide whether first and third regions have any effect on the gas holdup. Some researchers reported that typically no effects of those regions on the gas holdup were observed when the ratio was above 5 (Pino et al., 1992; Wilkinson et al., 1992). Eickenbusch et al. (1995) compared 3 columns having diameters 19, 29 and 60 cm with a height to diameter ratio of 10.2, 10.3 and 6.5, respectively. They reported domination of the heterogeneous flow regime and that no significant effect on the gas holdup was observed with different column diameter. On the other hand, Moustiri et al. (2001) studied two columns with 15 and 20 cm inner diameter in the homogeneous regime and reported pronounced increase of gas holdup with decrease in column diameter. This increase was attributed to the wall effect that decreases the bubble rising acceleration.

From the researches mentioned above it can concluded that there would be no significant effect of column diameter change on the gas holdup when the inner diameter of the column is below 20 cm. Furthermore, gas holdup continues to slightly decrease at column diameters greater than 20 cm and gradually reaches an asymptote due to the diminishing wall effect. However, gas holdup could be further influenced depending on the operating variables and the type of gas sparger used.

2.2.1.2.3 Effect of Gas Spargers on Gas Holdup

Gas spargers are important part of the design of bubble columns. There are several types of gas spargers, which differ mainly in their size, number of orifices, and orifices' pitch distances (Fig. 2.8).

Vial et al. (2001) compared three different gas dispersion methods: a single-orifice nozzle, a multiple-orifice sparger and a porous plate. They have performed regime analysis using evolution of the average gas holdup. They reported that the single-orifice nozzle operates always in the heterogeneous regime. On the contrary, homogeneous conditions prevail with the multiple-orifice nozzle when the superficial gas velocity is lower than 4 cm/s and fully established heterogeneous regime is reached at U_G = 11-12 cm/s. However, with the porous plate heterogeneous regime can be reached at a lower gas superficial velocity around 7-8 cm/s. Smith et al. (1996) tested three different types of spargers, namely, a fin porous glass frit, a flexible rubber membrane, and an annular shear sparger. They reported results of gas holdup and bubble size as functions of gas velocity for these sparger types. They reported a delayed transition to the heterogeneous flow regime when the shear sparger was used. Moreover, the interfacial area produced by the shear sparger operating in the homogeneous regime exceeds that produced by perforated and sintered plates operating in the heterogeneous regime.

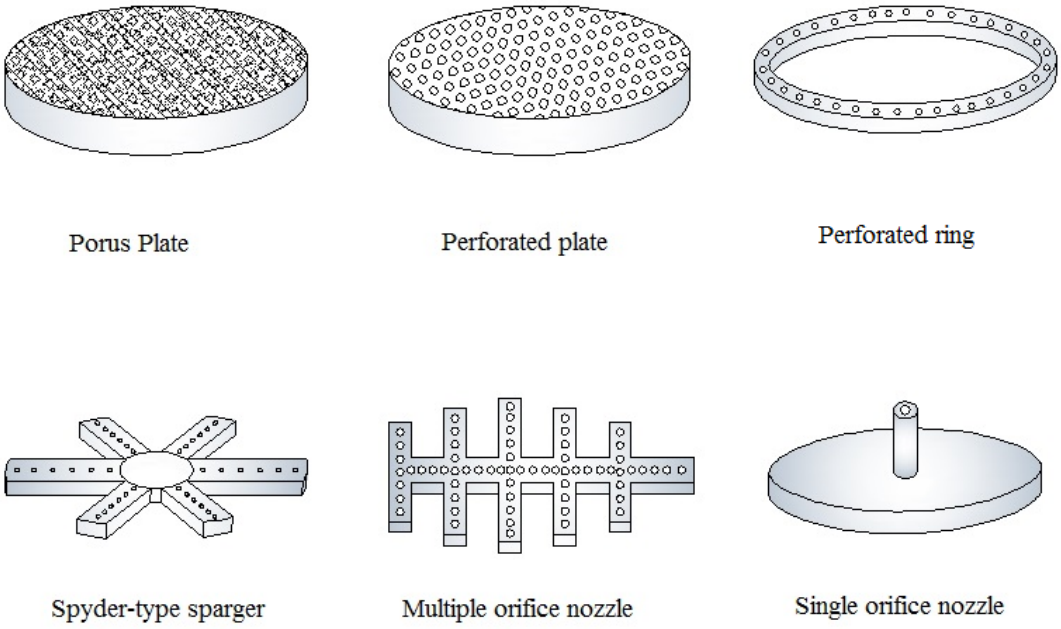

Figure 2.8. Various types of gas spargers used in bubble columns

Contrary to the previous studies, Pohorecki et al. (1999) found no significant effect of gas spargers on the gas holdup. They used several gas spargers with different geometries. They reported superficial gas velocity to be the only parameter to have effect on gas holdup and bubble diameter. They performed the experiments under elevated pressures and a range of temperature of 30-160°C. The vertical bubble column was 0.3 m diameter and 4 m high.

2.2.2 Dynamics of Gas Bubbles

Gas bubbles dynamics is ruled by their size, shape, and distribution in the column. Size of the bubbles determines the gas-liquid interfacial area which directly influences the overall rate of interaction occurring in the bubble column.

The distribution and behavior of the gas bubbles and the hydrodynamics of the flow are interrelated. Under homogeneous flow regime, gas bubbles nearly had uniform sizes with narrow size distribution (Pohorecki et al., 1999).

Increasing the superficial gas velocity enhances the bubble-bubble interaction which leads to collisions among bubbles and starts the transition regime. If time is enough, coalescence and breakup of bubbles take place. As the superficial gas velocity increases more, the frequency at which coalescence and breakup of bubbles increases and reaches to nearly a steady state in the heterogeneous regime. Upon coalescence bubbles would have different sizes. Large bubbles rises faster than smaller bubbles. With the turbulence created in the heterogeneous regime bubbles coalescence can occur even at the sparger. More on bubble coalescence behavior is discussed in the following sections.

2.2.2.1 Bubble Formation

The initial bubble size at the formation stage is subjected to different factors. The sparger type, the liquid height above the sparging level, the temperature of the liquid, and the superficial gas velocity are some of these factors. Generally the initial bubble diameter (d_b^*) directly after detachment from the nozzle is estimated by the following expression (Tsuge et al., 1981):

$$d_b^* = \left[\frac{6 d_o \sigma_L}{g(\rho_L - \rho_G)}\right]^{1/3} \tag{2.6}$$

Where d_o is orifice diameter, ρ_L and ρ_G are densities of liquid and gas respectively, and σ_L is surface tension of the liquid. This expression is based on the assumption that bubble formation takes spherical shape from the beginning of formation to the detachment under the buoyancy forces. Heignen and Van't Riet (1984) classified the bubble formation at sparger into three regimes as in (Fig 2.9).

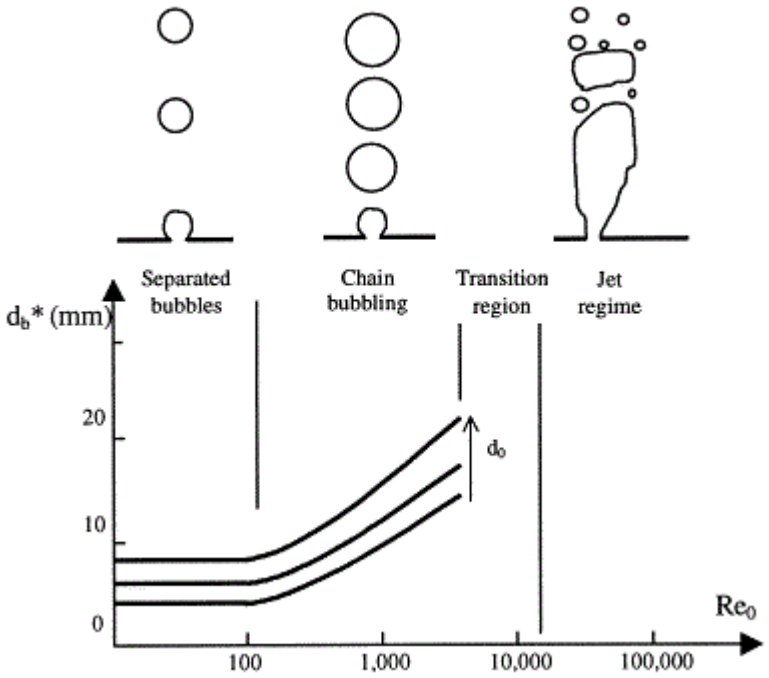

Figure 2.9. Air bubble formation regime at the orifice (Heijnen and Van't Riet, 1984)

According to Fig. 2.9, (d_b^*) increases with the increase in the orifice diameter (d_o). Moreover, for low orifice Reynolds number (Re_o), there would be no change in the size of bubbles at formation. As Re_o exceeds 100, regime transition to a chain bubbling takes place and d_b^* increases. The increase of d_b^* becomes higher with increase in the d_o. At farther elevated $Re_o$the bubble formation regime transfers to the jet regime where bubbles have irregular shapes and unpredictable sizes. They suggested that the column's optimum performance is achieved under the chain bubbling regime. This map was drawn under ambient temperature for single orifice nozzle with no neighboring bubbles which eliminates the bubble-bubble interaction.

2.2.2.2 Terminal Shape and Rise Velocity of Bubbles

Hydrodynamic behavior of a rising bubble has been a subject of both experimental and numerical studies for many years including some comprehensive studies and correlations regarding shape and speed of a rising bubble. Clift et.al. (1978) grouped

the behavior of a rising bubble in a viscous fluid under the influence of gravitational forces into three different regimes, namely; spherical, ellipsoidal, and spherical cap regime. Apparently, the terminal shape and velocity of a rising bubble depends greatly on their size as well as the surface tension of the bubble. Terminal velocity is defined as the velocity a rising bubble reaches when there is a balance between the driving force and the resistive force (i.e. buoyancy and drag forces). Once the terminal velocity is reached, bubbles stops accelerating and travel with the same velocity to the end of the course.

The regimes under which the terminal shape of bubbles is classified are achieved depending on three non-dimensional numbers; Reynolds number (Re), Bond number (Bo), and Morton number (Mo).

Bond number is calculated as:

$$Bo = \frac{g\Delta\rho d_b^2}{\sigma} \tag{2.7}$$

And Morton number is as follows:

$$Mo = \frac{g\Delta\rho\mu_l^4}{\sigma^3\rho_l^2} \tag{2.8}$$

Where, $\Delta\rho$ is the difference between the liquid and the gas densities, d_b is the bubble diameter, σ is the liquid surface tension, and μ_l is the dynamic viscosity of the liquid.

The shape regimes are illustrated in the Fig. 2.10:

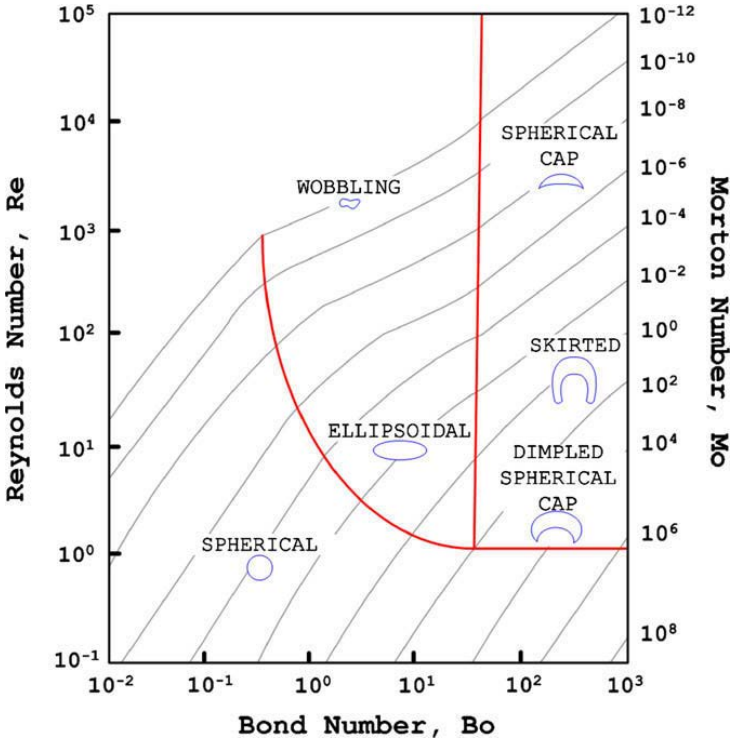

Figure 2.10. Shape regime map (Clift, 1978)

Terminal velocities on the other hand are governed according to different correlations for different regimes:

Spherical regime: This regime is dominated by surface tension and viscous forces. Original size of the bubble is small, usually less than 1.3 mm and is governed by the following equation:

$$U_t = \frac{g\Delta\rho d_b^2}{6\mu_l} \frac{1+\frac{\mu_g}{\mu_l}}{2+3\frac{\mu_g}{\mu_l}} \tag{2.9}$$

where, μ_g is the dynamic viscosity of the gas.

Ellipsoidal regime: This regime is mainly dominated by surface tension. Bubble size is intermediate, typically from 1.3 to 6 mm, and is governed by:

$$U_t = \sqrt{\frac{2.14\sigma}{\rho_l d_b} + 0.505 g d_b} \tag{2.10}$$

Spherical cap regime: This regime is governed by inertia force. Bubble size is large, usually bigger than 6 mm, and the following relation is used:

$$U_t = \frac{2}{3}\sqrt{\frac{g d_b}{2}\frac{\Delta\rho}{\rho_l}} \tag{2.11}$$

These relations assume that a bubble rise straight to the top and ignores the oscillatory motion and the possible bubble-bubble interaction.

It is concluded that the shape and rise velocity of a bubble is ruled by several parameters. Sparger type and gas flow rate mainly affect the initial bubble size. The inertia forces, surface tension, and liquid and gas viscosities and densities affect their rise velocity and shape.

Varying shape and rise velocity of individual bubbles increase the possibility of bubble-bubble interaction and may result in initiating the bubble coalescence and breakup phenomena. This phenomenon is a main concern to the researchers for its major impact on the mass and heat transfer between the two fluids.

2.2.2.3 Bubble Coalescence and Its Effect on Mass and Heat Transfer

Bubble coalescence takes place by bubbles blending into each other and forming larger lumps of air. It starts when bubbles collide and trap a certain amount of liquid between them. Once the liquid drained, the thickness of film between the two adjacent bubbles reduces to a critical point before it raptures.

This happens while the bubbles rise to the surface or even at the generation point. Upon coalescence of bubbles, the total gas–liquid contact area decreases and thus mass and heat transfer to the bubbles decrease (i.e., humidification decreases).

In their study of the lower region of the bubble column, Perry and Green (2001) found that the characteristics of the bubble coalescence depend on the design of the dispersion device. They pointed out that, in the manufacturing of the perforated spargers, the typical separation between the orifices centers should range from 2.5 to 4 times the orifice diameter. Camarasa et al. (1999b) and Pohorecki et al. (2001) studied the coalescence process in the central region of the bubble column where the bubble-break-up and the coalescence processes reached equilibrium. They have determined that there is a relationship between the bubble mean diameter, which is a function of the surface area, and the transport phenomena between the gas and the liquid phases. It is evident from these studies that the smaller the bubble diameter the greater the heat and mass transfer to it.

Mariano Martin et al. (2007) studied the effect of bubble coalescence on the liquid mass transfer as bubbles are leaving the sparger plate. They claim that although coalescence may decrease the mass transfer rate, the deformation of bubbles can balance this decrease in mass transfer rate.

Chen et al. (2011) investigated the coalescence of bubble pairs rising in a stagnant liquid numerically and compared the results with the experimental ones. The numerical results indicated that the rising velocity of the trailing bubble was larger than that of the leading bubble. They indicated that both the leading bubble and the trailing bubble rose faster than the single bubble. This is another factor that affects the rate of heat and mass transfer to the bubbles since faster rising bubbles decrease the interaction time and thus decreases the amount of heat and mass transferred. In

their study two different coalition patterns presented, namely; side and inline patterns (Fig. 2.11 & Fig. 2.12).

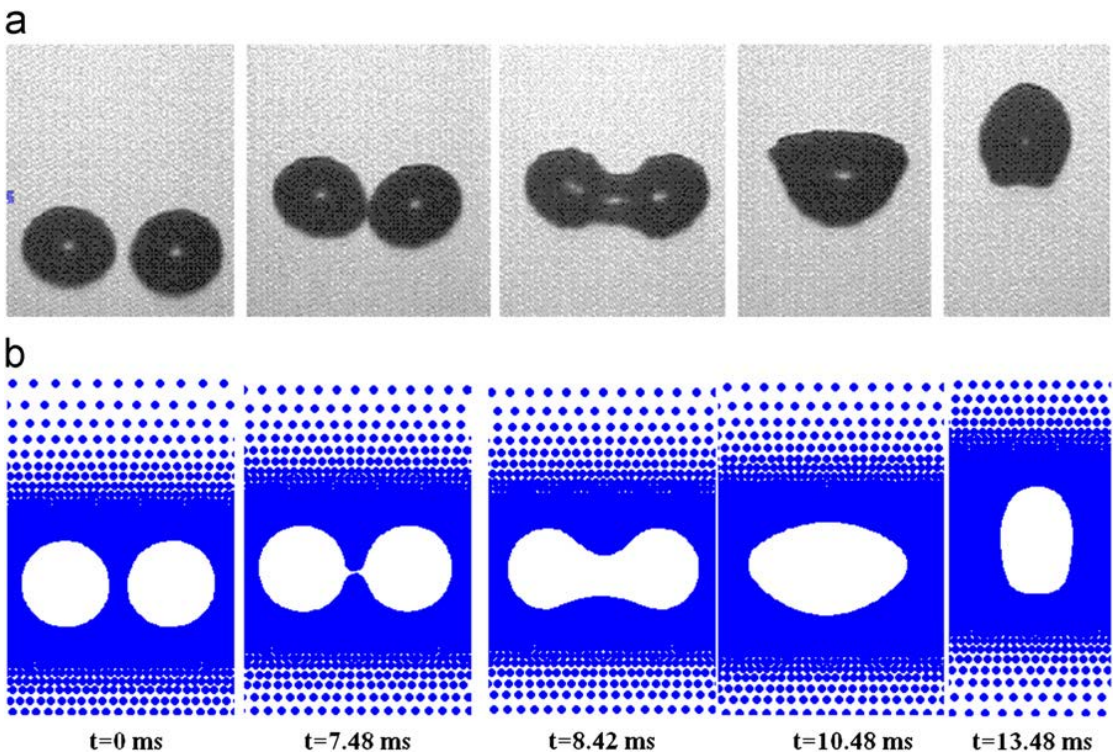

Figure 2.11. Numerical results and experimental observations of side by side coalescence between two identical bubbles (Krishna and van Baten, 2003)

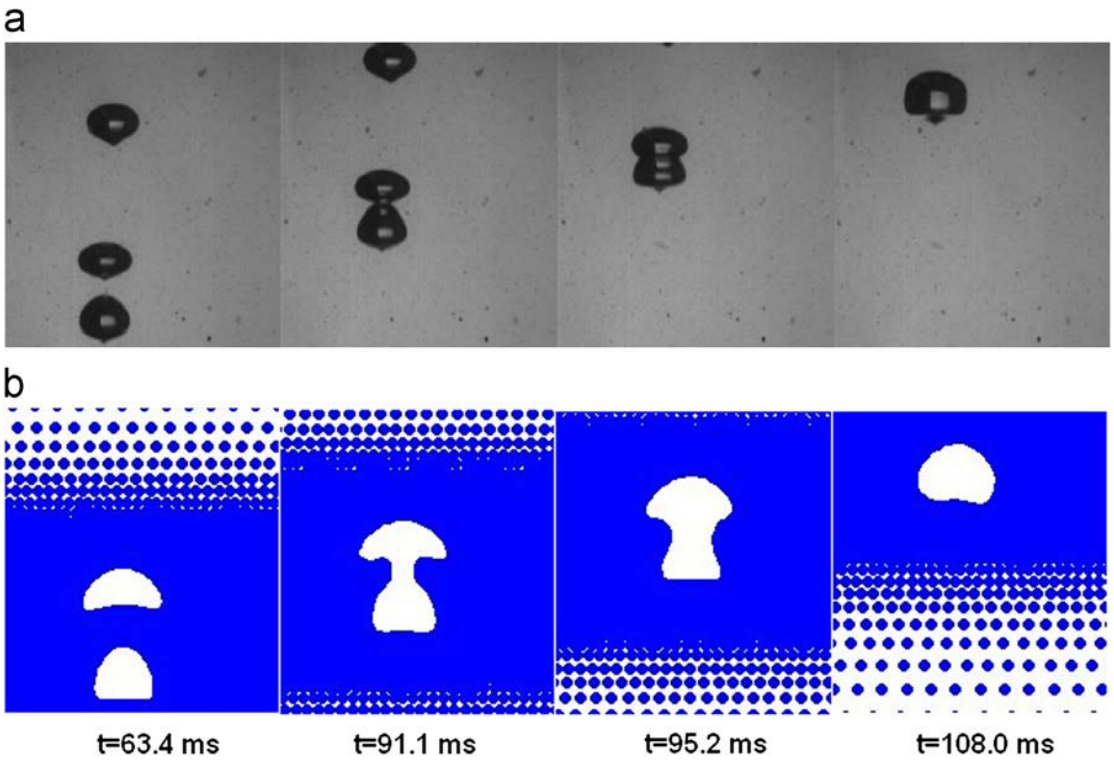

Figure 2.12. Numerical results and experimental observations of in-line coalescence between two identical bubbles (Krishna and van Baten, 2003)

R. Krishna et al. (2003)developed a computational fluid dynamics (CFD) model to describe the hydrodynamics, and mass transfer, of bubble columns. They concluded that mass transfer from the large bubble population is significantly enhanced due to frequent coalescence and break-up into smaller bubbles. This study assumes high break up rate that is almost as much as the coalescence rate, which is rarely the case. Some of the above mentioned researchers claimed that the recurrent bubble break-up and coalescence enhances mass transfer to the bubbles while others disagree.

2.2.3 Final remarks

It is clear from the previous studies that there are several parameters with varying importance which play role in the optimization of gas-liquid intra-transport phenomena, specifically heat and mass transfer.

From the mentioned studies the following notes can be drawn:

- Heat and mass transfer rate to and from the larger size bubbles are lower than the smaller size bubbles.
- As flow rate of air in water increased bubble coalescence increases.
- Heat and mass transfer from and to a bubble decreased as its diameter increases.
- The rising velocity of a bubble increased as its size increases.
- As the temperature of the liquid increased the terminal velocity of bubbles increases, giving less time for them to transfer heat and mass.
- Frequent coalescence and break-up of bubbles may enhance the mass transfer to a bubble.
- None of the available studies mentioned the effect of the temperature difference between the liquid and the gas on the rate of coalescence. As the temperature difference was increased the size of bubbles increases and thus the coalescence rate.

From the available literature it can be concluded that; whether bubble coalescence increases or decreases the heat and mass transfer, designing for multistage coalescence in the bubble column could be vital. At each stage bubbles would be regenerated and thus resized. Multistage bubble regeneration can provide adequate time for heat and mass transfer to take place thus enhances the humidification process.

Chapter 3

3 METHODOLOGY

Generally designing any system requires testing the performance of some models that are based on a specific technique before finalizing the design. In this study the practicability of the bubbling technique to be used in HDD systems is tested in laboratory environment before deploying the final solar design. The laboratory based tests would give insight of the working principle of the bubbling technique and shed a light on the weaknesses and help identifying the deficiencies that may be encountered when applying this technique. Thus, the possible remedies are spotted, applied, and tested for the optimum performance before finalizing the pilot solar design.

3.1 Experimental method

The main purpose of this study is to produce an efficient humidifier design, to be used in HDD systems, by employing the bubbling technique. The design incorporates air and water heating with humidification process in one unit (Fig. 3.1). The bubbling technique as discussed in the previous chapter is based on dispersion of a gas into liquid to allow direct contact between the two fluids. In this study relatively cold and dry air is dispersed in hot water to be humidified. Air is dispersed in water from a perforated sparger in form of bubbles. Bubbles ascend under the effect of buoyant and gravitational forces to the surface of the water bed. Upon travelling upwards, air bubbles receive vapor due to the difference in vapor concentration. The performance

of the device is evaluated for different parameters as discussed in the next section. The deficiency of the humidification process is treated by adding perforated baffles that regenerates bubbles and enhances the mass and heat transfer. Perforated baffles are used in the design of the final solar humidification unit. The solar humidification unit is then coupled with a condenser to complete a solar HDD system.

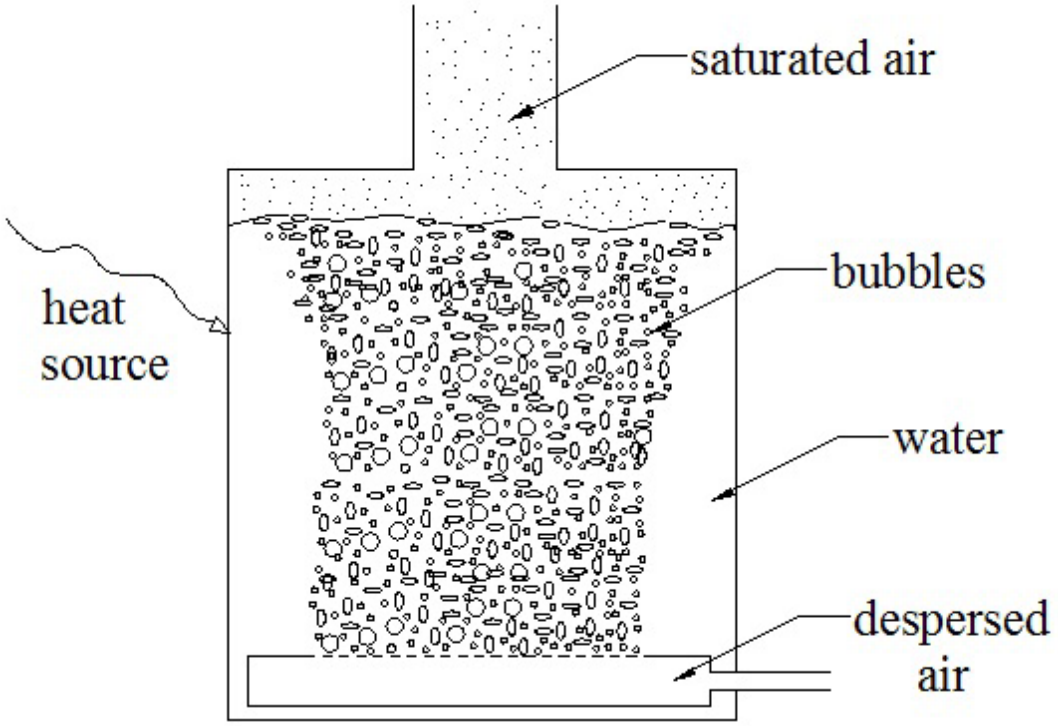

Figure 3.1. humidification by bubbling

In the coming chapters the experimental method and design parameters are presented in detail for each design separately.

3.2 Performance Measures and Evaluations

Performance measurement in the present work is made by quantifying the efficiency, effectiveness, and productivity of the humidifying system in order to find out ways of improving its ability to deliver favorable results. In the following subsections the

performance measures and evaluation methods under which the constructed setups were tested are presented. These performance measures are going to be used where applicable.

3.2.1 Efficiency and Effectiveness

Humidification Process Efficiency is defined as the ratio of actual increment in humidity to the maximum possible increment in vapor content at the saturated temperature of air. It is expressed in percentage as:

$$\eta_H = 100 \frac{\omega_{out-} \omega_{in}}{\omega_{out\,@sat.air-} \omega_{in}} \quad (3.1)$$

Where, ω_{out} and ω_{in} are the absolute humidity at the outlet and the inlet respectively, and $\omega_{out\,@sat.air}$ is the maximum possible amount of vapor carried by air at air temperature.

In the present work, another performance criterion, namely effectiveness, is introduced to assess the maximum increase in vapor content of air. Effectiveness of heat exchangers has been elaborately studied in the literature and a clear definition has been established and verified (Cengel, 1997). The equation used for determining the effectiveness of the heat exchangers cannot be satisfactorily used in humidifiers; they are only adaptable to humidifier effectiveness calculations. On the other hand cooling towers are possibly operated with the closest mechanism to a humidifier, although the aims are different. Targeting cooling towers, Cheremisinof et al. (1981) have presented a temperature-dependent effectiveness equation to test the effectiveness of a cooling tower as follows:

$$\epsilon_T = \frac{\Delta T}{\Delta T^{ideal}} \quad (3.2)$$

Where, ΔT is the temperatre difference between outlet and inlet air, and ΔT^{ideal} is the maximum possible temperatre gain in ideal case.

Since the aim of a cooling tower is to cool the hot water, rather than defusing vapor to air, the equation they have presented could be used as a measure of performance for a humidifier provided that the outlet air is saturated. Saturation of the outlet air is so important in HDD systems, as unsaturated air demands more, unnecessary, chilling energy to bring air to the dew point in order to start the condensation process. Jaber and Webb (1989) have presented a different definition to describe the effectiveness. Their expression involved the calculation of the actual over the maximum possible heat transfer rate:

$$\epsilon_J = \frac{Q_{act}}{\dot{m}_{min}^{mod}.\Delta h_a^{ideal}} \tag{3.3}$$

The expression they presented cannot be applied to our system since one of the fluids is stagnant while the denominator involves the calculation of the minimum flow rate in the system. Another way to express the effectiveness, presented by Nilles and Klein (2008), is by considering the ratio of the actual change in internal enthalpy of air to the maximum possible change. This expression was made to test the effectiveness of a coil type humidifier:

$$\epsilon_h = \frac{\Delta h_a}{\Delta h_a^{ideal}} \tag{3.4}$$

Where, Δh_a is the enthalpy difference between the outlet and inlet air, and Δh_a^{ideal} is the maximum possible enthalpy gain in ideal case.

The maximum effectiveness of a mass and heat exchanger can be achieved when the air exits saturated at the inlet liquid temperature. In the presented system water is still

and heat and water are added to compensate for heat and mass loss in order to keep temperature and level of water constant. The present work proposes that the easiest and most effective way for testing the effectiveness of the humidifier under study is by modifying the efficiency expression in Eqn. 3.1 to include the maximum possible increment in vapor content at the saturated temperature of water instead of saturated temperature of air:

$$\epsilon_{\omega} = 100 \frac{\omega_{out-} \omega_{in}}{\omega_{out\,@sat.water-}\omega_{in}} \quad (3.5)$$

where, is the maximum possible amount of vapor carried by air at water temperature.

3.2.2 Gas Holdup

Gas holdup ε_G serves as a measure of mass transfer efficiency in bubble column. Gas holdup ability of bubble columns was studied both analytically and experimentally by many researchers. The majority of the studies concentrated on the relationship between gas holdup ability and the superficial gas velocity in the system. Some researchers (Hikita et al., 1980; Kumar et al., 1976; Reilly et al., 1986) suggested relatively complex relation to calculate ε_G analytically. On the other hand some researchers (Camarasa et al., 1999a; Chaumat et al., 2005; Moshtari, 1999) have studied the gas holdup experimentally. All have used the usual pressure difference method (but employed different techniques) to measure the average gas holdup value.

In this study, the liquid displacement method was adopted to determine $\varepsilon_{G.}$ The humidifier was initially filled with water. Then, air was dispersed in water at different air mass flow rates. As a result some of the water inside the humidifier was displaced to allow dispersed air to replace it as the volume of the humidifier is fixed.

The gas holdup was calculated as of Eqn. 2.3, i.e., by dividing the displaced water by the water volume initially contained in the humidifier.

Generally the gas holdup of a liquid is plotted against the superficial gas velocity which is given in Eqn. 2.1.

3.2.3 Gained Output Ratio

One of the most commonly used performance measures for thermal based desalination is the gained output ratio (GOR). GOR is a dimensionless measure of the amount of product for a given net heat input.

$$GOR = \frac{\dot{m}_{PR} h_{fg}}{\dot{Q}_{in,net}} \tag{3.6}$$

where, $\dot{m}_{pr}$ is the rate of freshwater production, h_{fg} is the latent heat of evaporation, and $\dot{Q}_{in,net}$ is the received energy by the system. From Eq.3.6, a GOR of unity means that the energy required for evaporation of water and energy supplied to the system are equal. The ideal GOR for simple solar stills is unity. GOR is always less than unity in solar stills because of the losses accompanied in stills. However, GOR higher than unity means that the system regenerates energy (such as making use of energy released during condensation) which can be used to enhance evaporation. The advantage of using GOR is that it serves as the normalized output-gain value which can be used to compare different systems or same system with different parameters. In this work GOR will be used to compare the system running at different air mass flow rates and solar radiations.

3.2.4 Normalized Production (NP)

Normalization is a performance measure that is customized to compare different setups which work under different circumstances at their peak production period. NP takes into account the variables under which each system performs.

The introduced normalization of production takes into account hourly production of a system by the total solar energy gained in same duration and calculated as:

$$\boldsymbol{NP} = \frac{\boldsymbol{PR_{max}}}{\boldsymbol{I_{@PR_{max}} * A_{eff}}} \tag{3.7}$$

where PR_{max} is the maximum production at any period of time, $I_{@PR_{max}}$ is the average solar intensity during that period of time, and A_{eff} is the effective aperture area.

3.2.4 Normalized Gain (NG)

Another measure of performance can be obtained by plotting the humidifier effectiveness (i.e., Eqn. 3.5) as a function of normalized gain. The normalized gain (*NG*) is expressed as follows:

$$NG = \frac{(\mathbf{T_{out,av} - T_{in,av}})}{\mathbf{I_{av}}} \tag{3.8}$$

where $\boldsymbol{T_{out,av} - T_{in,av}}$ is the difference in average temperatures of air at the outlet and inlet of the humidifier and $\boldsymbol{I_{av}}$ is the average solar intensity, both taken at the collector's best performance. Equation 3.8 is usually used to compare the performance of solar air collectors working under different climatic conditions or at different days of the year.

3.3 Uncertainty Estimation

Uncertainty in experimental results is unavoidable concern regardless of the claimed precision and accuracy. In general, two factors affect the precision of a measurement and thus the results of an experiment. Those factors are the random errors that depend on the skill and capability of the experimenter, and the systematic errors resulted due to the limitation and precision of the measuring instruments. The data collection in the experimental setups of this study is carried out automatically using digital devices with known accuracy. The use of such devices limits the resultant uncertainty to the systematic errors accompanied with the instruments used.

Perers (1997) and Mathioulakis et al. (1999) have conducted uncertainty assessment for several elaborated models using variety of methods and techniques including the standardized method in ISO (1995) with the following form:

$$U_{\omega} = \sqrt{\sum_{i=1}^{n} \left(\frac{\partial \Gamma}{\partial x_i} * U_{x_i} \right)^2} \tag{3.9}$$

where x_i denotes independent variables between i = 1 and n, with uncertainty U_{x_i} affecting Γ, which is the calculated or measured value in the study. Equation 3.9 is be used for assessing uncertainty analysis.

3.4 Optimization Method

The tests performed in the laboratory environment would give maximum productivity under certain working conditions. The conditions under which the performance of the humidifier shows promising results would be used when designing the new solar setup. The solar humidifier is to be tested for its humidification effectiveness as a standalone unit before coupling with the rest of the

components which make the whole HDD system. Then the complete system is built and tested for its best performance.

Chapter 4

4 UTILIZING THE BUBBLING TECHNIQUE FOR HUMIDIFICATION: AN EXPERIMENTAL ASSESSMENT

A bubble column similar to the column reactors found in the literature is constructed and tested. The size of the bubble column presented in this chapter is a lot smaller than those of the column reactors. Since the ultimate aim is to use solar energy for heating the bubble column it is desired to keep its size as small as possible. In the present chapter the effectiveness of the bubble column is investigated and improvements are introduced for better humidification performance.

4.1 Design and experimental setup of the bubble column

4.1.1 Experimental setup

Basically, the performance evaluation has been conducted on a humidification test unit. Humidification process was performed by passing air into batch of brackish water. The system consists of three main units: humidification unit, air compressing and control unit, and a measuring and displaying device (acquisition system) (Fig 4.1).

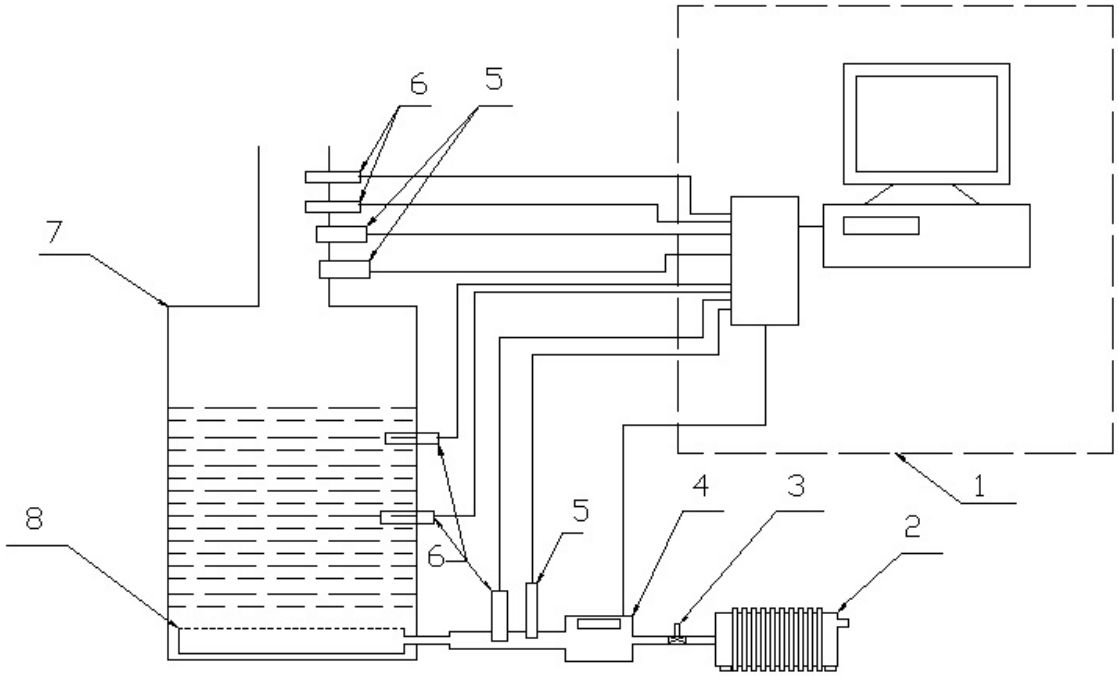

1)Data acquisition system 2) compressor 3) pressure control 4) flow controller
5) thermocouples 6) humidity sensor, 7) humidifying chamber, 8) sparger.

Figure 4.1. Experimental setup

4.1.2 The humidification unit

The humidification unit consists of three main parts (Fig. 4.2); The humidifier chamber, the gas sparger, and the heating element. The following is a description of how these components were utilized in the present work.

Figure 4.2. The humidification unit

4.1.2.1 The humidifier chamber

Unlike all the bubble columns discussed in the literature review, the shape of the humidification unit is rectangular. The rectangular façade displays real sizes and better vision of the flow pattern when monitored. The base size was chosen arbitrarily to give a hydraulic diameter of about 33cm in order to insure any flow regime other than the slug flow regime (see Fig. 2.6). The humidifier chamber is

simply a 0.33x0.33x0.8 m box with opened top. The box was manufactured using thermally treated glass sheets to enable visual inspection of the humidification process and to endure elevated temperatures. Thermal insulation was applied to the outer sides of the walls of the box except from the top and one of the sides to decrease the heat loss. The lid of the humidifier was deliberately left open to eliminate the effect of pressure on the saturation state of the gas.

Ignoring physical particularity and singularity for any system can lead to huge errors while analyzing that system. In HDD systems for instance, measuring the performance of the humidifier while attached to the whole system could lead to major errors. Calculating the actual absolute humidity of air without considering the pressure in the humidifier is one of these errors. Most of the theoretical and experimental works have considered or reported the air outlet of a humidifier to be saturated, and thus the humidifier efficiency were praised, merely because the wet bulb temperature is close enough or equal to the dry bulb temperature. In fact the absolute pressure in a humidifier of a running system is never atmospheric- it is even lower or greater than atmospheric pressure depending on the placement of the air pumping device as well as the flow rate at which the system runs. Figure 4.3 demonstrates the amount of vapor air can carry at different temperatures and under different pressures. From the Fig. 4.3 it can be seen that at 75°C the amount of vapor air could carry is 386, 298, 239, and 200gr/kga for 101.325, 120, 140, and 160 kPa respectively. From these results it can be concluded that analyzing a humidifier for efficiency should be done independently to ensure factual and accurate data.

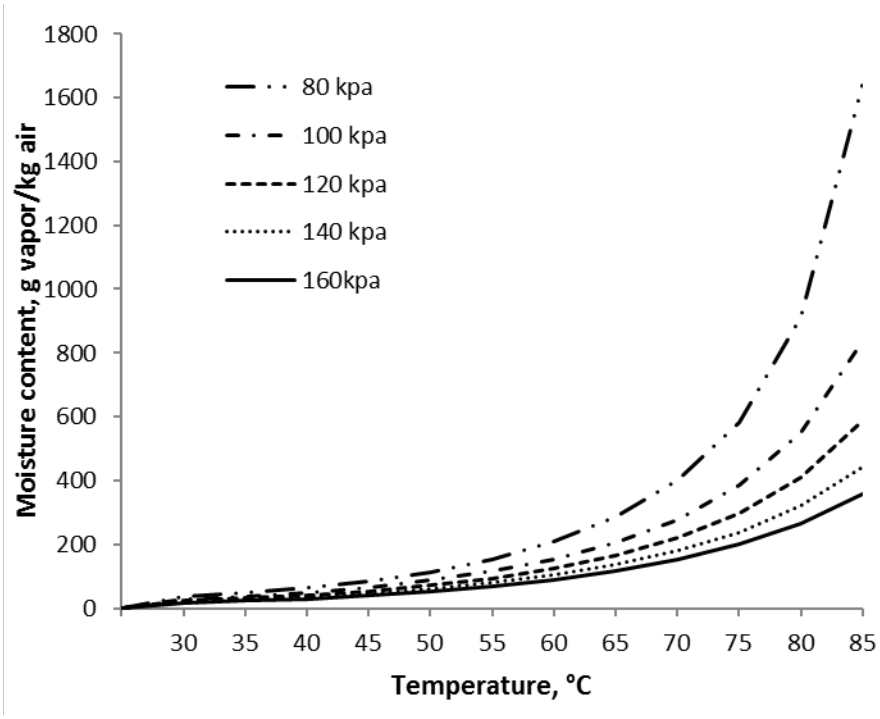

Figure 4.3. Moisture content of fully saturated air at different pressures and temperatures (produced using EES program)

4.1.2.2 The sparger design

The Sparger (dispersion device) was designed to be smaller than the base of the humidification chamber in order to eliminate the wall effect. It is simply a 0.22x0.22x0.06 m acrylic box with detachable forged lid (Fig. 4.4). The device is mounted on a removable frame that eases the lid changing process. Three identical lids were manufactured, with 1600 holes drilled on each. The holes were drilled by the aid of a CNC machine with a 1.5 mm diameter drilling pit. The initial bubble diameter at the detachment time is greatly influenced by the orifice diameter, the surface tension and the difference between the liquid and gas densities as evident from Eqn. 2.6. Knowing that fluid properties change with temperature change, the initial bubble diameter could be different for different temperatures. The temperature

of water in this experiment is varied between 20 to 70°C. Applying Eqn. 2.6 we get the results as in Table 4.1.

Table 4.1. Characteristics of bubble under different temperatures

Water temp.	Surface Tension	Water density	Air density	μ Dynamic Viscosity	Bubble diameter Eqn. 2.6	Bond number Bo Eqn. 2.7	Morton number Mo Eqn. 2.8	Terminal velocity U_t Eqn. 2.9
°C	N/m	kg/m^3	kg/m^3	$(N.s/m^2) *10^{-3}$	mm	_	_	m/s
20	0.0728	998.3	1.205	1.002	4.06	2.22	2.56E-11	0.242
30	0.0712	995.7	1.166	0.798	4.03	2.23	1.11E-11	0.241
40	0.0696	992.3	1.127	0.653	4.01	2.25	5.33E-12	0.239
50	0.0679	988	1.097	0.547	3.98	2.26	2.84E-12	0.238
60	0.0662	983	1.067	0.467	3.95	2.28	1.63E-12	0.237
70	0.0644	978	1.034	0.404	3.93	2.29	9.99E-13	0.235

As shown in Table 4.1 the initial bubble diameter at its detachment is around 4 mm for an orifice diameter of 1.5mm.

Predicting the bubble diameter at the detachment moment is very important when designing the pitch distance between orifices of the sparger. Since the bubble diameter is 4mm, the pitch distance should at least be 5mm in order to prevent bubble coalescence at the formation stage. According to Perry et al. (2001) the recommended center to center orifice separation ranges between 3.75-6mm for an orifice of 1.5mm.

The minimum center to center (pitch) distance between the adjacent holes is designed to be 5 mm. It was decided to test the humidifier for different pitch distance greater than 5mm as well. By covering some of the holes, it was possible to operate

the sparger for different pitch distances. Figure 4.5 is a schematic demonstration of the configurations where there are 196 holes left uncovered.

A plug was attached to the sparger to enable gas injection. The lid was sealed and secured with 16, 5mm screws to insure no air leak. The sparger was mounted on an aluminum frame 100 mm above the ground level to make room for the heating element. The heating element was immersed in the water at the bottom of the humidifier chamber. Then the frame that holds the sparger was submerged. The frame was designed and constructed such that it can be detached from the humidifier in order to ease the sparger's lid changing process.

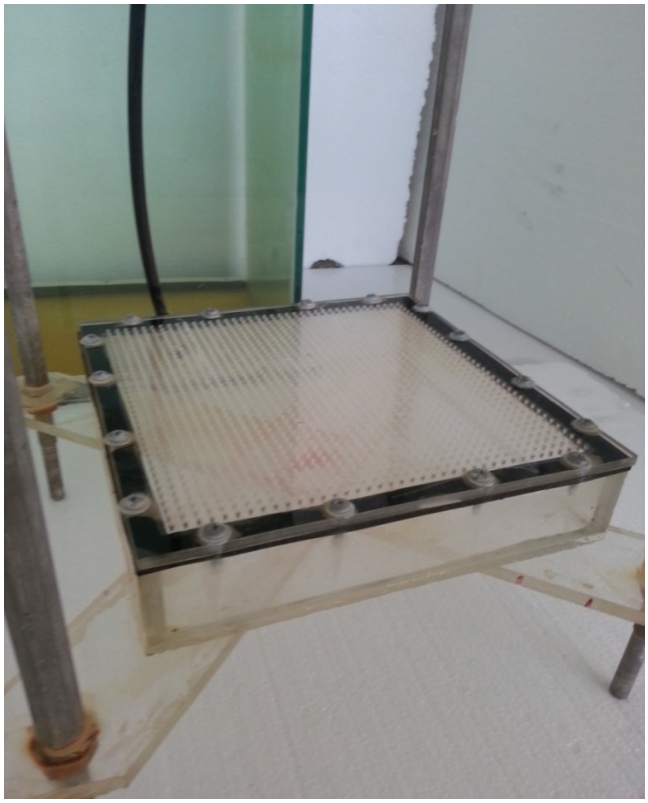

Figure 4.4. The sparger device

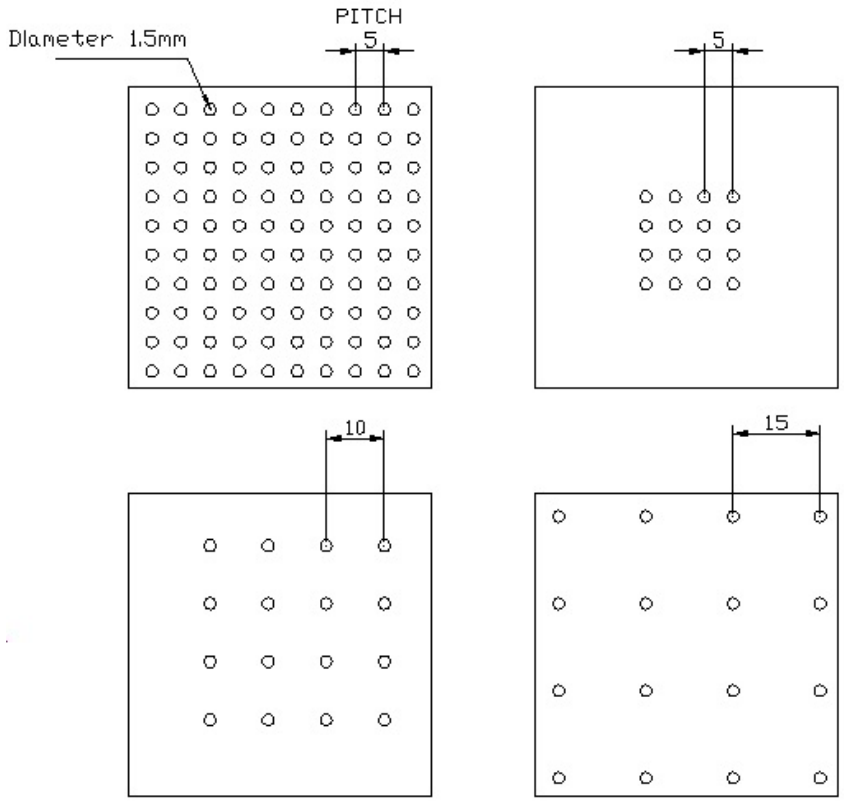

Figure 4.5. Configurations of the sparger's lid

4.1.2.3 Air compressing and control unit

In order to charge air into the sparger, a compression device is used to help overcome air path frictions and the static pressure on top of the dispersion device. The compression unit, shown in Fig 4.6, enabled full control of the pressure and flow rate of the dispersed air. It allowed conduction of the experiment under a steady state condition. An orifice meter was employed between the compressor and the sparger in order to calculate the air mass flow rate. Then air is injected to the sparger device through its port.

4.1.3 Data acquisition

The measurements taken in this work are the air flow rate, air pressure, relative humidity, water temperature, and temperature of the dispersed air at both the inlet

and outlet of the humidification unit. Water and air temperatures were recorded using three thermocouples, which were connected to an Xplorer GLX data logger. The same data logger was used to measure the pressure of the flowing air. Inlet and outlet humidity of air was acquired using an Omega Thermo Hygrometer RH411 with measurement range of 5-98% having accuracy of ±3%.

Figure 4.6. Air compressor and controlling unit

4.2 Experimental procedure

The experimental setup shown in Fig. 4.1 was used in all experiments. Air was charged in the Sparger by the attached hose. Due to the pressure in the dispersion device, air bubbles form at the surface of the lid and then detach and travel upward in the water under the effect of gravity.

The experiment was performed for different hole diameters, different pitch distance, and different water levels above the sparger's lid. Summary of the all the setups is given in Table 4.2. Water temperature was changed incrementally by 5 degrees from 30 to 70°C for each setup. At each set temperature, the air flow rate was varied as well. The mass flow rates used in this experiment are presented in the next section. For all runs of the experiment, the air temperatures and the humidity ratio was recorded at steady state conditions.

Table 4.2. The parameters under which the humidifier was tested

Orifice diameter mm	Pitch distance mm	Water height cm	Water temperature °C
1.5	5, 10, 15	20, 30, 40	30, 35, 40, 45, 50, 55, 60, 65, 70

4.3 Flow rate measurement and superficial gas velocity

The flow rate was measured by considering the pressure difference across an orifice meter with pipe and orifice diameters of 2.5 and 1.25 cm respectively. The volume flow rate was calculated according to the following expression:

$$\dot{V} = C_f A_o \sqrt{2\Delta P/\rho} \tag{4.1}$$

Where A_o is the cross sectional area of the orifice, ΔP is the pressure difference across the orifice, ρ is fluid density, and C_f is the flow coefficient calculated as follows:

$$C_f = \frac{C_d}{\sqrt{1-\beta^4}} \tag{4.2}$$

Where β is the ratio of the orifice diameter to the pipe diameter and C_d is the discharge coefficient. There are many empirical equations for calculating C_d, one of which is that defined by ASME:

$$C_{d,ASME} = \left[\left(0.5959 + 0.0312 * \beta^{2.1} - 0.184 * \beta^8 + 0.0385 * \beta^{2.5} + 0.195 * \left(\frac{\beta^4}{1-\beta^4}\right)\right) * \frac{1}{(1-\beta^4)^{0.5}}\right] \tag{4.3}$$

C_d was found to be 0.6408 and the corresponding C_f is 0.6618.

The mass flow rate is calculated according to:

$$\dot{m} = \rho \dot{V} \tag{4.4}$$

and ρ is calculated using the ideal gas equation:

$$\rho = P/RT \tag{4.5}$$

where R is the gas constant, P and T are the pressure and temperature of the gas at the orifice upstream.

The resultant air mass flow rate, the corresponding superficial gas velocities U_G, and the orifice Reynolds number (R_o) at each flow rate are as given in Table 4.3. U_G is calculated as in Eqn. 2.1.

Comparing the U_G from Table 4.3 with Fig. 2.6 and Fig. 2.7 it is expected that the process should be governed by the homogeneous flow regime. Moreover, comparing

the Reynolds number at the orifice with Fig. 2.9, the initial bubble diameter at the formation is expected to stay nearly the same for all the given mass flow rates. Furthermore, at high flow rates, around 100 kg/h, air bubble formation regime falls at the transition region between the separated bubbles regime and chain bubbling regime.

Table 4.3. Characteristics of the air flow

$\dot{m}$ kg/h	R_o _	U_G m/s
5.0	62	0.97
7.7	82	1.27
10.1	93	1.44
12.4	101	1.56
14.7	107	1.65

4.4 Results and discussion

4.4.1 The flow regime

The conducted experiment exposed a different kind of flow regime than the expected. It was expected to witness a homogeneous regime at low water levels and low flow rates and a heterogeneous regime as the water level and air flow rate increases. When gas was dispersed into stagnant liquid a turbulent flow was observed even at low water level. Moreover, the turbulence increases with the increase in water level and air flow rate. This behavior is attributed to the wall effect and bubble coalescence. The sparger does not cover the whole cross section area of the humidifier. Therefore, there is a room for the formation of vortexes and eddies, between the air stream and the humidifier's walls, that result in more turbulent flow regime. Furthermore, according to the calculated Morton number and Bond number presented in Table 4.1, the bubble shape is within the ellipsoidal region. This

indicates that the distance between the adjacent bubbles decreases with the distance travelled. Therefore, bubble coalescence was inevitable at high water levels.

4.4.2 Air temperature and humidity

The water and air temperatures and air relative humidity are the results obtained from the experiments conducted. The air outlet temperatures against water temperatures for 1.5 mm diameter hole with pitch distance of 10 mm are plotted in Fig 4.7 for different water levels and 5 different air flow rates. The air inlet temperature during the experiment is 18±1 °C. The temperature of air increases as it comes into contact with the hotter water as shown in the figure. The higher the water temperature the higher the outlet air temperature. In Fig. 4.7a it can be seen that the outlet air temperatures for different flow rates at low water temperatures are very close. Then the gap starts to increase as the water temperature increases. This behavior could be attributed to the immature flow regime due to the low water level. The increase in air temperature in Fig. 4.7a and 4.7b is more stable with slightly higher temperatures recorded with water level of 400mm at low flow rates.

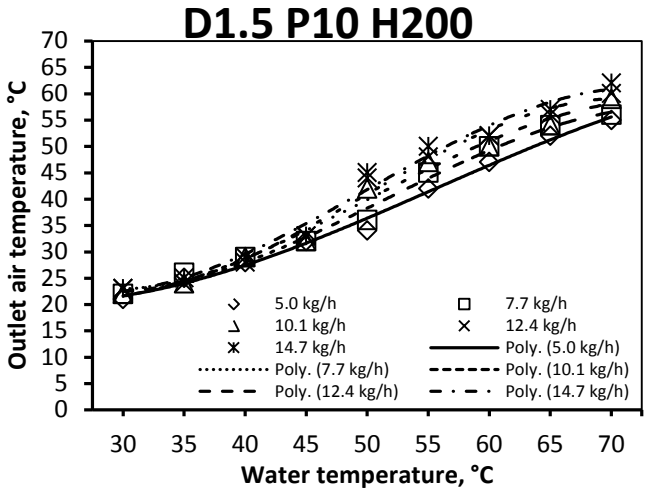

a)

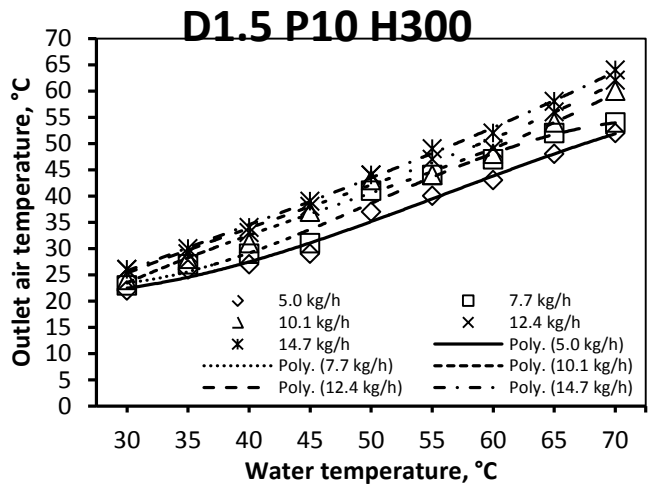

b)

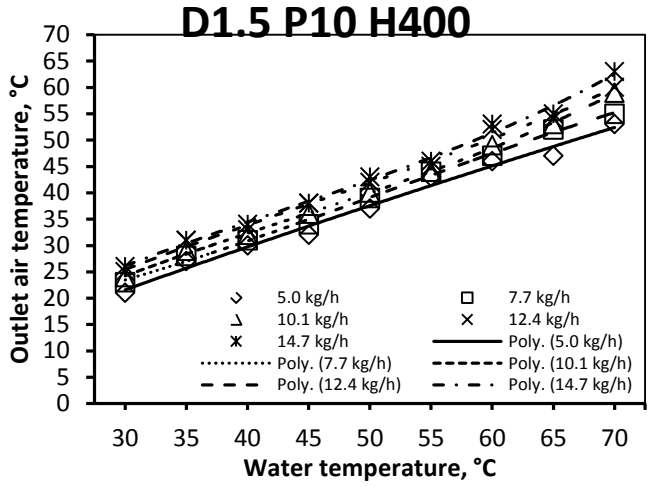

c)

Figure 4.7. Outlet air temperatures with respect to water temperature for different flow rates

The relative humidity at the exit of the humidifying chamber of the test is plotted against the water temperature in Fig. 4.8. Unlike the temperature profile, the relative humidity change with water temperature doesn't increase linearly. From Fig. 4.8 it is observed that regime change took place at least once with increasing temperature. The regime change manifests itself by the deflection of the plotted curve. It can be seen from Fig. 4.8a and 4.8b that for water levels of 200mm and 300mm the relative

humidity of air at lower mass flow rates is greater than that of higher flow rates at any temperature. However, dispersed air under water level of 400mm in Fig. 4.8c shows higher relative humidity at higher flow rates. The relative humidity continues to increase until the water temperature reaches 55-60°C then, shows greater relative humidity at low flow rates beyond (60°C).

From productivity point of view, the relative humidity is not a performance indicator. Since water content in air at any pressure depends on air temperature and relative humidity, the differential amount of vapor content between the inlet and outlet of air should be compared. Figure 4.9 plots the absolute humidity difference Vs. water temperature.

It can be seen from Fig. 4.9 that the absolute humidity difference at higher flow rates is greater than that of lower air flow rates. At higher flow rates of air, i.e., higher Reynolds numbers, the heat and mass transfer are enhanced. Moreover, it can be deduced from Fig. 4.9 that although the absolute humidity difference for the level of 200mm is less than the others at low temperatures, in general, water level has a negligible effect on the absolute humidity difference.

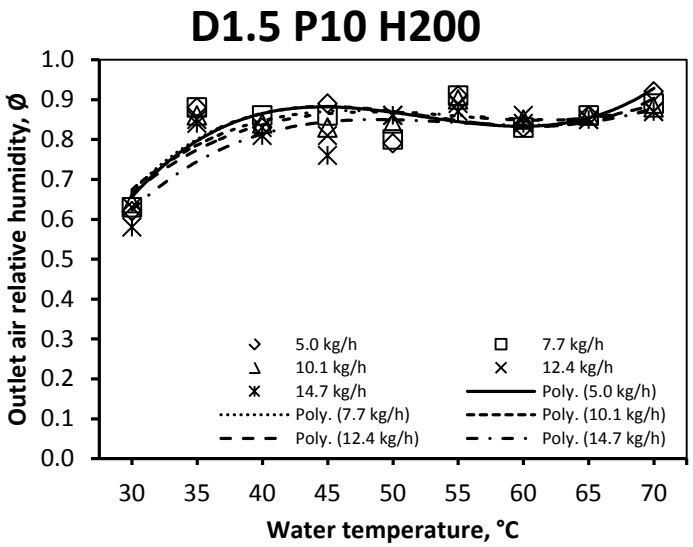

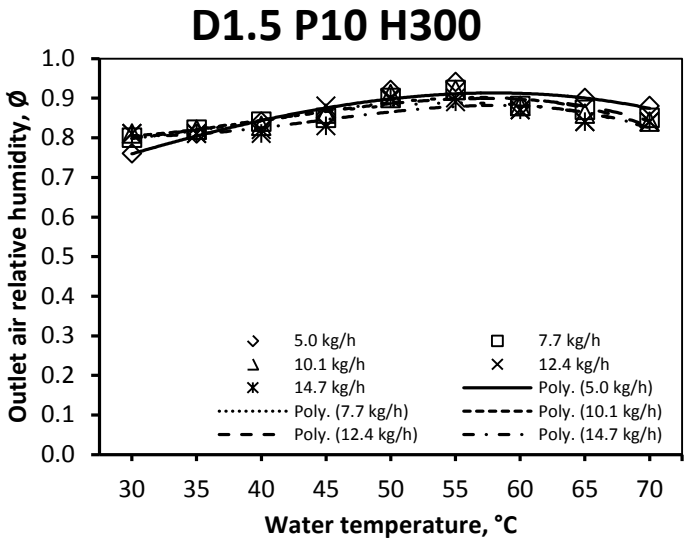

b)

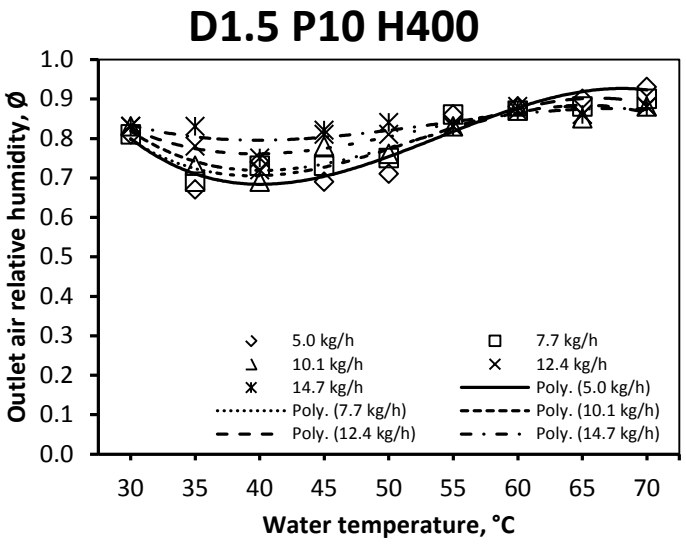

c)

Figure 4.8. Outlet air relative humidity with respect to water temperatures for different flow rates

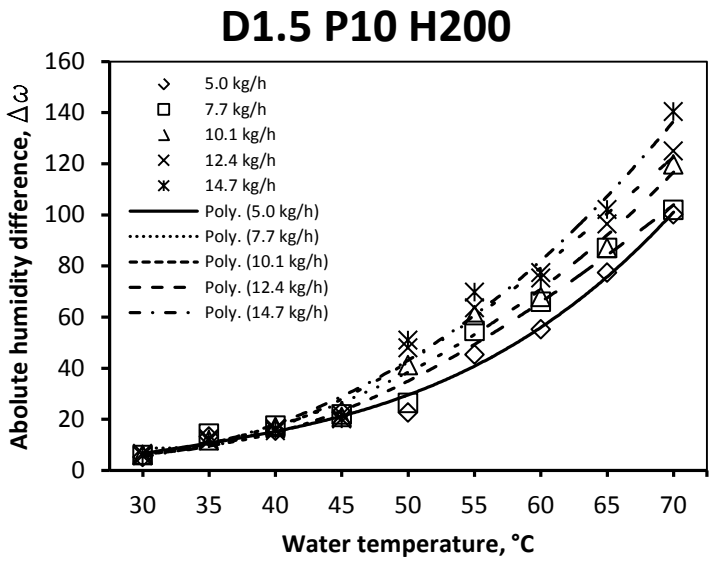

a)

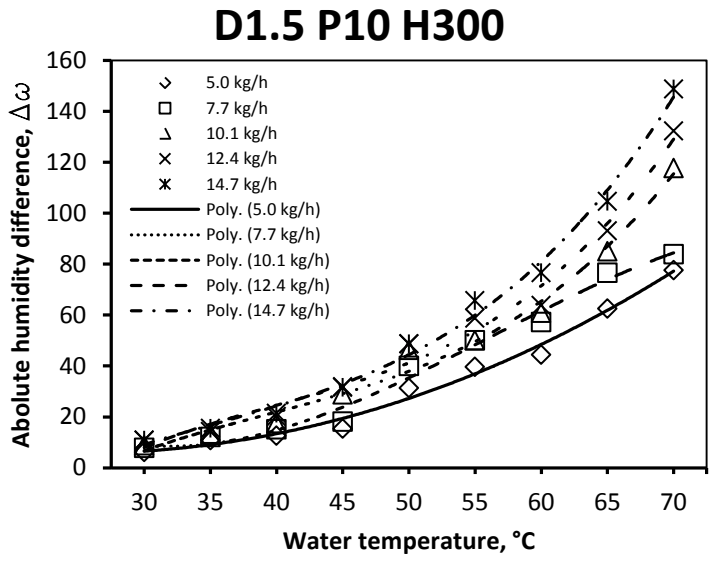

b)

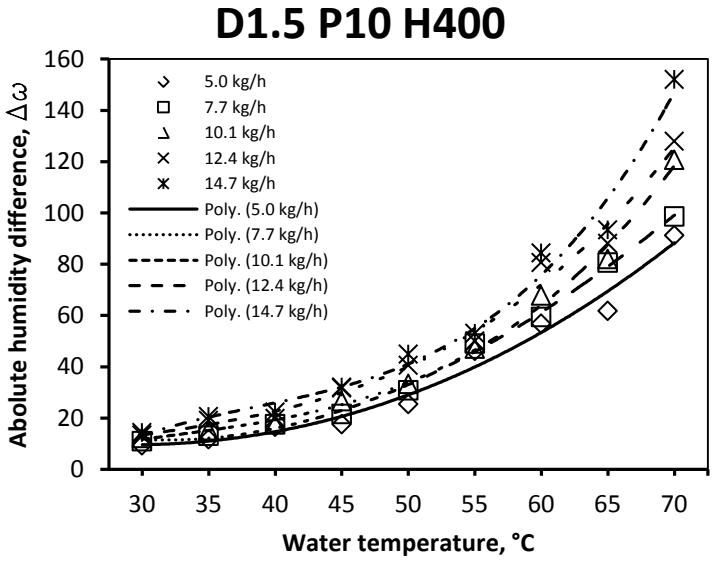

c)

Figure 4.9 Absolute humidity changes with respect to water temperatures

4.4.3 Efficiency and effectiveness

Equation 3.1 was used to obtain the humidification process efficiency. Figure 4.10 plots the humidification efficiency vs. temperature under different operating conditions. Similar to the relative humidity curves it can be seen that the humidification efficiency at lower flow rates outperforms the efficiency at higher flow rates in Fig. 4.10a and Fig. 4.10b. However in Fig. 4.10c, with water level of 400mm, the humidification efficiency at high flow rates outperforms that of lower flow rates for temperatures less than 55°C. It can be seen that in Fig. 4.10a and Fig. 4.10c there are two deflection points indicating two regime changes. However, Fig. 4.10b shows one deflection that indicates a single regime change.

The similarity of the relative humidity and the efficiency curves is not a coincidence. It is an expected result of the tests performed in a laboratory environment with almost constant inlet relative humidity at low temperature. This indicates that if air at the outlet of the humidifier approaches saturation point, using Eqn. 3.1 would result in 100% efficiency of the system. However, the result could be deceiving if the outlet air temperature of the air was less than the water temperature, which is the case as can be seen from Fig. 4.7. For this reason Eqn. 3.5 was taken into consideration in order to indicate the performance of the system relative to the maximum performance it can reach.

Figure 4.11 shows the performance results of the system under different water levels. According to the figure, the performance of the system, or the humidification effectiveness, does not exceed 60% level at its best. Moreover, it can be observed that the performance of the system is greater at higher air mass flow rates. It is

obvious as well that performance of the system is almost constant at any temperature except at very low temperatures in the case of low water level of 200mm.

Figure 4.12 illustrates a comparison of the calculated air absolute humidity difference for the entire experiment. The given graphs plot $\Delta\omega$ under the effect of each parameter (ie. Water levels and temperatures, pitch distances, and mass flow rates)

It can be concluded that the humidifier performed best at higher water levels and temperatures, higher air mass flow rates, and at orifice pitch distance of 10mm.

In order to improve the humidification effectiveness of the unit, a crucial modification is needed. The next section presents suggested modification that boosted the humidification effectiveness of the humidification unit.

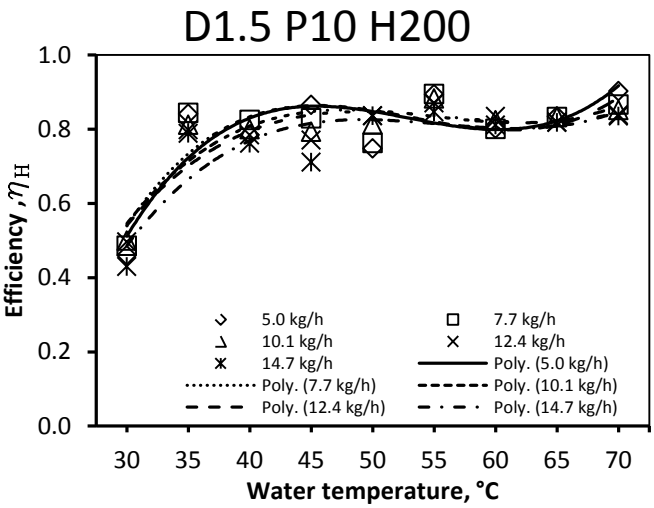

a)

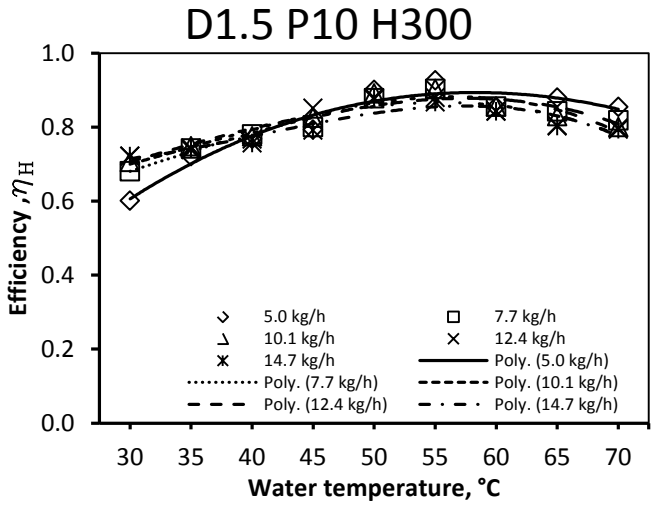

b)

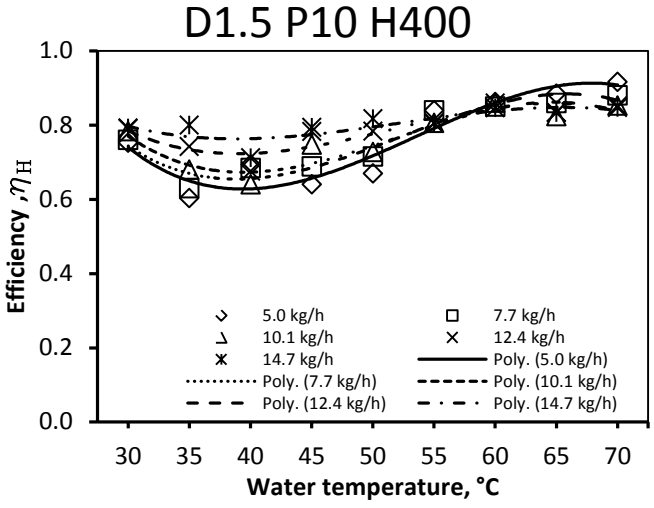

c)

Figure 4.10. Humidifier efficiency vs. water temperature

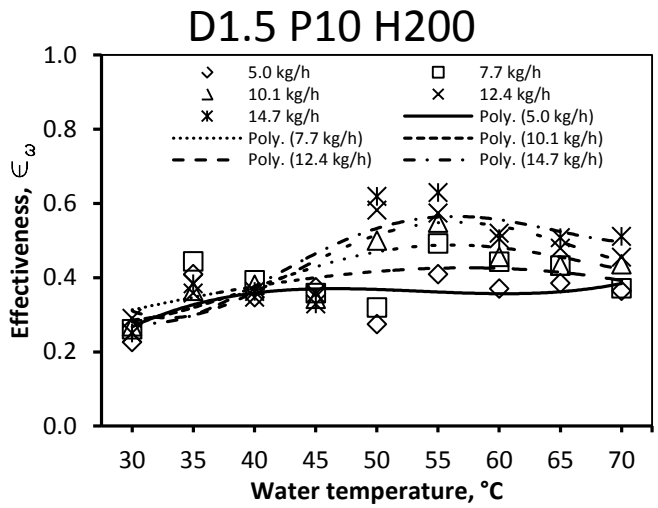

a)

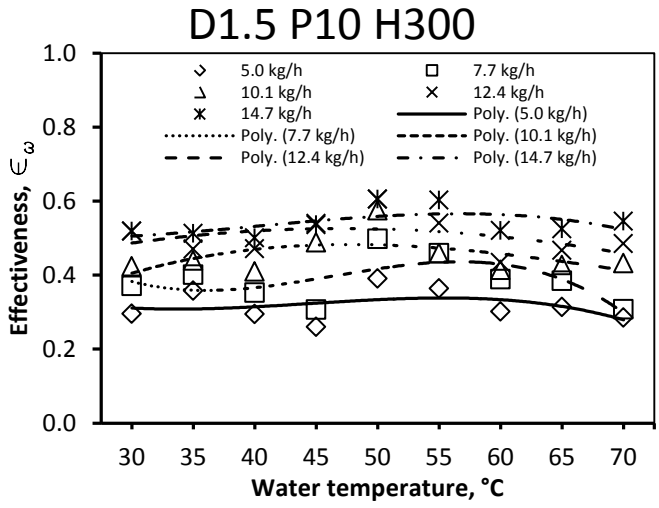

b)

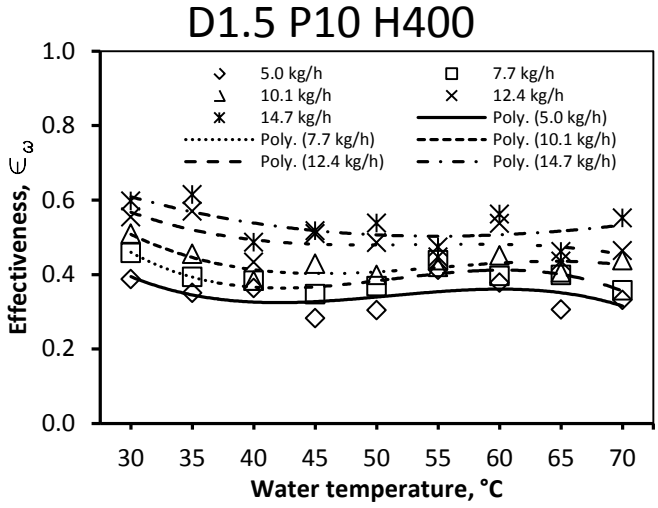

c)

Figure 4.11. Humidification effectiveness vs. water temperature

Figure 4.12 performance of the humidification unit, in terms of absolute humidity difference under different parameters

Figure 4.12 performance of the humidification unit, in terms of absolute humidity difference under different parameters. (A3 page)

4.5 The modified bubble column

From the available literature and the above discussion, one can conclude that; in a humidification process of any flow regime, the effectiveness of the humidification process is poor but increases with the increasing flow rates. Moreover the higher water levels may enhance the humidification effectiveness. On the other hand, bubble coalescence may increase or decrease the heat and mass transfer.

Whether the bubble coalescence increases or decreases the heat and mass transfer, designing for controlled bubble coalescence and brake up may enhance the humidification performance. Adding a number of bubble regeneration stages upstream of the sparger results in resizing the bubbles. It can provide more time for heat and mass transfer to take place as well, thus enhancing the humidification process.

In order to achieve the resizing of bubbles multi stage bubble generator was implemented by adding converted perforated trays (sieves) as shown in Fig. 4.13. The ascending air bubbles from the sparger collapse under the first sieve and create air pocket before escaping through the sieve holes as regenerated bubbles to travel in the contained water before they collapse again under the next sieve. The sieves are each perforated until the middle and placed transversely as shown in Fig 4.14. The process is repeated at each sieve.

a)

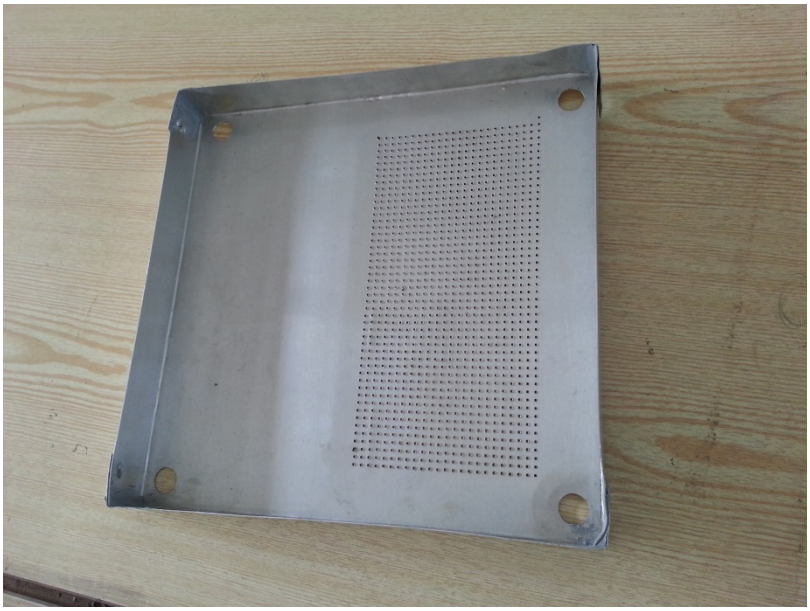

b)

Figure 4.13. a) the perforated sieve, b) the modified humidifier with 8 sieves configuration.

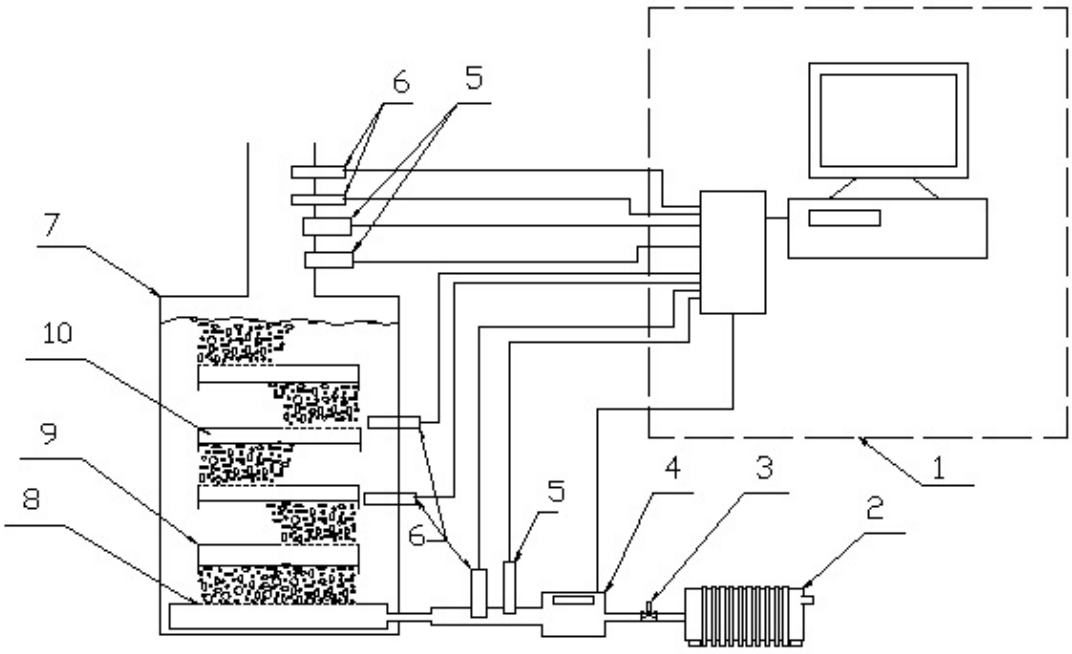

1)Data acquisition system 2) compressor 3)pressure control 4)flow controller 5)thermocouples 6) humidity sensor, 7)humidifiyng chamber, 8)sparger, 9)perforated seive tray 10) air pocket.

Figure 4.14. The modified humidifier testing unit

The main expected advantages of the stack of inverted sieves are as follows:

- air is held for longer periods under the inverted sieves than it would otherwise be held in water as it is freely travelling in the basic setup, thus more time is provided for heat and vapor transfer into the air bubbles.
- air comes into contact with the absorber itself (i.e., the inverted sieves), thus heat transfer takes place more effectively and the air temperature approaches to that of the sieves. High temperature causes air expansion, thus increasing its vapor carrying capacity.
- air bubbles are regenerated at each stage, thus the size of the bubbles are kept relatively smaller maintaining higher contact surface area.

4.5.1 Apparatus setup and procedure

Except for the introduced converted sieves, the rest of the setup is as of the main testing setup. The procedure followed is unchanged too. At water levels of 200mm, 300mm, and 400mm, 4, 6, and 8 converted sieves where used respectively. The base-to-base distance between each of the sieves was 50mm. Thus the last sieve for each testing level was at the same relevant water level.

4.5.2 Results and discussion

The performed test resulted in fully saturated air at any temperature, air mass flow rate, and water level. This result means that 100% humidification efficiency was attained. But this doesn't mean that the maximum performance of the humidifier was reached unless the thermal efficiency (temperature-dependent effectiveness Eqn. 3.2) was at its maximum as well.

Figure 4.15 presents the outlet air temperature vs. water temperature from the performed tests. It is expected that the outlet air temperature would be enhanced by the introduced sieves. It is interesting to note that the outlet air temperatures from the tests where 8 sieves were used became equal to the water temperature at any flow rate. This means that the thermal efficiency has reached the maximum, and thus the effectiveness of the humidifier is at its maximum.

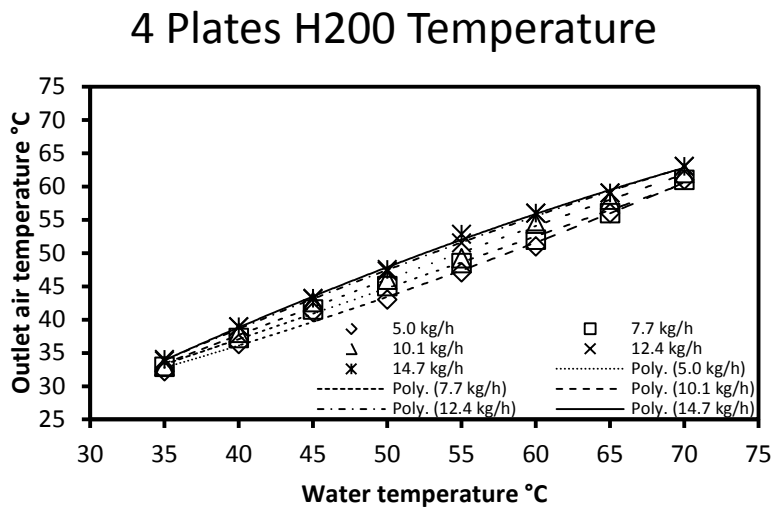

a)

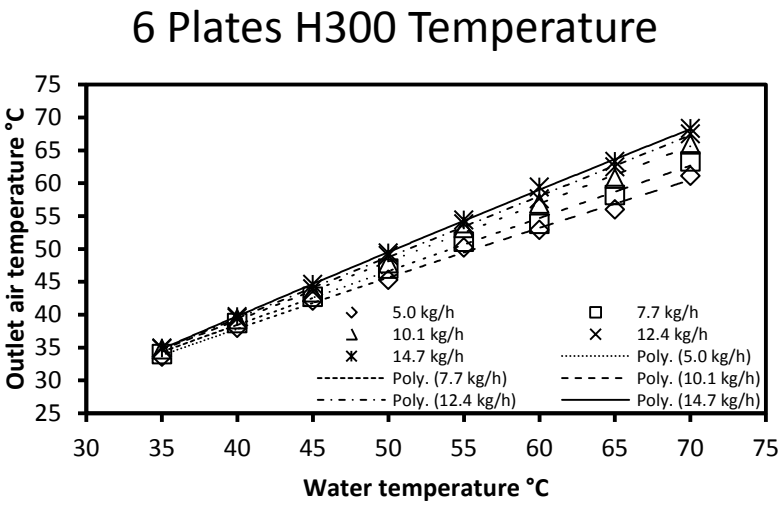

b)

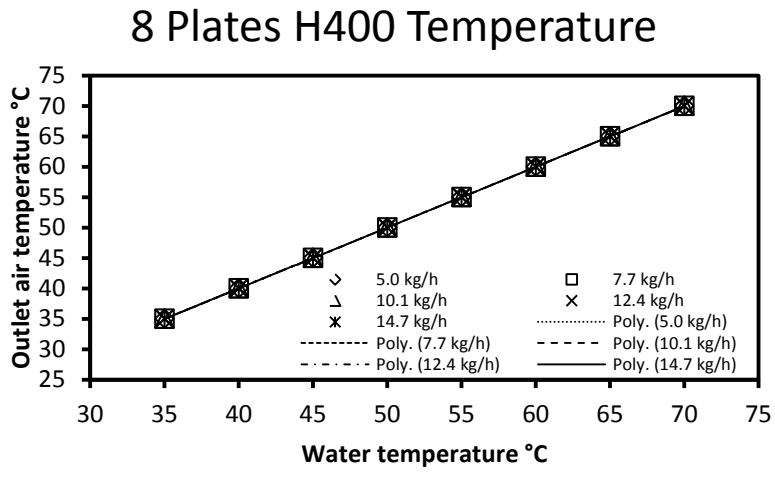

c)

Figure 4.15. Temperature variation of the outlet air with bubbles regeneration

Figure 4.16 presents the thermal efficiency calculated using Eqn. 3.2. Fig. 4.16 shows the high performance attained as a result of using the bubble regeneration concept in such humidifiers. In the case of 4 sieves the thermal efficiency reaches its maximum 90±2% at higher flow rates, but it is lower for lower flow rates. In the case of 6 sieves the thermal efficiency approaches unity at high flow rates, and decreases with lower flow rates. However, the thermal efficiency of the system is unity for the case of 8 sieves at any flow rate; with fully saturated air at the outlet, the effectiveness of the humidifier should reach to its maximum.

Figure 4.17 compares the effectiveness of the humidifier for the three cases. In the case where 4 sieves were used, the effectiveness of the system reaches its maximum at low temperatures and high flow rate. The same applies for the case of 6 sieves but with relatively higher values. However, the system reaches its maximum performance at any temperature and any flow rate in the case where 8 sieves were used.

The decreasing in effectiveness vs. water temperature for 4 and 6 plates are presented in Fig. 4.17a and Fig. 4.17b does not mean that the productivity of the system is decreasing too. It is simply an indication that air could not extract the maximum possible amount of vapor under the testing conditions. Moreover, Fig. 4.17 shows the benefit for using sieves for bubble regeneration, i.e., the effectiveness increases as the number of sieves were increased. It proves the whole concept of bubble regeneration. Obviously the system reaches its maximum productivity by optimizing the number of stages under which collapsing and regeneration of bubbles take place.

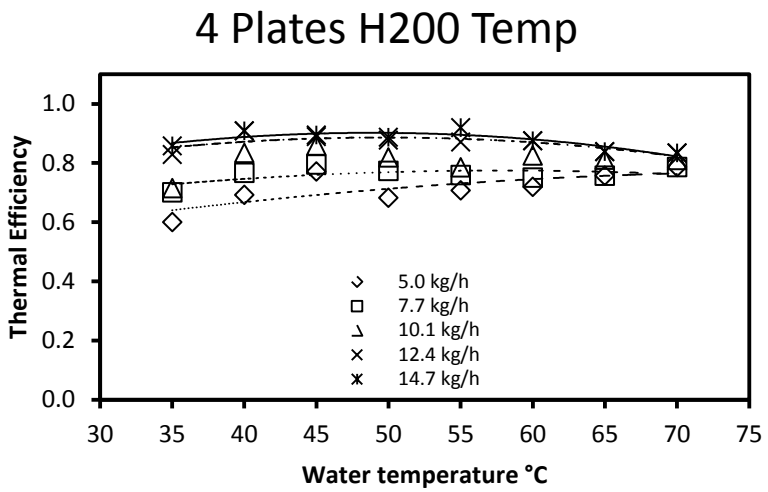

a)

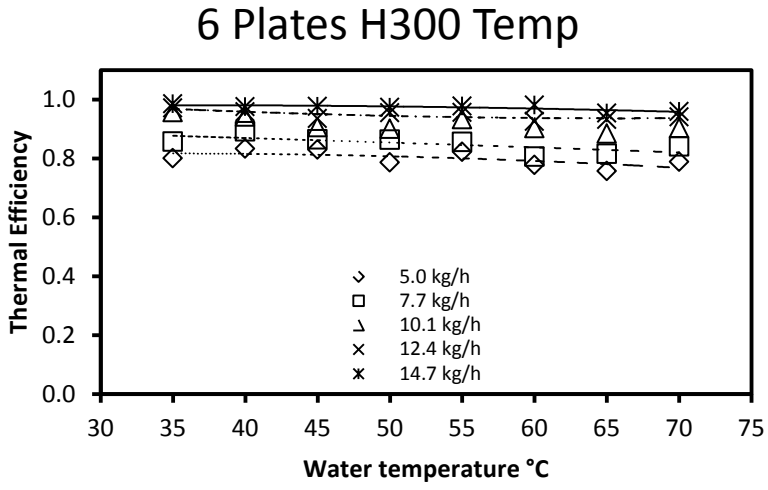

b)

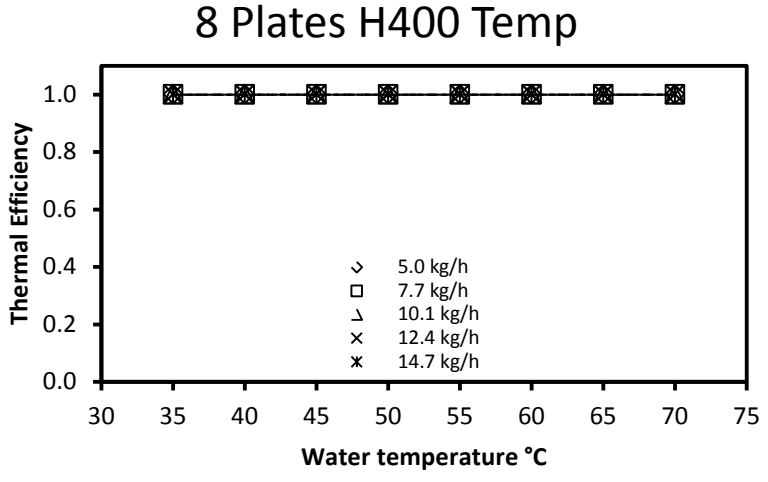

c)

Figure 4.16. Thermal efficiency of the humidification unit with bubbles regeneration

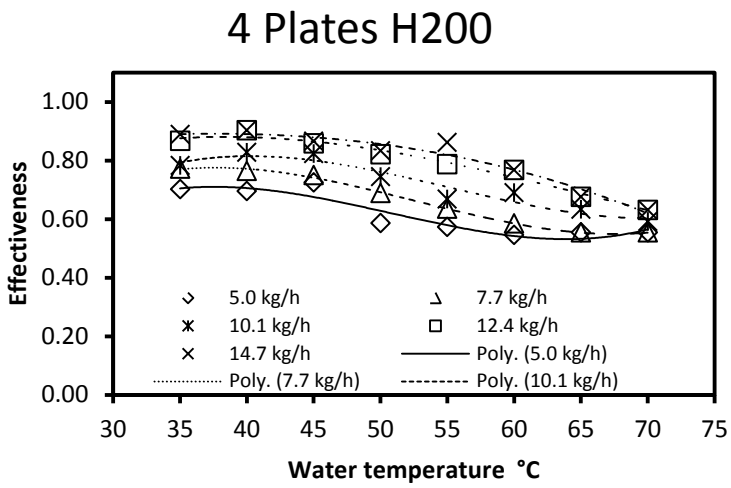

a)

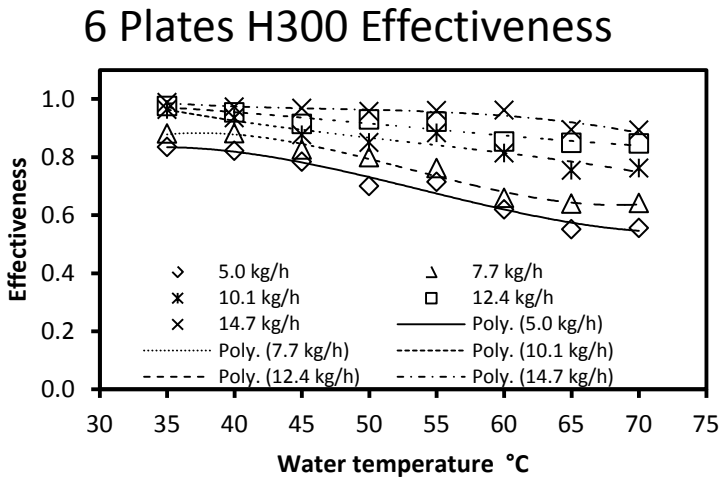

b)

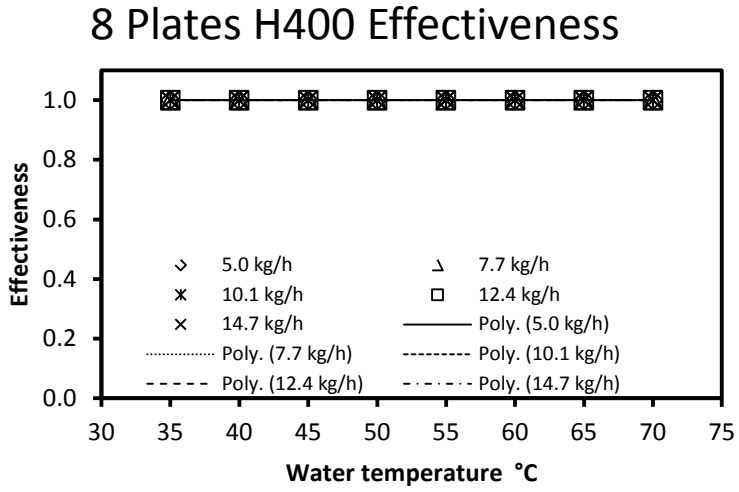

c)

Figure 4.17. Effectiveness of the humidification unit with bubbles regeneration

Figure 4.18 illustrates the productivity of the system as the amount of the vapor extracted by air throughout the test. It is well known that the vapor carrying ability of air is exponentially related to its temperature. Thus the amount of extracted vapor in the test is expected to increase exponentially with the increase in temperature of water and thus the air temperature.

Figure 4.19 summarizes the effect of using the sieves on the amount of extracted moisture. It compares the system's productivity in the case of the highest productive sieve-less test of D1.5 P10 H400 with the cases in which different number of sieves where used. The figure shows that at water level of 200mm with 4 sieve plates (4PH200) the extracted vapor is greater than that of the sieve-less case of D1.5 P10 H400 at any temperature. Moreover, comparing the cases where the same water level was used, the case of 8 sieve plates (8P400) was found to outperform the sieve-less case (D1.5 P10 H400) by 70% at water temperature of 70°C.

Having proved the viability of the system, the solar version was designed constructed and tested.

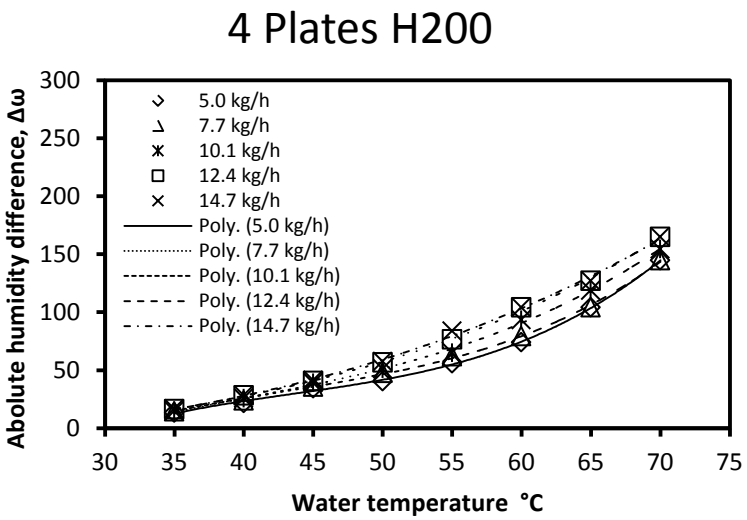

a)

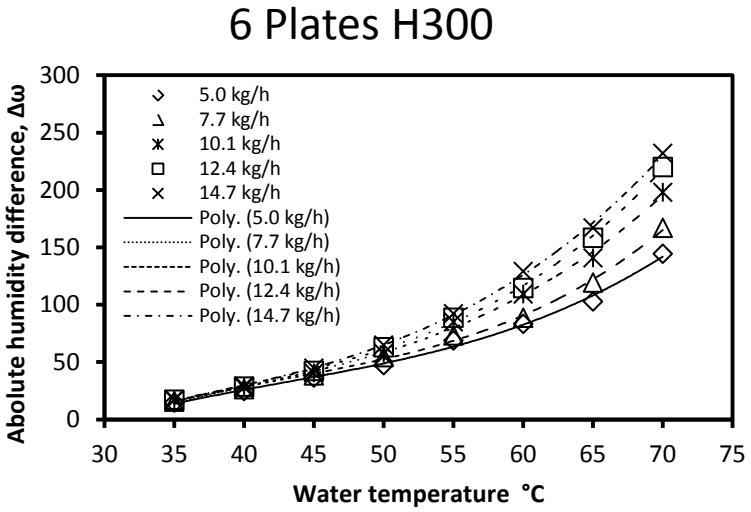

b)

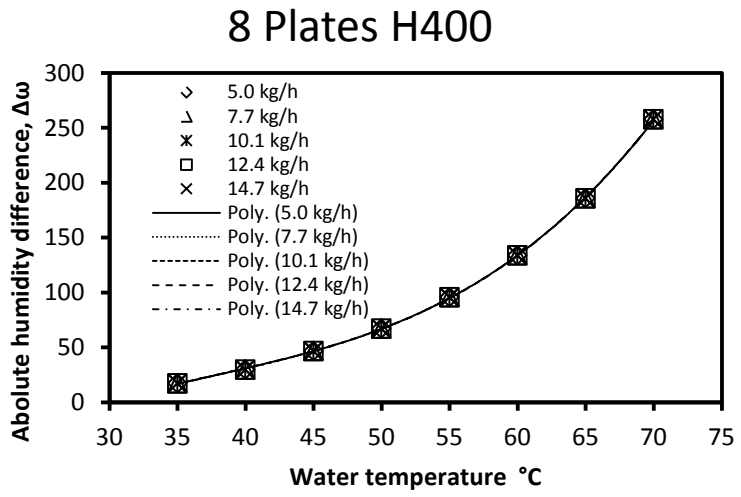

c)

Figure 4.18. Absolute humidity differences between the outlet and the inlet points of the humidifying unit

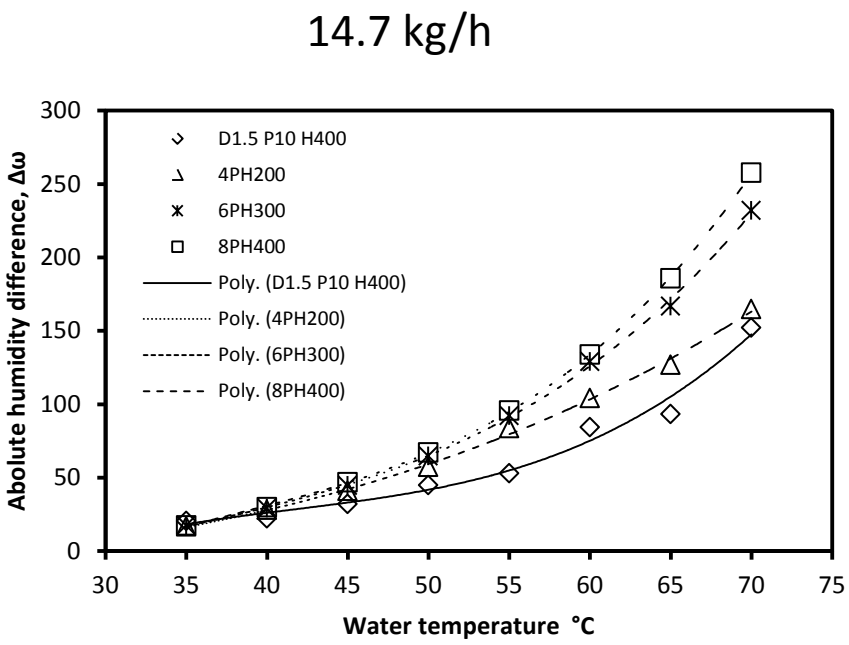

Figure 4.19. Comparison of the absolute humidity difference, between the inlet and outlet of the humidifier, of the best performed configuration of the basic bubble column and the modified column

Chapter 5

5 SOLAR HUMIDIFICATION UNIT

The main goal from the laboratory-based experiment was to have hands on the key characteristics that make the humidification by bubbling appealing. This was possible by addressing the main problems responsible for humidification deficiency and low system effectiveness. Having spotted these main issues, a bright solution represented by the intrusion of inverted sieve plates for bubble regeneration was suggested. The main advantage this system brings is the ability of having efficient humidification in a small humidifier with little amount of water. Since the system is going to take advantage of solar energy for water heating, it is crucial to concentrate the gained energy in order to elevate the water temperature. The experiment stated clearly that the product is exponentially related to the water temperature. Thus, concentrating the solar energy in smaller volume of water increases the quality of such energy and thus the productivity for the same amount of energy. Where, it is not the quantity, but the quality of energy that matters in such systems.

In this chapter the solar HDD system with its building stages is presented. Firstly the solar humidifier is considered alone before discussing the whole system.

5.1 Solar Heating and Humidification

It is important mentioning that the forerunner technique of the solar HDD systems is the solar still which has had limited use in industry, due to its poor process efficiency

and energy losses. The overall deficiency of the solar still results from the fact that all functions of the system take place in one single component which leads to huge loss of latent heat of condensation through the glass cover which cannot be recovered. When the evaporation, condensation and the heating processes are carried out in different units the overall efficiency is increased and the HDD system becomes economically attractive (Al-Hallaj et al., 2006; Yuan et al., 2011).

The main objective of this experiment is to investigate experimentally the feasibility of merging the processes of the water heating, the air heating, and the humidification into one compact unit with the condensation process kept separate (Fig. 5.1). The humidification system should implement the bubbling technique which was discussed in the previous chapter. It is also aimed to build two different configurations and compare them with the basic setup in order to test the ability of enhancing the effectiveness of the humidifier bed.

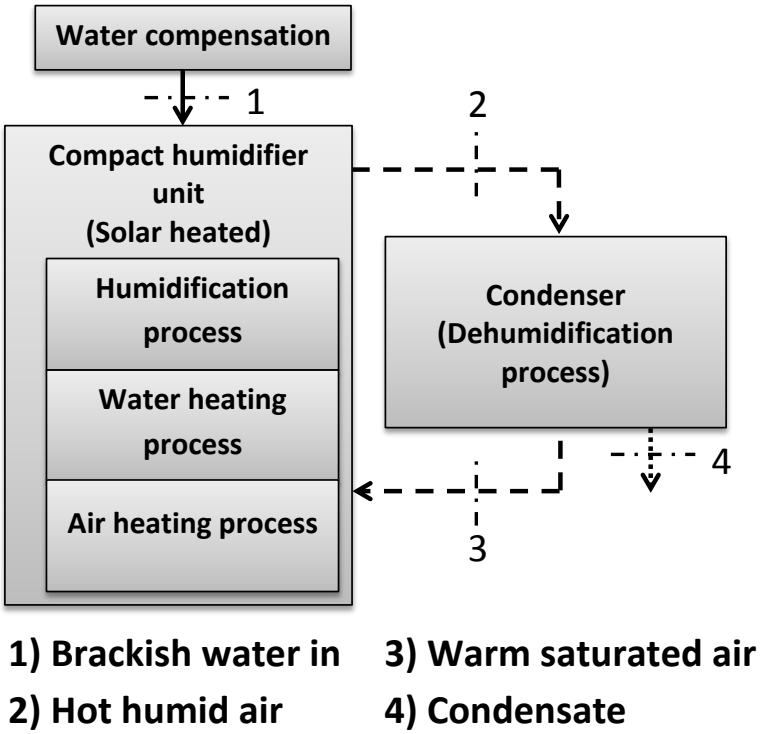

Figure 5.1. The proposed humidifier schematic diagram

5.2 Test apparatus

A compact solar humidifier which also houses the solar air and water heating processes was designed and manufactured in the Department of Mechanical Engineering at the Eastern Mediterranean University. The unit is filled with water and the air is driven from the bottom by the use of a compressor. Figure 4.2 shows the scheme of the experimental setup together with the instrumentation to monitor the performance. Three configurations of the compact humidifier unit have been tested. These are; setup 1, where the unit is filled with brackish water and the air is charged through it, which is also referred to as the basic setup; setup 2, which is the basic setup with the addition of the air bubbles-regenerative fins (inverted sieve plates); and setup 3 incorporates a reflective mirror to setup 2.

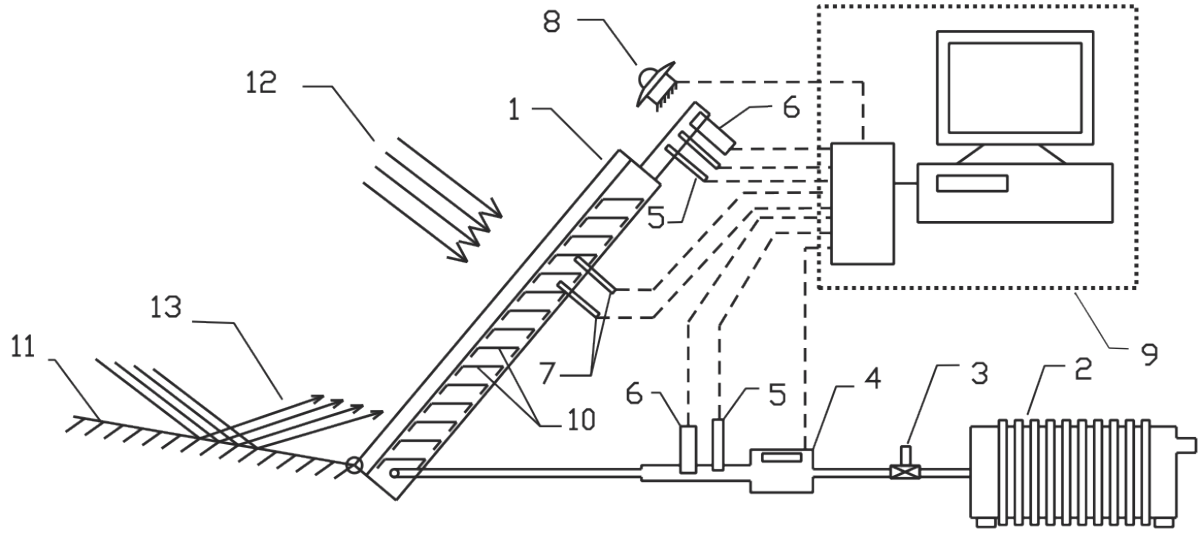

1) Humidifier, 2) Compressor, 3) Pressure controller, 4) Flow controller, 5) Thermocouples, 6) Humidity sensors, 7) Embedded thermocouples, 8) Pyranometer, 9)Data acquisition system,10) Converted bank of sieves (used in setups 2 & 3), 11) Reflector mirror (used in setup 3), 12) Direct solar radiation, 13) Reflected solar radiation.

Figure 5.2. Schematic diagram of the experimental setup

The common major components which were used in the three setups are; the humidifier bed, the compressor, and the data retrieving devices (Fig.5.2). These components are briefly explained as follows:

5.2.1 The humidifier bed

The humidifier bed is constructed by fastening a galvanized metal sheet at the bottom of an acrylic framing and placing glass sheets on the top serving as the aperture. The whole bed was then insulated and enclosed in a wooden box, except the glazed aperture side. The cavity between the glass and the galvanized metal absorber plate is filled with water. The sun light is allowed to penetrate from the glazed-side and through the water to the 2 mm absorber plate. The aperture is double glazed with a glass thickness of 8 mm from inside, in order to withstand the pressure of the water, and 4 mm from outside. The aperture has a width of 50 cm and a length of 100 cm. A half inch diameter and 600 mm long copper pipe was inserted all the way through a hole, that was drilled from one side of the bed, to the opposite side of the bed and

was fixed internally. The pipe had 2 mm diameter holes drilled 10mm apart from each other (center-to-center), along 500 mm of its length. The purpose of this pipe is to generate air bubbles by compressing air through it into the water. The distance between the inner glazing and the absorber plate was 5mm. To allow air exit the system, one inch Plexiglas pipe was attached to a hole in the upper part of the frame. The whole bed was mounted on a metal frame and was tilted at 50° facing south.

5.2.2 Compressor and controllers

An electrically driven two-piston compressor was used to supply air to the system. The compressor was equipped with a 200L storage tank, air flow controller, and pressure controllers to control the air in the tank as well as the inlet air to the system.

5.2.3 Data acquisition and measuring devices

The data collected in this work to study the performance of the humidifier were global solar radiation, air flow rate, water temperature, inlet and outlet air temperatures and humidity. Solar intensity on the surface of the system was measured using a Pyranometer coupled with a digital multimeter. The Eppley radiometer Pyranometer has an accuracy of ±0.5 for the range from 0 to 2800W/m^2. Water temperature was recorded by using two thermocouples, which were connected to an Xplorer GLX data logger. Inlet and outlet humidity and temperatures of the air were acquired using an Omega Thermo Hygrometer RH411 with measurement range of 5 to 98% relative humidity and 0 to 49ºC Temperature. The measurement accuracy of the hygrometer is specified as ±0.8ºC for temperature and ±3% for relative humidity. The air flow rate was measured using a hot wire anemometer. The Tecpel AVM 714 anemometer has the accuracy of ±3%.

5.3 Experimental procedure and data processing

The experimental setup shown in Fig. 5.2 was used in all experiments. Experiments were conducted in mid-winter by recording hourly data of the solar intensity, water temperature, air relative humidity, and air temperatures at the inlet and outlet of the humidifier unit. The measurements were taken between 9:30 am and 3:30 pm every day for air flow rates of 8.2, 10.4 and 12.6 kg/h. The same procedure was repeated for all humidifier setups, which are described in detail as follows.

5.3.1 Setup 1: The basic design

The humidification process is facilitated by bringing the unsaturated air (i.e. air bubbles) into contact with water in order to enable the saturation of air. In the most basic arrangement of the proposed humidifier, the cavity between the lower glass and the metal plate is filled with water, into which air bubbles are fed in as can be seen in Fig. 5.3. If the air bubbles do not join to form larger volumes of air as they freely travel through still water in the cavity, it will be possible to maintain maximum contact surface area with hot water, leading to increased mass transfer rate of water vapor into the air movement.

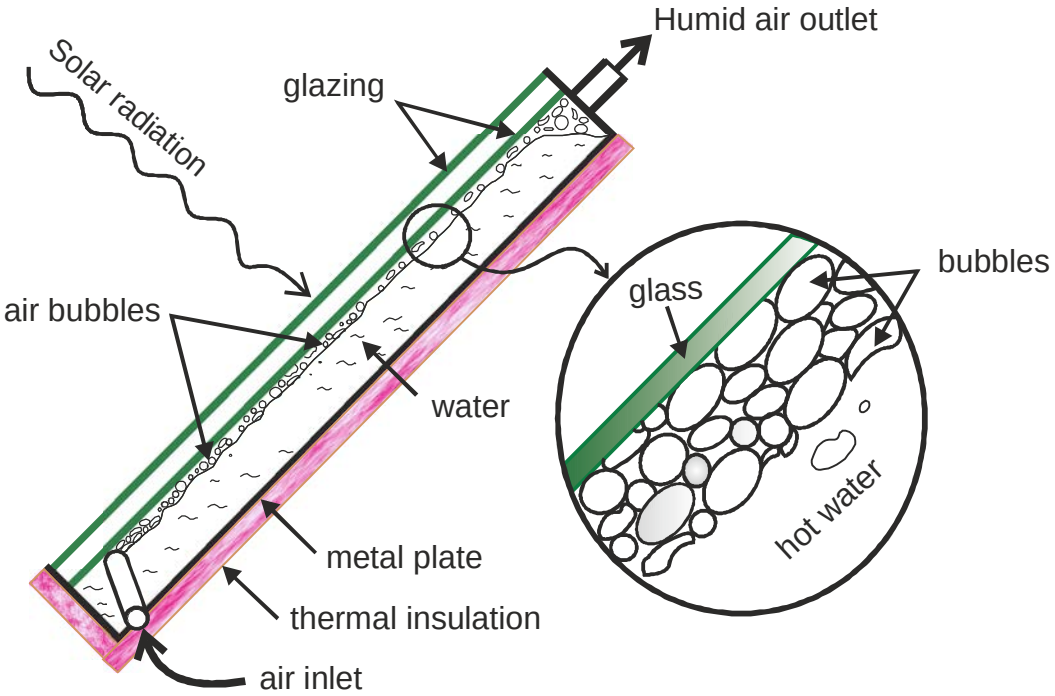

Figure 5.3. The cross-sectional view of Setup 1 showing the process

The air is injected into the water by means of a compressor. Air passes through several holes drilled on a pipe, immersed in water at the bottom of the humidifier turning into bubbles which then ascend vertically under the buoyancy effect. The main energy source utilized (i.e. energy used for water and air heating) is solar energy. The evaporation chamber is merged into the solar collector to serve as one unit. In other words, water and air heating and humidification processes take place in the same inclined chamber. The south facing bed allows the solar energy to penetrate through the glazing and fall onto the black painted absorber plate. The absorber in return transfers the absorbed heat to the contained water increasing its temperature. The hot water, not only transfers heat to the rising air bubbles, but also transports water mass in the form of vapor.

5.3.2 Setup 2

The major difference of setup 2, in comparison to setup 1, is the introduction of black painted 15 inverted stainless steel sieves which are designed to act as absorber and bubble regenerator (Fig. 5.4). The ascending air bubbles from the inlet copper tube meet the first sieve where they collapse and create air pocket before escaping through the sieve holes as regenerated bubbles to travel in the contained water before they meet the next sieve. The process is repeated at each sieve as can be seen in Fig. 5.5.

Figure 5.4. A stack of Inverted sieves (heat absorber and bubble regenerator)

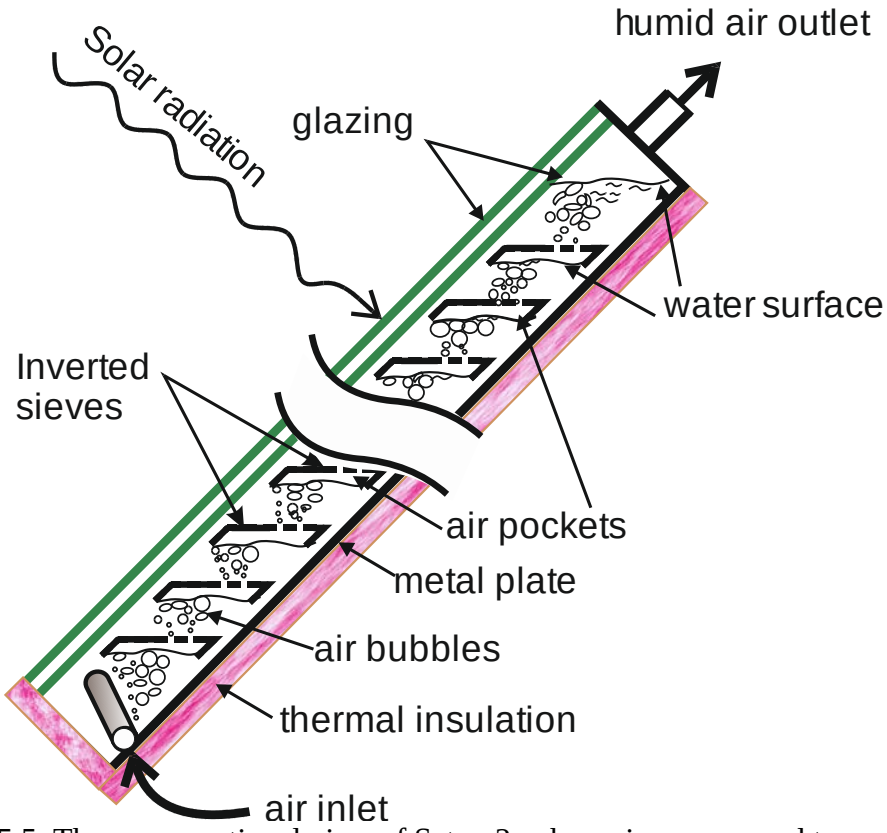

Figure 5.5. The cross-sectional view of Setup 2, where sieves are used to regenerate bubbles

The pitch distances of the orifices located on the sieves are configured according to the findings in the previous chapter as 10mm. The custom made sieves have approximately 300 holes with diameters of 1.5 mm drilled along the rear top side of the sieves. The main advantages of the stack of inverted sieves are given as:

- air is held for longer periods under the inverted sieves than it would otherwise be held in water as it is freely travelling in the basic setup, thus more time is provided for heat and vapor transfer into the air bubbles.
- air comes into contact with the absorber itself (i.e., the inverted sieves), thus heat transfer takes place more effectively and the air temperature approaches

to that of the sieves. High temperature causes air expansion, thus increasing its vapor carrying capacity.

- air bubbles are regenerated at each stage, thus the size of the bubbles are kept relatively smaller maintaining higher contact surface area.

5.3.3 Setup 3

In setup 3, a reflector mirror is added to the arrangement of setup 2. This arrangement can be seen in Fig. 4.2. A $1m^2$ mirror was attached horizontally to the bottom of the humidifier bed in order to reflect extra solar energy on the aperture area.

5.3.4 Data processing

The absolute humidity is estimated by measuring the air temperatures and the relative humidity at the inlet and exit of the humidifier. The measurements are taken by the Hygrometer. The data is processed by a computer program that utilizes thermodynamic tables to find the corresponding saturated vapor pressure of air at different temperatures. The following relation is found by curve fitting technique as a perfect fit for temperature range from 5°C to 50°C with R^2=1 and a standard deviation σ = 0:

$$P_g(T) = A * T^3 - B * T^2 + C * T + D \quad (5.1)$$

where the constants *A, B, C*, and *D* are: 0.00008, 0.0008, 0.0761, and 0.4836 respectively. The following thermodynamic relation can be used to relate the vapor partial pressure and the relative humidity to the absolute humidity:

$$\omega = \frac{0.622\mathrm{Pv}}{P-\mathrm{Pv}} \quad (5.2)$$

Knowing that $P_v = \emptyset * P_g$, The characteristic equation can be written in the following form:

$$\omega = \frac{0.622*\emptyset*(A*T^3 - B*T^2 + C*T + D)}{P - (\emptyset*(A*T^3 - B*T^2 + C*T + D))} \quad (5.3)$$

Then the difference between the inlet and outlet values of absolute humidity is calculated to give the increase in water vapor content in air through the process.

Productivity of the system is found by multiplying the flow rate by the average humidity difference between the inlet and the outlet of the humidifier:

$$PR = \dot{m} * \Delta\omega_{av} \quad (5.4)$$

The independent variables in the characteristic equation are the temperature and the relative humidity. Employing the uncertainty expression from Eqn. 3.9 to the characteristic equation gives:

$$U_\omega = \left[\left(\frac{\partial\omega}{\partial T}\right)^2 U_T^2 + \left(\frac{\partial\omega}{\partial\emptyset}\right)^2 U_\emptyset^2\right]^{1/2} \quad (5.5)$$

where;

$$\frac{\partial\omega}{\partial T} = \frac{0.622*P*\emptyset*P_g'(T)}{\left[P - (\emptyset*P_g(T))\right]^2} \quad (5.6)$$

and;

$$\frac{\partial\omega}{\partial\emptyset} = \frac{0.622*P*P_g(T)}{\left[P - (\emptyset*P_g(T))\right]^2} \quad (5.7)$$

Likewise, the uncertainty in the productivity of the system is found by applying the same method to the productivity equation:

$$U_{PR} = \left[\left(\frac{\partial PR}{\partial\dot{m}}\right)^2 U_{\dot{m}}^2 + \left(\frac{\partial PR}{\partial(\Delta\omega_{av})}\right)^2 U_{\Delta\omega_{av}}^2\right]^{1/2} \quad (5.8)$$

Then the fractional uncertainty is estimated by dividing each uncertainty by the corresponding result from the related equations. The fractional uncertainty of the absolute humidity and the productivity are found to be 0.0632 and 0.0707 respectively.

5.4 Results and discussion

Figure 5.6 displays the hourly relative humidity measured at the inlet and outlet of the humidifier for an air flow rate of 8.2 kg/h on a typical winter day. Although the relative humidity at the inlet was different for each day, the relative humidity at the outlet for all the setups was almost 100%. This result is deceiving since it shows no real effect on the modifications done to the basic design on the productivity of the system. It can be noted that the air humidity at the outlet was not affected by the inlet conditions. This shows that the performance objectives are substantially met.

Figure 5.7 displays a plot of the irradiance, the inlet and outlet temperatures of air, and the water temperature measured during the experiment. It can be seen that in the basic design there is a significant gap between the outflowing air temperatures and water temperatures. In setups 2 and 3, the air temperatures at each hour have almost reached the same values as the water temperatures. The air temperature cannot exceed the water temperature in the collector, as heat is transferred from water to air. In terms of heat transfer this is the ideal result that can be achieved in the design of heat exchangers. This result is desired since the vapor carrying capacity of air is increased as its temperature is increased provided air is under constant pressure.

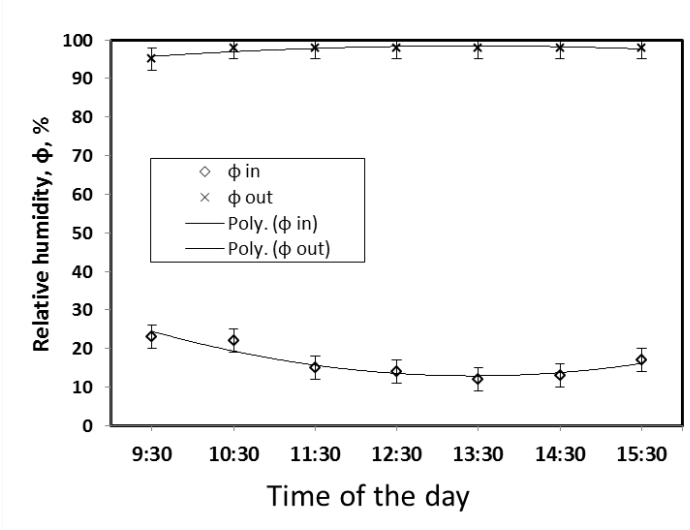

(a)

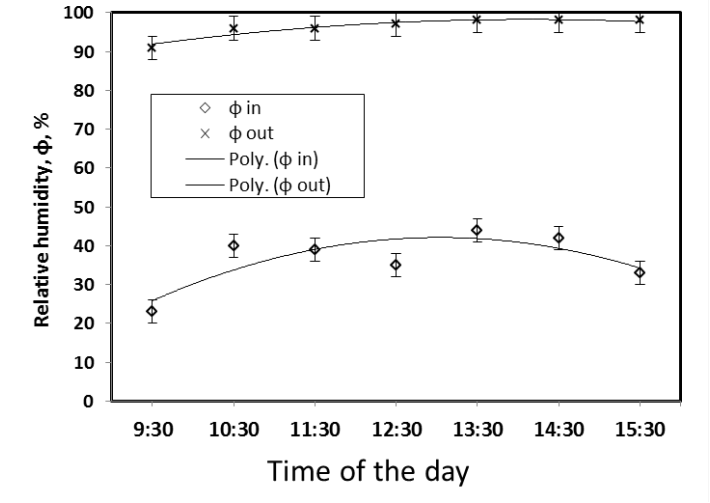

(b)

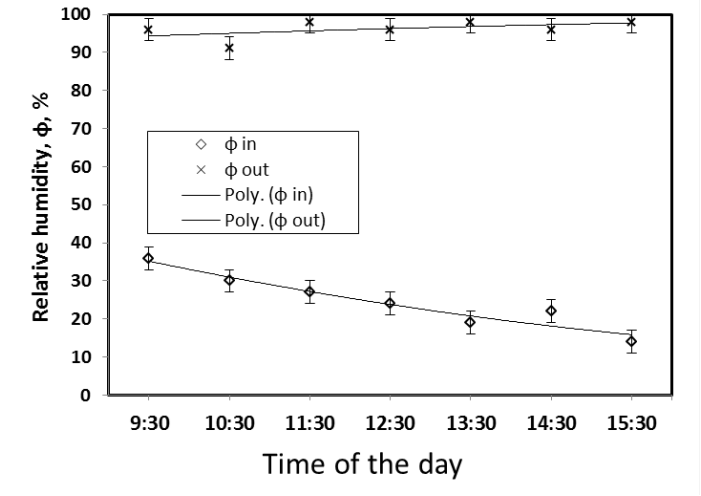

(c)

Figure 5.6. The inlet and outlet relative humidity of air for different setups at a flow rate of 8.2 kg/h. a) setup 1, b) setup 2, c) setup 3

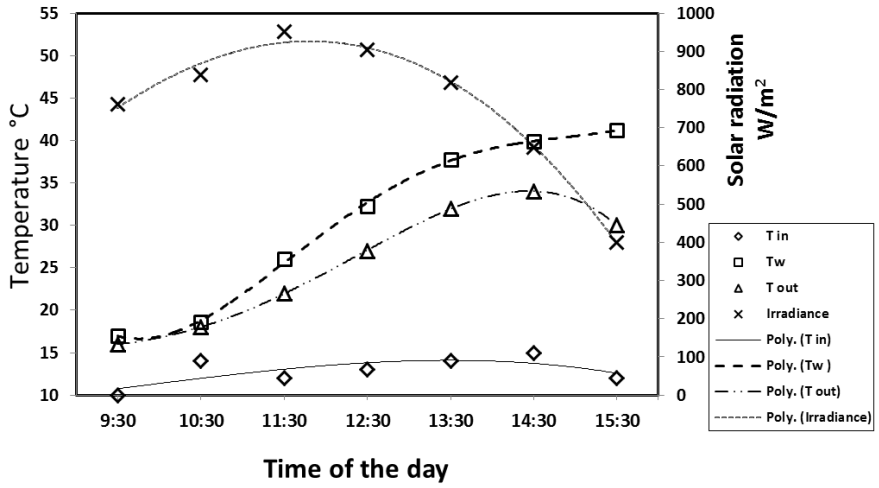

(a)

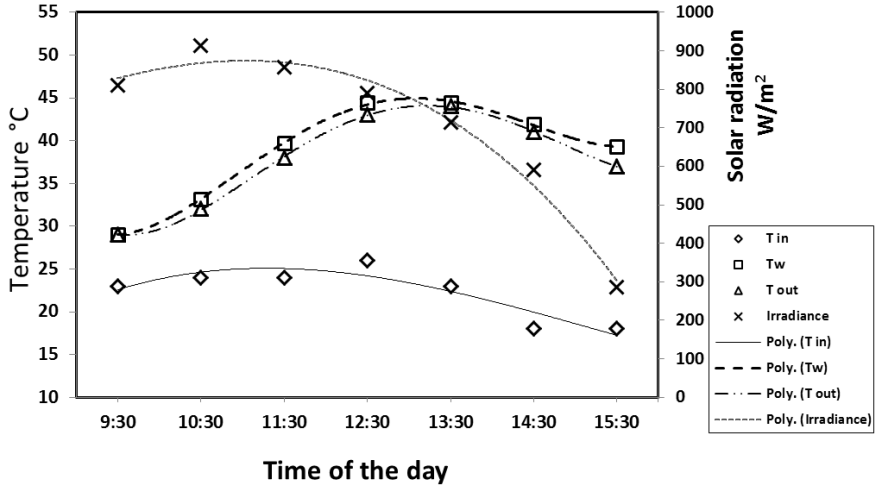

(b)

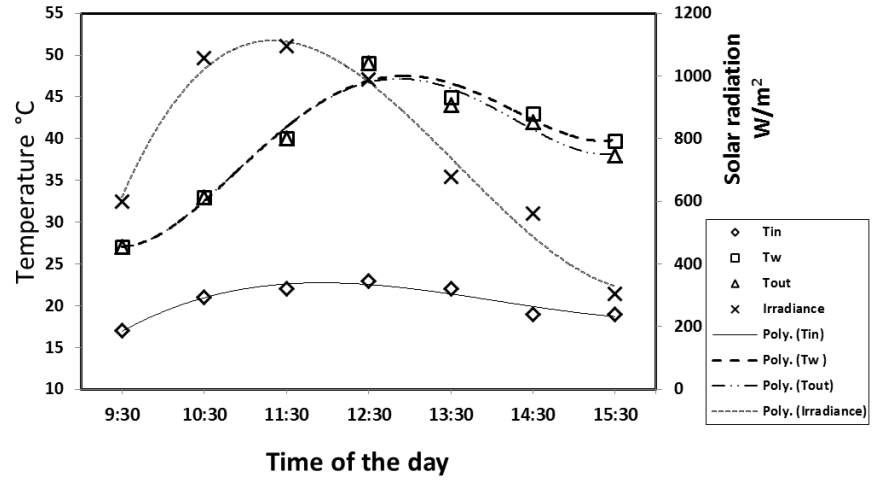

(c)

Figure 5.7. The effect of the improved design on the outlet temperature of air for air flow rate of 8.2 kg/h. a) setup 1, b) setup 2, c) setup 3

The effect of higher outlet air temperatures on the productivity manifests itself by the increase in the effectiveness of the humidification which is illustrated in Fig. 5.8.

In the basic setup the efficiency of the humidifier was recorded to be between 95 and 100%. The maximum temperature that air can reach was not taken into account in the efficiency calculation (refer to Eqn. (3.1)), and therefore, the actual maximum vapor carrying capacity of air was not considered. Similar levels of efficiency were obtained with the other configurations. However, the effectiveness defined by Eqn. (3.5) implied that setups 2 and 3 performed better than the basic setup. The effectiveness of the basic setup fell sharply (see Fig. 5.8(a)) as a result of the increasing gap between the outlet air temperature and the water temperature through the day.

Figure 5.8 depicts the effect of the different configurations on the both the efficiency and effectiveness of the humidification process vs. time of the day. While the efficiency of the humidification process is very high in the basic design, the effectiveness of the humidification process it displays, is relatively lower compared with the other setups. The average effectiveness of the basic design is 70% while it can reach 95-98% for both of the other setups for the same flow rate.

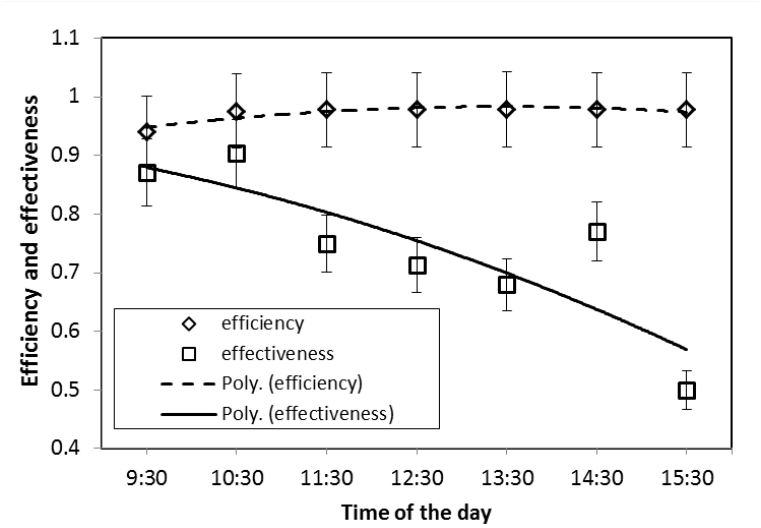

a)

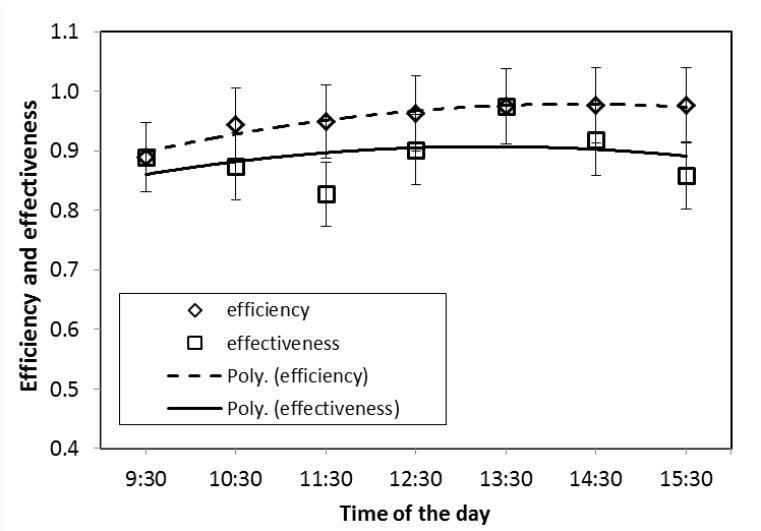

b)

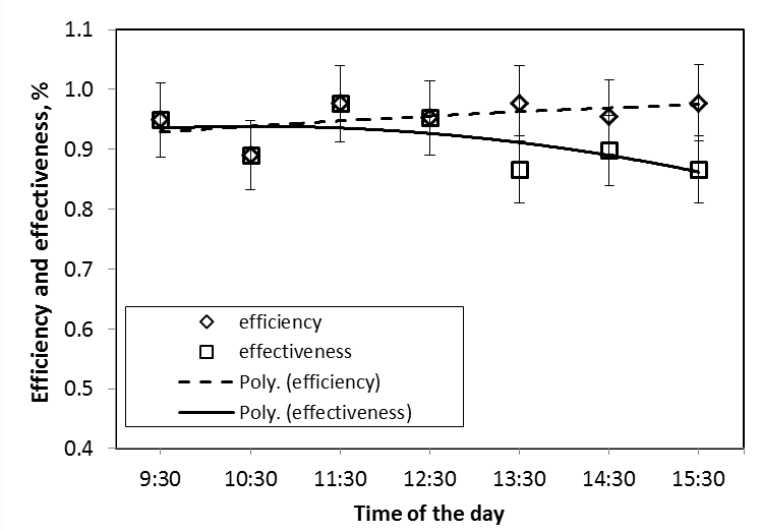

c)

Figure 5.8. The efficiency and effectiveness of the humidification process. a) Setup 1, b) Setup 2, c) Setup 3

The effect of the high effectiveness of the humidification process reflects higher productivity of the modified systems compared to the basic one. Figure 5.9 illustrates the moisture content differences between the inlet and outlet air for each setup, for different air flow rates (i.e., 8.2, 10.4, 12.6 kg/h.) The higher moisture content increment in setup 2 and setup 3 is due to the higher temperatures of the air bubbles reached, the smaller diameter of the regenerated bubbles, and as a result of employing a reflective mirror. As air temperature was increased the moisture carrying capacity of the air was also increased. It can be clearly seen that mass transferred is greater for greater flow rates as well.

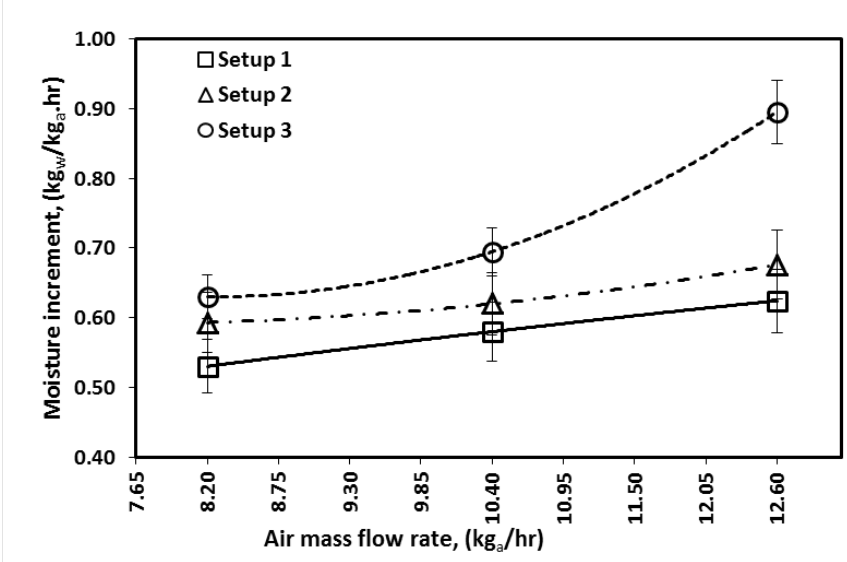

Figure 5.9. The effect of the improved design on the productivity of the system

The normalized gain of the humidifier is potted against its effectiveness in Fig. 5.10. Better performing heaters are expected to be in the top right portion of the graph in Fig. 5.10, where the high latent heat gain is delivered at a high sensible heat gain. From the figure we can conclude that the second setup with bubbles regeneration has a better performance compared to the basic setup. Furthermore, the addition of a

reflecting mirror, as in the third setup, enhances the performance and thus further increases the total enthalpy gain of the humid air.

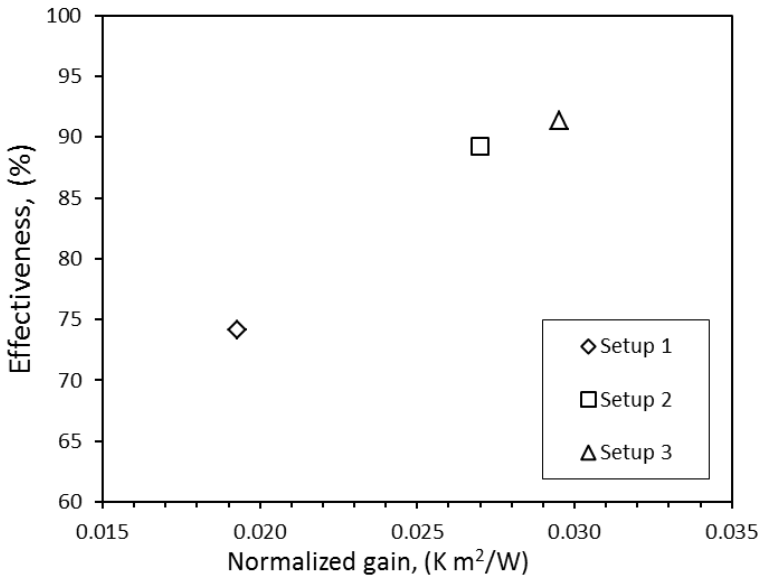

Figure. 5.10. Effectiveness of the three setups plotted as a function of the normalized gain

5.5 Final remarks

In this chapter a novel solar humidification technique incorporating the heating of water, the heating of the air stream and the humidification of air in one compact unit is proposed. The air is driven into the humidification unit in the form of bubbles and the effects of water temperature, bubble coalescence, bubble regeneration, and increased radiation by reflection on its performance have been studied and the following conclusions were reached:

1. Direct contact bubbling humidification is an efficient technique which can be used in solar HDD systems.
2. Employing sieves to act as solar absorbers enhances heat transfer which increases the air temperature and thus the moisture carrying capacity of air.

3. Reflection increases the system's temperature and improves the effectiveness of the humidification process. The absolute humidity of air is increased by 32% for mass flow rate of 12.6 kg/h.
4. The third configuration, as in setup 3, has increased the average effectiveness of the humidification process from 75% to 90%.

In the next chapter, a complete HDD system will be introduced and tested for productivity and performance.

Chapter 6

6 SOLAR HDD SYSTEM – THE COMPLETE SYSTEM

In this chapter, a case study of the complete HDD system comprising the developed humidification unit and a condenser for fresh water harvesting is presented.

The humidifier is further improved in the complete system with some key differences. Similar to the previous one, the humidifier is a three in one system in which water and air are heated while vapor is transferred to the air due to the direct contact of air with water in the unit. Thus, the main approach is kept. However, the design of the humidification unit has encountered some changes.

6.1 The humidifier design

Three main modifications have been made to the design presented in chapter 5. Firstly, in the new design the humidifier bed is rotated 90° in order to decrease the head against which the pump does work. Secondly, this is accompanied by placing the baffles in transverse order as can be seen in Fig. 6.1. As a result the air mass flow rate in the system has increased for the same air pump.

The third modification is the replacement of the glass cover. In the previous design two glass covers were used. The inner glass cover which was in contact with water was replaced by a stainless steel sheet to eliminate algae formation. The new cover

can withstand higher air pressure that can build up as a result of any flow constraints at the outlet or downstream of the humidifier.

The humidifier is still a closed container but with three ports. Two of the ports are for the inlet and outlet of air and the third is for water addition and compensation. The inner dimensions of the container (stainless steel tray) are given as 1 meter by 0.5 meter and 5 cm deep, as of the previous design but rotated by 90°. The stainless steel cover is secured to the tray and sealed in order to prevent any water leakage during its usage as it is tilted. The cover, in this case, acts as an absorber that receives the solar energy and conveys it to the inner region. Attached to the cover there are 8 perforated and buckled baffles (sieves) that hold air when ascending through the humidifier (13 in the previous design). The reason of using this many baffles is due to the performance of the 8 baffles in the laboratory based experiments. The sealed tray is insulated by 5 cm polystyrene sheets and enclosed in a wooden box. The top side of the box is glazed. One meter long baffles are perforated halfway through and placed transversely as shown in Fig. 6.1 and 6.2. Each baffle has six arrays of 2mm in diameter drilled holes with total of 294 holes.

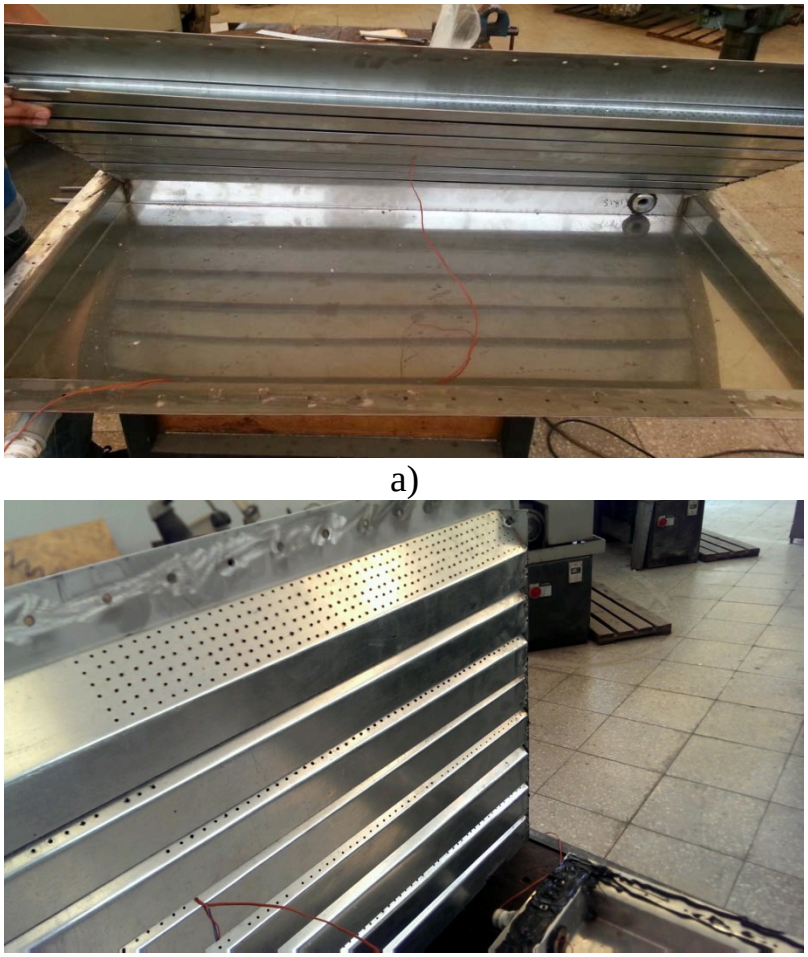

Figure 6.1. A view of the humidification unit a) from inside showing the tray and the cover, and b) showing the bubble regeneration sieves

Upon dispersion under the first baffle from the unperforated part, air is forced to travel horizontally to the perforated side. Air is forced by gravity to pass through the holes and break up as bubbles in water at the top of the baffle. Then bubbles collapse under the next baffle before the air stream travels horizontally to the second baffle's perforated region and ascend vertically through the holes of the second baffle. The process continues through the eight baffles before air exits through the outlet of the humidifier. Besides to the mentioned benefits of the baffles, this extra horizontal

movement of air, is ought to further enhance heat and mass transfer to air by increasing the contact time of air with the baffles and the hot water.

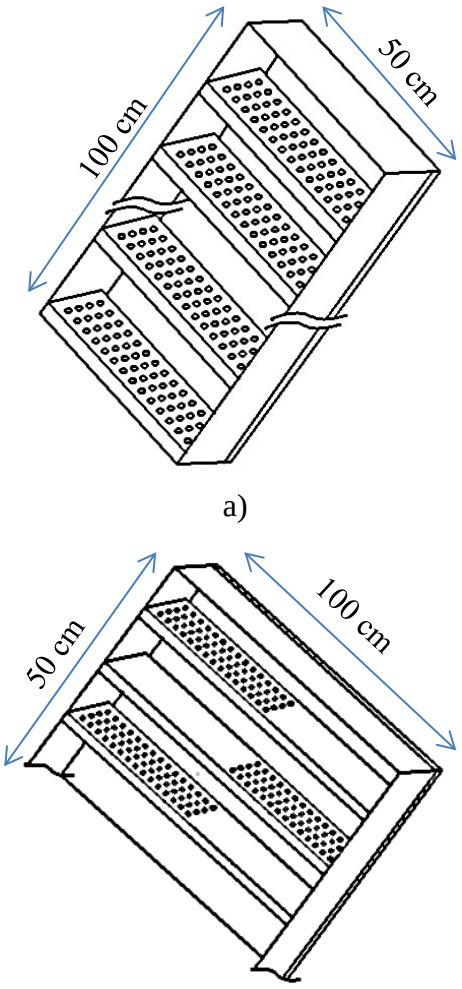

Figure 6.2. Comparison of a) the original design and b) the improved design

6.2 Experimental setup

The experimental setup is illustrated in Fig 6.3. The main parts of the system are the humidifier in which water heating and air heating and humidifying take place, and the dehumidifier or condenser.

The humidifier stands on a frame with an adjustable angle as can be seen in Fig 6.4. The angle was adjusted to 35 degrees to match the latitude of the testing area as it is the best angle for solar energy collection during the summer season (the season at which the experiment was performed). The tilted frame, and thus the humidifier, was adjusted to face south. Air was pumped to the humidifier using a 120 Watts single phase 240V tank-less aquarium-type air pump. The air stream passed through a type SJ-16 orifice meter device manufactured by Air Flow Developments Ltd. having accuracy of 2-4%.

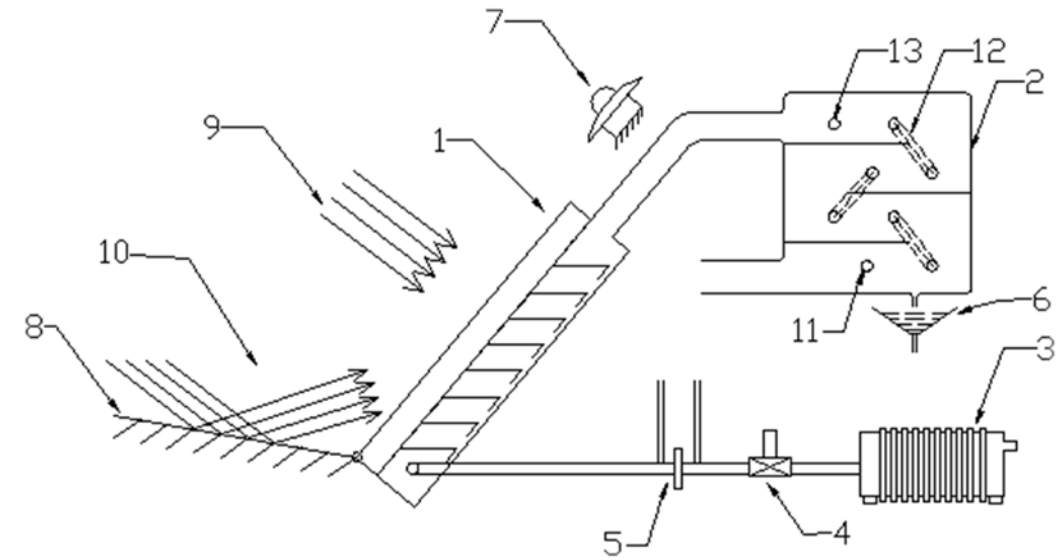

1. Humidifier, 2.Condenser, 3. Compressor, 4. Bypass valve, 5.Orifice meter, 6. Freshwater collector, 7. Pyranometer, 8.Reflector, 9. Direct solar radiation, 10. Reflected solar radiation, 11. Cooling water inlet, 12. Cooling water pipe (connecting the radiators), 13. Cooling water outlet.

Figure 6.3. Schematic diagram of the experimental setup

1.Humdifier, 2.Condenser, 3. Compressor, 4. Bupass valve, 5.Orifice meter, 6. Fresh water collector, 7.Pyranometer, 8.Humidifier air inlet, 9.Humidifier air outlet, 10.Cooler, 11.Condenser air inlet, 12.Condenser air outlet.

Figure 6.4. Photo showing the humidifier and the experimental setup.

Hooked to the humidifier is a dehumidification unit (condenser) that consists of four identical radiator type compact cross-flow water-to-air heat exchangers with both fluids unmixed. Each heat exchanger has a heat transfer area of 11.25 m^2 (total 45 m^2) and a density ratio of 1125 m^2/m^3. The heat exchangers are connected in series and air passes perpendicular to their narrow sides. Each heat exchanger consists of several tubes fed and drained by two headers. The heat exchangers are connected in series; the outlet of the first heat exchanger is the inlet to the second heat exchanger, and etc. The circulating water is cooled in a bath which simulates the underground water temperature (15-18 $^{\circ}$C in test area) as it is thought to be an optional cooling system. Water is cooled and circulated in the dehumidifier. The outlet of the bath is the inlet of the forth radiator and the outlet of the first radiator is the inlet of the cooling bath. Condensate water is collected from eight ports (two ports for each radiator) in a calibrated condensate reservoir. As the system is an open-air system air exiting the dehumidification unit is released into the atmosphere. A T-junction was

attached to the top port and then to water tank acting as a compensator for water loss during the humidification process.

6.3 Experimental procedure

The atmospheric air was pumped into the water batch from the bottom port and exited as hot humidified air from the top port. Humid air then was forced to pass through the dehumidifier for water extraction before discharged to the atmosphere. All inlet and outlet air temperatures were measured using k-type thermocouples coupled with a digital data logger with accuracy of ±0.1°C. The relative humidity of air at each port were measured and recorded as well. The collector water temperatures were measured at three different points in the collector (bottom, middle, and top of the humidifier) and the average temperatures were recorded. The volume of compensation for water and temperatures were recorded at each reading. The condensate water temperature and flow rate was measured as well. Solar intensity on the surface of the collector was measured using radiometer coupled with a sensitive multi-meter. The Eppley radiometer Pyranometer has an accuracy of ±0.5 for the range from 0 to 2800W/m^2. The experiment was performed for four different air mass flow rates (8.3, 12.6, 14.2, 15.2 kg/h) at different days. The system was started an hour before any recording was taken (i.e., at 8:30), and the measurements were recorded each hour until 17:30.

6.4 Results and discussion

6.4.1 Temperature and humidity changes

Figure 6.5 displays the hourly recorded solar intensity together with relevant air temperatures for the air mass flow rate of 12.6 kg/h. The temperature curves in the figure represent the ambient temperature, the humidifier inlet and outlet air

temperatures, and the average temperature of the water in the humidifier. Ambient air temperature variation was a few degrees (2-3 ^{o}C) between 09:30 and 17:30. Although the variation in the ambient temperature was not significant, the inlet temperature kept increasing in the following hours. This is due to the heat gained by air at this stage from the compression process. The inlet air temperature of the humidifier is the outlet temperature of the compressor. Solar intensity increases until the mid of the day and then decreases. As solar intensity increased, both the outlet air temperature and the average water temperature also increased. Due to the energy stored in the system outlet air temperature and average water temperature decrease in a slower pace as solar radiation decreased. The outlet air temperature is higher than the average water temperature. The recorded water temperature at the bottom is lower than the middle and the temperature at the top is as high as the outlet air temperature. Two possible reasons for the stratification of temperature distribution are; the normal buoyancy driven stratification that drives the hotter fluid to float on top of the colder fluid, and the chilling effect of the inlet air as its temperature is relatively lower than the water temperature.

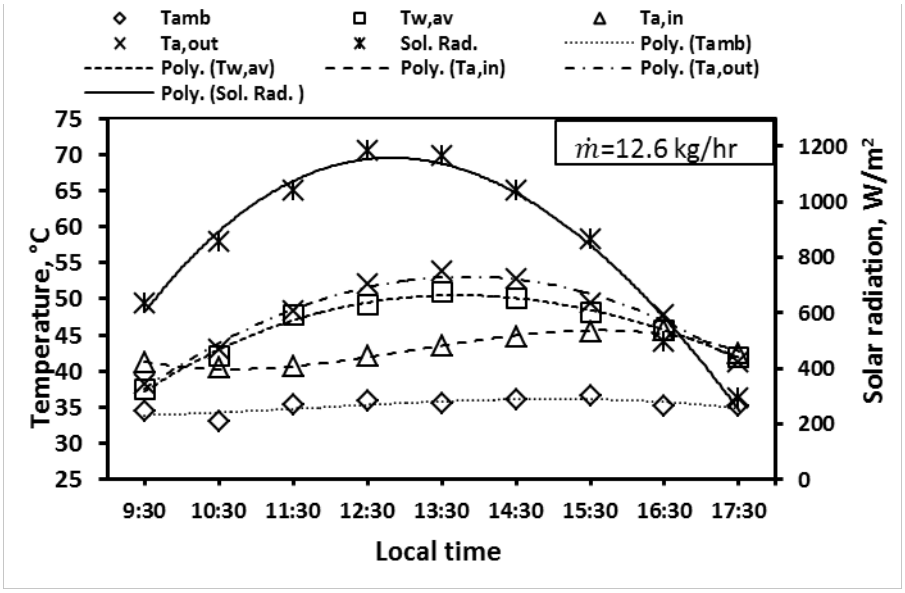

Figure 6.5. Hourly change in temperature due to the change in solar radiation and heat extraction

Fig. 6.6 displays the hourly relative humidity measured before the air pump at the humidifier inlet and outlet, plotted with respect to time of the day.

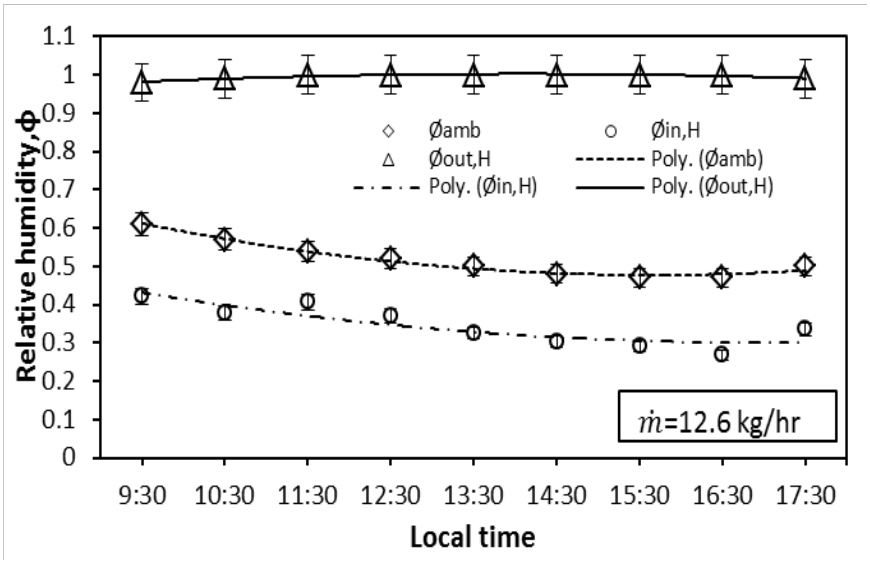

Figure 6.6. Hourly changes in humidity due to humidification process

The compressed air temperature increases due compression before entering the humidifier. The relative humidity of the compressed air decreases as its temperature increased. The absolute humidity, however, is constant throughout the pumping process. As air passes through the humidifier both the temperature and the relative humidity were increased. The humidified air relative humidity ranged between 97-100%.

6.4.2 Productivity and performance measure

6.4.2.1 Productivity

Figure 6.7 presents the effect of air flow rate on the system's production of fresh water. The figure clearly shows the dependency of the water production on water temperature. As the water temperature is increased, due to the increase of solar intensity, the production of water is increased in all flow rates.

As air passes through water, heat and mass transfer take place simultaneously. Some of the energy transfers from the water in the form of sensible heat to increase the air temperature and some as latent heat as vapor is transferred to air. Increased water temperature increases the driving force for both heat and mass transfer and thus influences the amount of extracted vapor. The higher the temperature of air the higher it's vapor carrying capacity.

There are two benefits of having the pump other than conveying air; pump has increased the air temperature and therefore decreased the relative humidity. As the air temperature was increased by pumping to a degree close to the water temperature, the sensible heat flux to air was decreased. As the relative humidity was reduced the

specific vapor pressure (or vapor concentration) difference between liquid and gas was increased and thus the driving force for mass transfer was increased.

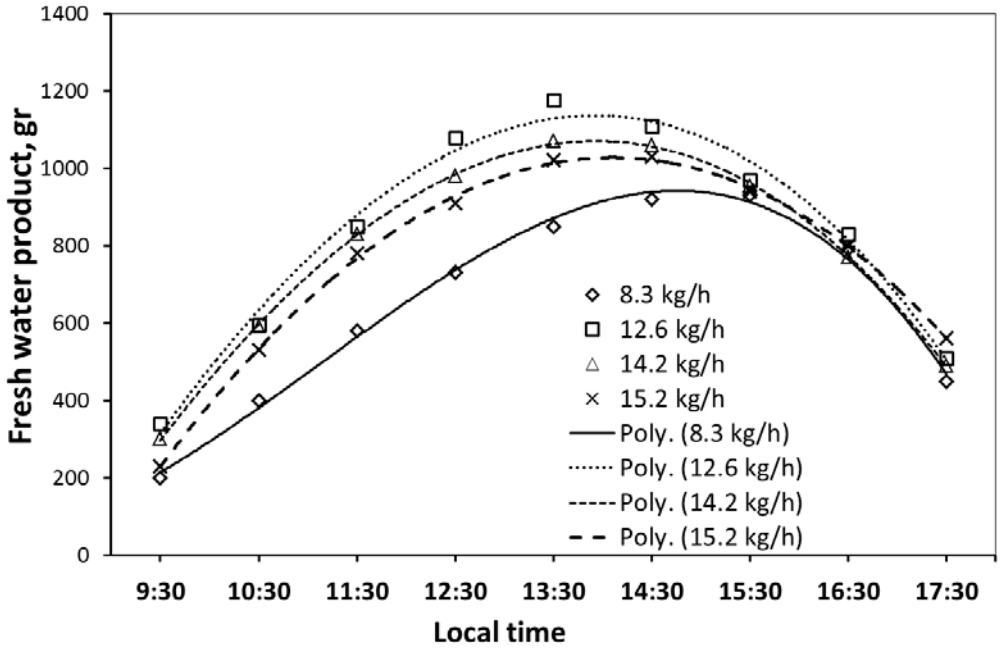

Figure 6.7. Hourly freshwater production for different flow rates

Figure 6.8 shows the cumulative fresh water product for four different flow rates. Water productivity increases continuously but at a slower pace during the last two hours. From Fig. 6.7 and Fig. 6.8 it is clear that increasing the flow rate does not necessarily mean increased productivity. The productivity of the system reached maximum at the flow rate of 12.6 kg/h. Productivity is less at lower and higher air mass flow rate. At high mass flow rates the convective chilling effect of the flowing air decreases the water temperature, and thus the air temperature is decreased too. Subsequently, the vapor carrying capacity of air decreases resulting in overall declination of the product amount. On the other hand, at relatively low air flow rates, the water temperature and air temperature increases. Even though the vapor carrying

capacity of air increases at higher temperatures, the total amount of extracted vapor decreases as the volume flow rate decreased. But, the shortage in vapor removal results in higher thermal loss from the aperture and thus decreases the overall efficiency of the unit. Figure 6.9 compares the productivity under each air mass flow rates.

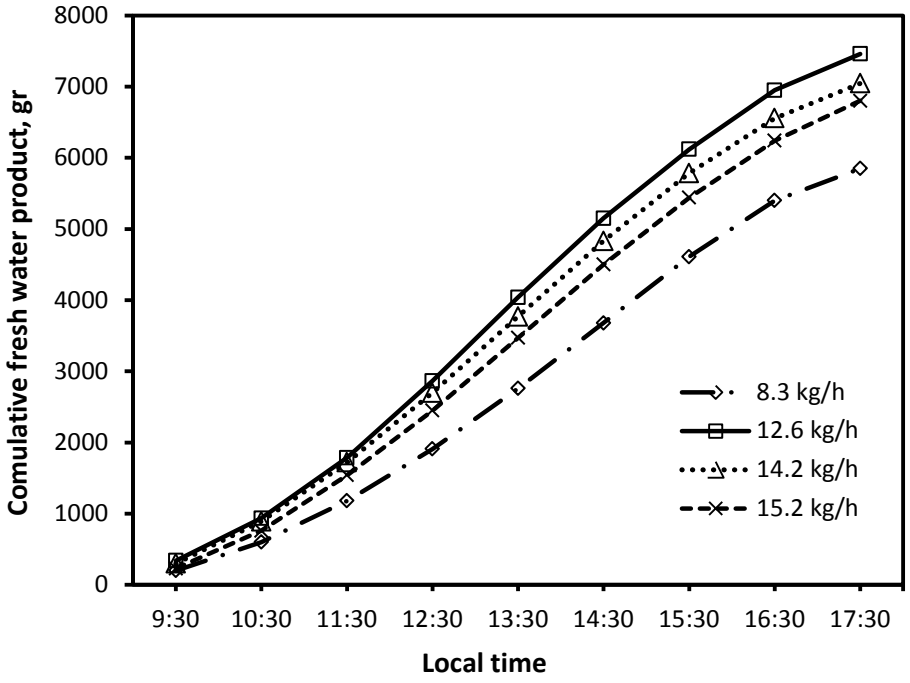

Figure 6.8. Cumulative freshwater production for different flow rates

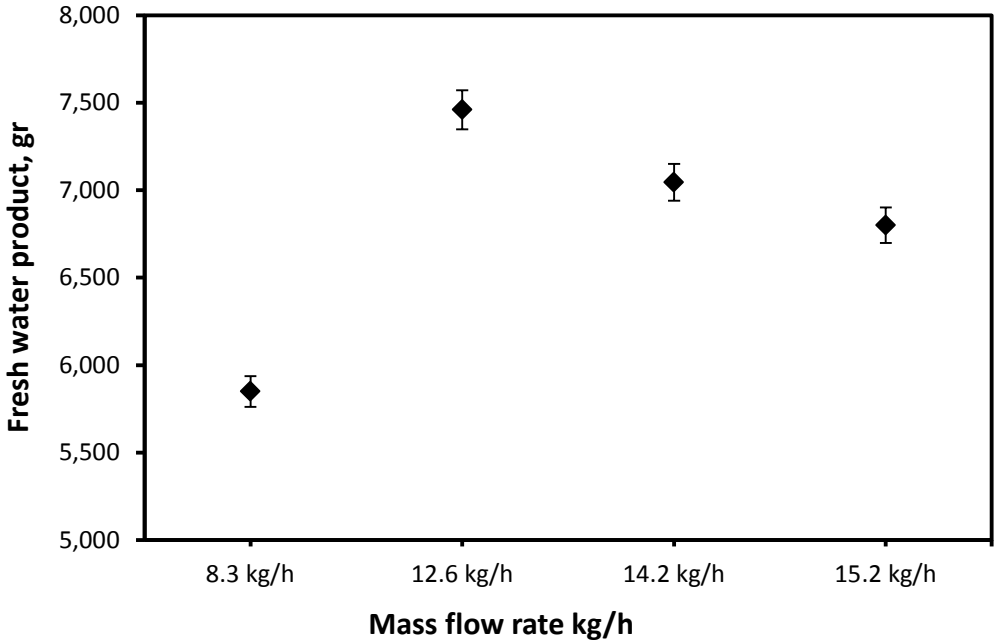

Figure 6.9. Total freshwater production for different flow rates

6.4.2.2 Gas Holdup

Figure 6.10 is a comparison between the gas holdup values of this study with reproduced values from analytical studies for different flow rates available in the literature. In general all the relations show increase in gas holdup capacity of the liquid with increasing superficial gas velocity. Moreover, the relationship between the gas holdup and the superficial velocity is almost linear in each case. The gas holdup of the system presented in this study lays at the average of these relations where no baffles were employed. However, the system showed superiority when the baffles were introduced (see Fig. 6.10)

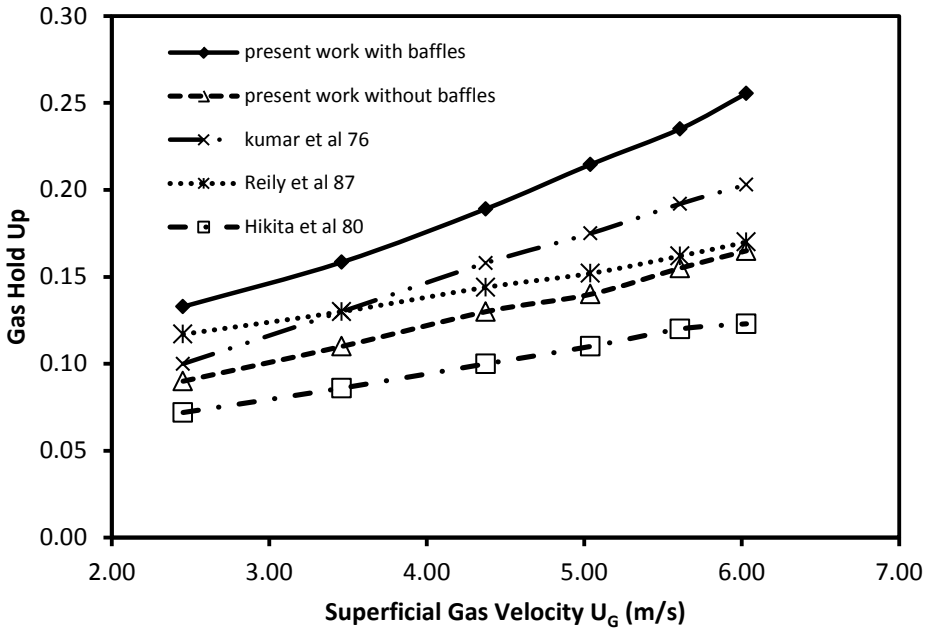

Figure 6.10. Comparison of gas holdup with different suggested formulas

Figure 6.11 compares the results from the present study with recent experimental studies available in the literature. From the figure it is clear that the holdup capacity increases with increasing air mass flow rates. The advantage of employing perforated baffles is obvious as the gas holdup values are higher compared with other studies, for the tested air mass flow rates. The gas holdup values achieved in the case without baffles are in good agreement with the experimental results of (Chaumat et al., 2005)study. The high values of gas holdup witnessed in Camarasa study is due to the height of the column used which was 2 meters. The obtained results in the system with baffles are higher compared with Camarasa's study. It is clear that, the introduction of baffles increased the gas holdup capacity of the system thus; the performance of the system was improved

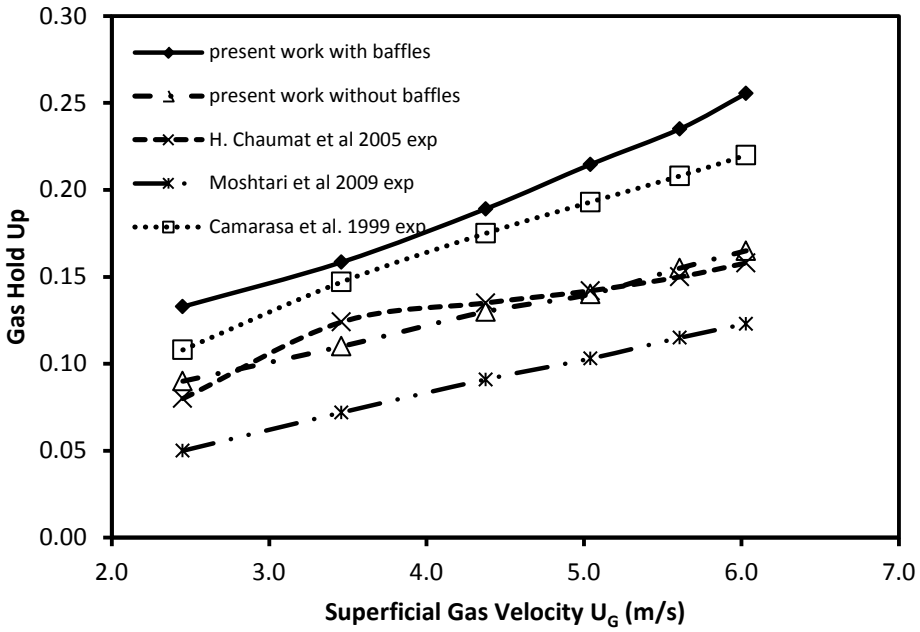

Figure 6.11. Comparison of gas holdup with different experimental results

Most of the studies concentrated on defining the transition point at which the flow regimes turns from homogeneous to heterogeneous. Nevertheless, none of the studies aimed to increase the holdup ability of the column in the homogeneous regime.

6.4.2.3 Gained Output Ratio

Figure 6.12 represent the GOR with respect to time of the day at various mass flow rates. The latent heat of vaporization was calculated by using the following developed equation

$$h_{fg} = -0.002T_w^2 - 2.222T_w + 2498.8 \quad (6.1)$$

In this equation T_w was taken as the average water temperature in the humidifier.

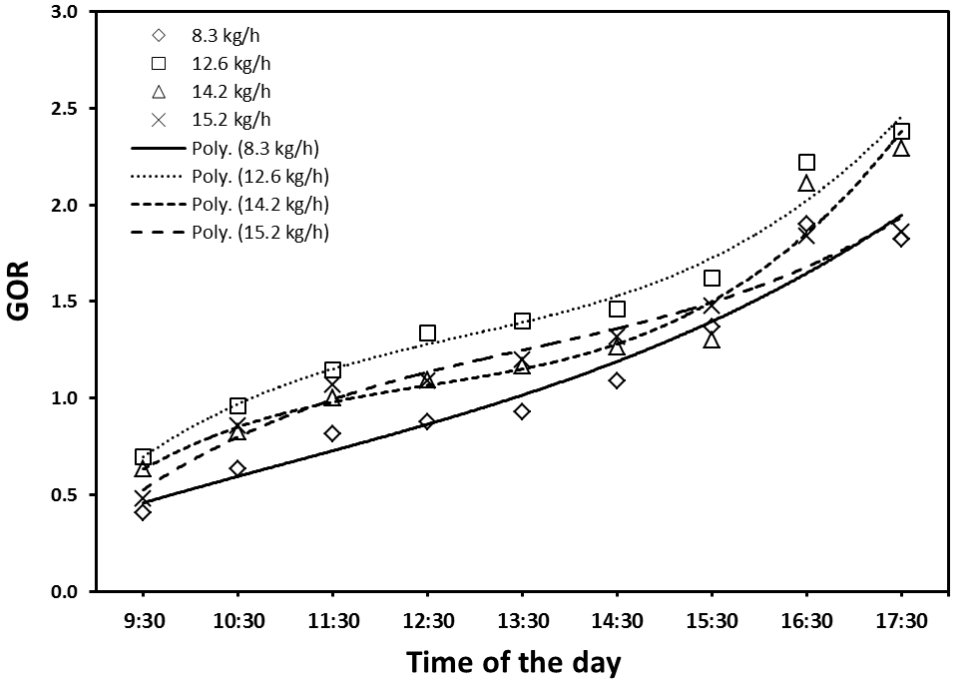

Figure 6.12. GOR for different flow rates

All the curves show almost the same trend and can be divided into three distinct regions. From 9:30 to 11:30 water temperature is low but rising by time, that is the reason for the low GOR at in beginning of the production. From 11:30 to 2:30 the curve almost experiences a plateau that shows a balance between the product water and gained energy. From 2:30 to 5:30 the curve builds up a gentle heap and the GOR is more than unity. Nevertheless, the fresh water production is less in this region than the preceding one. The declination in the solar energy supplied over weighs the declining of the fresh water product. The fresh water product declines at a slower pace due to the stored energy of the contained water and the humidifier components. If we take the plateau region as the representative region for the GOR we find that the GOR, of the higher productive air mass flow rate of 12.6 kg/h, is averaged at 1.5. This is followed by the two higher flow rates of 14.2 and 15.2 kg/h with a GOR

average at almost 1. The lowest GOR was achieved at 8.3 kg/h mass flow rate where the water production was also the lowest.

6.4.2.4 Normalized Production

Table 6.1 provides a normalized productivity comparison between the present work and other experimental works. NP is calculated according to Eqn. 3.9.

Table 6.1. Comparison of the normalized production for the present work with other works in the letirature

Research name	(Hermosillo et al., 2012)	(Nafey et al., 2004)	(Yuan et al., 2011)	Present work
Max productivity (L/h)	1.45	1.3	125	1.175
Effective are (m^2)	-	2.5 (0.5 m^2 solar air heater + 2 m^2 solar concentratin g water heater)	114 (100 m^2 solar air heater + 14 m^2 solar water heater)	0.5
Solar intensity (W/m^2)	Simulated	900	760	1166 (with reflection)
Total solar energy (W)	1120	2250	86640	583
Normalized production (L/kW.h)	1.29	0.58	1.44	2.02

The present setup provides higher NP compared to other setups presented in Table 6.1.

6.5 Final remarks

A compact desalination unit working under the air humidification dehumidification principle was presented. A modified humidification unit incorporated air and water heating besides to air humidification was utilized to maximize the air vapor carrying capacity before passing it into a condenser for water production. The introduced perforated baffles increased the fractional holdup of air in the humidification unit

resulted in higher humidification efficiency. The effectiveness of the system manifested itself by higher normalized productivity when compared to other pilot and commercial systems at their maximum productivities. The overall system freshwater production was 15 L/m^2 day.

Chapter 7

7 INNOVATION IMPLICATIONS IN THE DESIGN OF SOLAR HDD SYSTEMS

Solar energy based HDD systems occupy a considerable area since they use solar collectors to collect the energy. In such systems, apart from the cost of the occupied land, solar collectors may form the largest portion of the total investment. Thus compact designs of solar HDD systems are essential in order to reduce the area needed and decrease the overall cost. Integration by merging some of the HDD processes leads to more compact designs. When thinking of Compact designs, the designer should bear in mind that performance of the system shouldn't be the price. In order to improve the compactness of HDD systems, one should work on both the cycle and the components. For example, in this work the proposed cycle incorporated air heating, water heating, and the humidification processes. The main goal sought from the humidifying unit is maximizing the temperature and the saturation level of the outlet air stream. Thus the humidification capacity is increased and dehumidification load is decreased.

Saturated air is a mixture of incondensable gas and condensable vapor. The incondensable gas absorbs great amount of energy in the humidifier and increases the resistance to condensation from the mixture in the dehumidifier. The mass fraction of the condensable vapor increases with increasing air temperature and/or with

decreasing pressure. Figure 4.3 shows that at 80kpa the possible moisture content of air is almost double that of air at 100kpa at the same temperature. Thus, in order to increase the vapor carrying capacity of the gas stream, the temperature of the gas should be kept as high as possible while the pressure in the evaporator is kept low. In order to make this possible, a number of innovative approaches can be adopted.

Speaking of the pressure inside the humidifier, the location and type of the air pump (compressor) is important. If the pump is located upstream of the humidifier, air in the humidifier would be under high pressure. Thus the vapor carrying capacity of the air, although the air could be saturated, would be weakened. Placing the pump downstream of the dehumidifier would create vacuum on air and thus the specific volume of air would increase. Since the amount of vapor in air is at least not increasing, the dew point of air would decrease as a result of increasing specific volume of air. In both of the cases the water production-performance of the HDD systems would not be at its best. However, if the air pump is placed between the humidifier and the dehumidifier, air in the humidifier would be under vacuum that helps increase the vapor carrying capacity. Even a vacuum of 20kpa would double the amount of vapor carried by air at 85°C. Also the dehumidifier would be under slightly high pressure that helps the condensation process. Further, in order to decrease some of the head pressure against which the air pump exerts work, the water level should be decreases as much as possible.

The temperature of the air passing through the water in the humidifier is highly influenced by the temperature of water. The water temperature, on the other hand, is governed by the amount of water in the humidifier, solar intensity, inlet temperature

and mass flow rate of the air, compensation water temperature, and heat losses from the humidifier.

- The mass of water is determined by the volume of the humidifier housing it. The humidifier is designed to be a shallow cube with the top façade having the largest area. The depth of the humidifier does not affect the amount of received solar energy. However, decreasing the depth of the humidifier would result in higher water temperatures as the received solar energy accumulate in a smaller volume of water. On the other hand, decreasing the depth of the humidifier poses a limitation on the amount of air flow. Although the humidifier should be tested for different depths, it is predictable that it can only be shallow to an extent.
- Global solar intensity is the only input to the system that cannot be manipulated. Attempting to increase the collected solar radiation by increasing the aperture area would increase the amount of heat loss from the humidifier. However, the solar energy can be concentrated by adding reflectors on all sides of the receiver. As a result, both the temperature of the absorber and of the water in the humidifier would increase. But increasing the temperature of the receiver would result in an increased heat loss from the aperture area. This problem can be solved by attempting to design a double-pass humidifier system.
- The lost energy from the absorber can be collected by passing the inlet air between the glazing and the absorber. Thus inlet air would be preheated before being injected to the humidifier. Double-pass systems are proven for their effectiveness in solar air heaters and would pay off in solar HDD systems if they are utilized.

- Heating the air prior to feeding it into the humidifier is a vital practice in HDD systems even if the system is based on water heating. The cooling effect resulted from the withdrawal of sensible and latent heat by the colder air passing in hot water would decrease if air was preheated. It is even more vital if air preheating was made possible attempting to recover the heat loss from the system. Apart from the absorber, heat losses also take place in compressors due to friction between its moving parts. The temperature of high capacity compressors reaches as high as 100°C. The compressor needed for the system proposed in this work is relatively small. The temperature in such compressor can reach 70°C leading to considerable heat losses that can be used to preheat the inlet air to the compensate water fed into the humidifier.
- Air mass flow rate is a very important variable in HDD systems. It has direct and indirect effects on the effectiveness of the humidifier and the productivity of the whole system. Systems designed with higher flow rates do not necessarily have higher water productivity as can also be seen from Fig. 6.9. If the air flow rate is above an optimum value there will be insufficient humidification or lower humidifier effectiveness. Moreover, higher flow rates result in further cooling of the water in the humidifier which results in lowering the temperatures of the fluids and thus hindering the amount of the carried vapor. On the other hand, when the air mass flow rate is below the optimum value early saturation of air takes place. In this case, although the efficiency and effectiveness of the humidification process can be maximized, the productivity of the system is limited. The optimum flow rate in solar HDD systems depends on the amount of solar radiation. Thus, an automatic control system can be incorporated to the

HDD system to modify the flow rate to achieve the best performance. However, as the variables are many, it is more convenient to optimize the components before adding intelligence to the system. In this work humidification by bubbling was investigated. The experimental work conducted in the laboratory revealed that there is an optimum pitch distance between the sparger holes. Additionally, when bubble regeneration was introduced it was discovered that an optimum number of regeneration stages was available. These key points, besides others, were used in designing the final solar HDD system in order to eliminate the deficiency factors.

- In its present state, the HDD system is optimized for saturation under the highest flow rate the suggested pump can deliver. But for the maximum effectiveness the saturated outlet air temperature should match the water temperature in the humidifier. And this can be accomplished by adding a simple feedback system. Since the design of the humidifier guarantees the saturation of the air stream at the outlet, the controller should work on maximizing the outlet air temperature. The outlet air temperature should match the water temperature for maximum effectiveness. A differential temperature controller can be added to measure the difference in water and outlet air temperatures. The controller then would increase or decrease the air flow rate in order to keep the difference in temperature below some preset value. This simple control mechanism would improve the productivity of the system. However a more sophisticated controller that can predict the productivity of the system under different flow rates for a given set of variables can be put into use. As a scenario, suppose a system that works based on the controlling mechanism discussed above-which takes care of

the effectiveness rather than the productivity of the system. The system would work with the instantaneous optimum flow. However the cooling effect of the high flow rate may decrease the water temperature. In this case effectiveness of the system would have been maximized but the overall productivity would be decreased. Given all the variables, a controller that can predict the productivity of the system should consider the cooling effect resulted from the high flow rate and keep booth the effectiveness and productivity at their maximum. A flow chart illustrates the outlines of the controlling process is shown in Fig. 7.1.

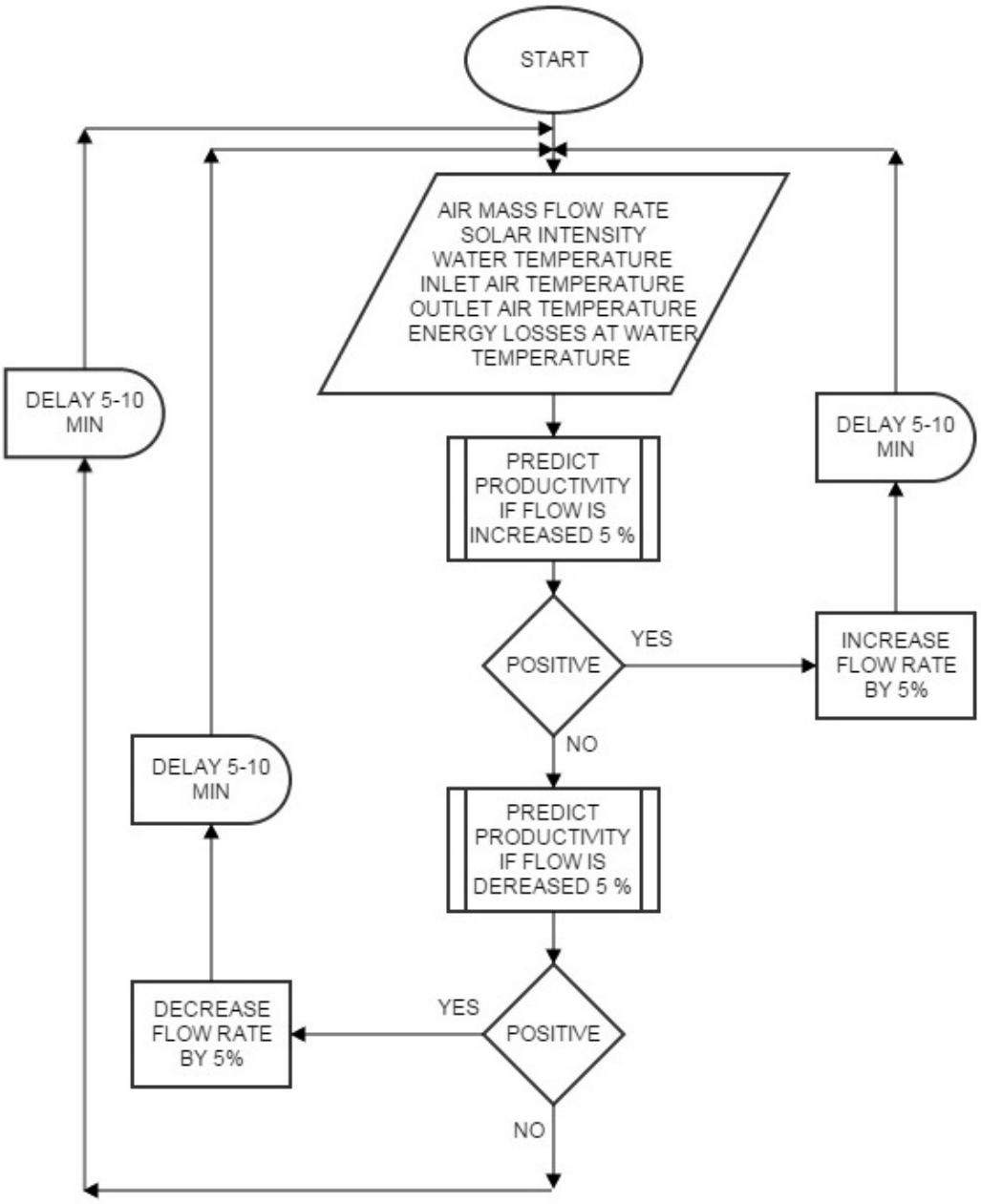

Figure 7.1. Proposed flow chart of a HDD controller subroutine that insures maximum productivity

Chapter 8

8 CONCLUSION

It has always been desired to improve the performance of solar HDD systems while at the same time reducing the size of the whole system. For this purpose, a humidification unit that incorporates the bubbling technique is built and tested in the laboratory environment. The air is driven into the humidification unit, which is basically a container full of water, in the form of bubbles. Upon contact with water in the humidifier, air bubbles become saturated with vapor. Efficiency and effectiveness of the humidifier was analyzed. The humidifier performance was improved by air bubble regeneration technique. Based on the lessons learned from this work, a novel compact solar humidification unit incorporating the heating of water, the heating of the air stream, and the humidification of air is proposed. The effects of water temperature, bubble regeneration, and increased radiation by reflection on the performance of the humidifier are studied. Based on the analysis and the experimental results, the following conclusions are reached:

- Direct contact bubbling humidification is an efficient technique which can be used in HDD systems.
- Introducing inverted sieves (perforated trays) to the system helps resizing the air bubbles that helps maximizing the air-water contact surface area.
- Bubble regeneration increases the gas holdup ratio in the humidifier, thus increases the mass and heat transfer.

- Using eight bubble regeneration stages maximizes the effectiveness of the humidification process even at low temperatures and high flow rates.
- Employing sieves to act as fins attached to the solar absorber enhances heat transfer which increases the air temperature and thus the moisture carrying capacity of air.
- Reflection increases the system's temperature and improves the effectiveness of the humidification process.
- The GOR increases until an optimum air flow rate is reached and decreases as the flow rate exceeds the optimum.
- The system shows normalized production of 2.02 L/kW.h which is significantly higher than systems in other studies available in literature.
- The daily fresh water production of the system reaches 15 L/m^2.

The suggested humidification unit shows promising use for humidification by bubbling technique. However employing this technique is yet not common in HDD systems. Thus, further investigations should be conducted based on the lessons that have been learned from this work. Suggestions for further work are as follows:

- Air could be circulated in the system by using a vacuum air pump that is positioned between the humidifier and the dehumidifier.
- Utilizing a double-pass aperture for air preheating could decrease the heat losses from the absorber.
- Significant amount of latent heat can be recovered if the compensate water is passed through the first stage of the condenser.
- Utilizing a controller can increase the performance of the whole system.

REFERENCES

Al-Enezi, G., Ettouney, H., Fawzy, N. (2006) Low temperature humidification dehumidification desalination process. *Energy Conversion and Managemen*t 47, 470-484.

Al-Hallaj, S., Farid, M.M., Tamimi, A.R. (1998) Solar desalination with a humidification - dehumidification cycle: Performance of the unit. *Desalination* 120, 273-280.

Al-Hallaj, S., Parekh, S., Farid, M.M., Selman, J.R. (2006) Solar desalination with humidification–dehumidification cycle: Review of economics. *Desalination* 195, 169-186.

Bacha, H.B., Damak, T., Bouzguenda, M., Maalej, A.Y. (2003) Experimental validation of the distillation module of a desalination station using the SMCEC principle. *Renewable Energy* 28, 2335-2354.

Ben Amara, M., Houcine, I., Guizani, A., Măalej, M. (2004) Experimental study of a multiple-effect humidification solar desalination technique. *Desalination* 170, 209-221.

Bourouni, K., Chaibi, M.T., Tadrist, L. (2001) Water desalination by humidification and dehumidification of air: State of the art. *Desalination* 137, 167-176.

Camarasa, E., Vial, C., Poncin, S., Wild, G., Midoux, N., Bouillard, J. (1999a) Influence of coalescence behaviour of the liquid and of gas sparging on hydrodynamics and bubble characteristics in a bubble column. *Chemical Engineering and Processing*: Process Intensification 38, 329-344.

Camarasa, E., Vial, C., Poncin, S., Wild, G., Midoux, N., Bouillard, J. (1999b) Influence of coalescence behaviour of the liquid and of gas sparging on hydrodynamics and bubble characteristics in a bubble column. *Chemical Engineering and Processing*: Process Intensification 38, 329-344.

Cengel, Y.A. (1997) *Heat Transfer, A Practical Approach*. McGraw-Hill Press.

Chafik, E. (2003a) A new seawater desalination process using solar energy. *Desalination* 153, 25-37.

Chafik, E. (2003b) A new type of seawater desalination plants using solar energy. *Desalination* 156, 333-348.

Chafik, E. (2004) Design of plants for solar desalination using the multi-stage heating/humidifying technique. *Desalination* 168, 55-71.

Chaumat, H., Billet-Duquenne, A.M., Augier, F., Mathieu, C., Delmas, H. (2005) Mass transfer in bubble column for industrial conditions—effects of organic medium, gas and liquid flow rates and column design. *Chemical Engineering Science* 60, 5930-5936.

Chen, R.H., Tian, W.X., Su, G.H., Qiu, S.Z., Ishiwatari, Y., Oka, Y. (2011) Numerical investigation on coalescence of bubble pairs rising in a stagnant liquid. *Chemical Engineering Science* 66, 5055-5063.

Clift, R. (1978) Bubbles, drops, and particles / R. Clift, J. R. Grace, and M. E. Weber. *Academic Press*, New York.

Cooper, P.I. (1973) The maximum efficiency of single-effect solar stills. *Solar Energy* 15, 205-217.

Dai, Y.J., Wang, R.Z., Zhang, H.F. (2002) Parametric analysis to improve the performance of a solar desalination unit with humidification and dehumidification. *Desalination* 142, 107-118.

Dai, Y.J., Zhang, H.F. (2000) Experimental investigation of a solar desalination unit with humidification and dehumidification. *Desalination* 130, 169-175.

Deckwer, W.D., Louisi, Y., Zaidi, A., Ralek, M. (1980) Hydrodynamic properties of the Fischer-Tropsch slurry process. *Industrial & Engineering Chemistry Process Design and Development* 19, 699-708.

Eickenbusch, H., Brunn, P.O., Schumpe, A. (1995) Mass transfer into viscous pseudoplastic liquid in large-diameter bubble columns. *Chemical Engineering and Processing*: Process Intensification 34, 479-485.

El-Agouz, S.A. (2010) A new process of desalination by air passing through seawater based on humidification–dehumidification process. *Energy* 35, 5108-5114.

El-Agouz, S.A., Abugderah, M. (2008) Experimental analysis of humidification process by air passing through seawater. *Energy Conversion and Management* 49, 3698-3703.

Elgozali, A., Linek, V., Fialová, M., Wein, O., Zahradník, J. (2002) Influence of viscosity and surface tension on performance of gas–liquid contactors with ejector type gas distributor. *Chemical Engineering Science* 57, 2987-2994.

Farid, M., Al-Hajaj, A.W. (1996) Solar desalination with a humidification-dehumidification cycle. *Desalination* 106, 427-429.

Garg, H.P., Adhikari, R.S., Kumar, R. (2003) Experimental design and computer simulation of multi-effect humidification (MEH)-dehumidification solar distillation. *Desalination* 153, 81-86.

H. Jaber, a.R.L.W. (1989) Design of Cooling Towers by the Effectiviness-NTU Method. *ASME Journal of Heat Transfer* 111, 837-843.

Heijnen, J.J., Van't Riet, K. (1984) Mass transfer, mixing and heat transfer phenomena in low viscosity bubble column reactors. *The Chemical Engineering Journal* 28, B21-B42.

Hermosillo, J.-J., Arancibia-Bulnes, C.A., Estrada, C.A. (2012) Water desalination by air humidification: Mathematical model and experimental study. *Solar Energy* 86, 1070-1076.

Hikita, H., Asai, S., Tanigawa, K., Segawa, K., Kitao, M. (1980) Gas hold-up in bubble columns. *The Chemical Engineering Journal* 20, 59-67.

Houcine, I., BenAmara, M., Guizani, A., Maâlej, M. (2006) Pilot plant testing of a new solar desalination process by a multiple-effect-humidification technique. *Desalination* 196, 105-124.

Krishna, R., Ellenberger, J. (1996) Gas holdup in bubble column reactors operating in the churn-turbulent flow regime. *AIChE Journal* 42, 2627-2634.

Krishna, R., van Baten, J.M. (2003) Mass transfer in bubble columns. *Catalysis Today* 79–80, 67-75.

Kumar, A., Degaleesan, T.E., Laddha, G.S., Hoelscher, H.E. (1976) Bubble swarm characteristics in bubble columns. *The Canadian Journal of Chemical Engineering* 54, 503-508.

Martín, M., Montes, F.J., Galán, M.A. (2007) Bubble coalescence at sieve plates: II. Effect of coalescence on mass transfer. Superficial area versus bubble oscillations. *Chemical Engineering Science* 62, 1741-1752.

Mathioulakis, E., Voropoulos, K., Belessiotis, V. (1999) Assessment of uncertainty in solar collector modeling and testing. *Solar Energy* 66, 337-347.

Moshtari, B.B., Ensieh; Moghaddas, Jafar (1999) Experimental Study of Gas Hold-up and bubble behavior in Gas – Liquid Bubble Column Petroleum & Coal 51, 27-32.

Moustiri, S., Hebrard, G., Thakre, S.S., Roustan, M. (2001) A unified correlation for predicting liquid axial dispersion coefficient in bubble columns. *Chemical Engineering Science* 56, 1041-1047.

Müller-Holst, H., (2007) Solar thermal desalination using the multiple effect humidification (MEH) method, *solar desalination for the 21st century*., pp. 215–225.

N.P. Cheremisinoff, P.N.C., (1981) *Cooling towers: selection, design, and practice,* Ann Arbor Science Publishers Inc. Ann Arbor Michigan.

Nafey, A.S., Fath, H.E.S., El-Helaby, S.O., Soliman, A. (2004) Solar desalination using humidification–dehumidification processes. Part II. An experimental investigation. *Energy Conversion and Management* 45, 1263-1277.

Narayan, G.P., Sharqawy, M.H., Summers, E.K., Lienhard, J.H., Zubair, S.M., Antar, M.A. (2010) The potential of solar-driven humidification–dehumidification desalination for small-scale decentralized water production. *Renewable and Sustainable Energy Reviews* 14, 1187-1201.

Nawayseh, N.K., Farid, M.M., Al-Hallaj, S., Al-Timimi, A.R. (1999) Solar desalination based on humidification process—I. Evaluating the heat and mass transfer coefficients. *Energy Conversion and Management* 40, 1423-1439.

Nellis, G., and Klein, S. (2008) *Heat Transfer*. Cambridge University Press.

Orfi, J., Laplante, M., Marmouch, H., Galanis, N., Benhamou, B., Nasrallah, S.B., Nguyen, C.T. (2004) Experimental and theoretical study of a humidification-dehumidification water desalination system using solar energy. *Desalination* 168, 151-159.

Parekh, S., Farid, M.M., Selman, J.R., Al-hallaj, S. (2004) Solar desalination with a humidification-dehumidification technique — a comprehensive technical review. *Desalination* 160, 167-186.

Perers, B. (1997) An improved dynamic solar collector test method for determination of non-linear optical and thermal characteristics with multiple regression. *Solar Energy* 59, 163-178.

Pino, L.Z., Solari, R.B., Siquier, S., Estevez, L.A., Yepez, M.M., Saez, A.E. (1992) Effect of operating conditions on gas holdup in slurry bubble columns with a foaming liquid. *Chemical Engineering Communications* 117, 367-382.

Pohorecki, R., Moniuk, W., Zdrójkowski, A. (1999) Hydrodynamics of a bubble column under elevated pressure. *Chemical Engineering Science* 54, 5187-5193.

Pohorecki, R., Moniuk, W., Zdrójkowski, A., Bielski, P. (2001) Hydrodynamics of a pilot plant bubble column under elevated temperature and pressure. *Chemical Engineering Science* 56, 1167-1174.

R.H. Perry, D.W.G. (2001) *Engineering manual of liquids, 4a ed*. McGraw-Hill, Madrid.

Reilly, I.G., Scott, D.S., De Bruijn, T., Jain, A., Piskorz, J. (1986) A correlation for gas holdup in turbulent coalescing bubble columns. *The Canadian Journal of Chemical Engineering* 64, 705-717.

Shah, Y.T., Kelkar, B.G., Godbole, S.P., Deckwer, W.D. (1982) Design parameters estimations for bubble column reactors. *AIChE Journal* 28, 353-379.

Smith, J.S., Burns, L.F., Valsaraj, K.T., Thibodeaux, L.J. (1996) Bubble column reactors for wastewater treatment. 2. The effect of sparger design on sublation column hydrodynamics in the homogeneous flow regime. *Industrial and Engineering Chemistry Research* 35, 1700-1710.

Thorat, B.N., Kataria, K., Kulkarni, A.V., Joshi, J.B. (2001) Pressure drop studies in bubble columns. *Industrial and Engineering Chemistry Research* 40, 3675-3688.

Tsuge, H., Tanaka, Y., Hibino, S.-i. (1981) Effect of the physical properties of gas on the volume of bubble formed from a submerged single orifice. *Canadian Journal of Chemical Engineering* 59, 569-572.

UNESCO, (2014) Water and Energy, in: UNESCO, World Water Development Report, *Unesco Publishing*, Paris.

Vandu, C.O., Krishna, R. (2004) Influence of scale on the volumetric mass transfer coefficients in bubble columns. *Chemical Engineering and Processing*: Process Intensification 43, 575-579.

Vial, C., Lainé, R., Poncin, S., Midoux, N., Wild, G. (2001) Influence of gas distribution and regime transitions on liquid velocity and turbulence in a 3-D bubble column. *Chemical Engineering Science* 56, 1085-1093.

Wallis, G.B. (1969) *One Dimensional Two Phase Flow*. McGraw Hill, New York.

Wilkinson, P., Spek, A., van Dierendonck, L. (1992) Design parameters estimation for scale-up of high-pressure bubble columns. *AIChE Journal* 38, 544-554.

Winterbottom, J.M. (1993) Bubble column reactors. By Wolf-Dieter Deckwer. John Wiley & Sons Ltd, Chichester, 1992, ix + 533 pp., price: 110.00. ISBN 0 471 91811 3. *Journal of Chemical Technology & Biotechnology* 58, 403-404.

Wu, Y., Cheng Ong, B., Al-Dahhan, M.H. (2001) Predictions of radial gas holdup profiles in bubble column reactors. *Chemical Engineering Science* 56, 1207-1210.

Yamali, C., Solmus, I. (2008) A solar desalination system using humidification-dehumidification process: experimental study and comparison with the theoretical results. *Desalination* 220, 538-551.

Yamashita, F. (1998) Effect of clear liquid height and gas inlet height on gas holdup in a bubble column. *Journal of Chemical Engineering of Japan* 31, 285-288.

Younis, M.A., Darwish, M.A., Juwayhel, F. (1993) Experimental and theoretical study of a humidification-dehumidification desalting system. *Desalination* 94, 11-24.

Yuan, G., Wang, Z., Li, H., Li, X. (2011) Experimental study of a solar desalination system based on humidification–dehumidification process. *Desalination* 277, 92-98.